UNIVERSITÀ DELLA CALABRIA

UNIVERSITA' DELLA CALABRIA

Dipartimento di Ingegneria per l'Ambiente e il Territorie e Ingegneria Chimica – DIATIC

Dottorato di Ricerca in

Scienze e Ingegneria dell'Ambiente, delle Construzioni e dell'energia – SIACE

CICLO

XXXIII

TITOLO TESI

Experimental investigation of system performance for combined desalination processes with membrane capacitive deionisation (MCDI)

Settore Scientifico Disciplinare CHIM/06 – Chimica Organica

Coordinatore: Ch.mo Prof. Salvatore Critelli

Firma _____

Supervisore/Tutor: Ch.mo Prof. Bartolo Gabriele   Ch.mo Dott. Alberto Figoli

Firma_

Ch.mo Prof. Jan Hoinkis

Firma_____

Dottorando: Dott. Edgardo E. Cañas Kurz

Firma ____

UNIVERSITÀ DELLA CALABRIA

PhD Thesis, XXXIII Cycle

Universitá della Calabria

SSD: CHIM/06 – Organic Chemistry

EXPERIMENTAL INVESTIGATION OF SYSTEM PERFORMANCE OF COMBINED DESALINATION PROCESSES WITH MEMBRANE CAPACITIVE DEIONISATION (MCDI)

PhD Candidate:

Edgardo E. Cañas Kurz

Supervisors:

Prof. Bartolo Gabriele [1]

Prof. Jan Hoinkis [2]

Dr. Alberto Figoli [3]

[1]Department of Chemistry and Chemical Technologies, University of Calabria (UNICAL), Rende, Italy
[2]Center of Applied Research, Karlsruhe University of Applied Sciences (HKA), Karlsruhe, Germany
[3]National Research Council, Institute on Membrane Technology (CNR-ITM), Rende, Italy

PhD Coordinator:

Prof. Salvatore Critelli

Dottorato di Ricerca in
Scienze e Ingegneria dell'Ambiente,
delle Costruzioni e dell' Energia
SIACE

UNIVERSITÀ DELLA CALABRIA

Hochschule Karlsruhe
University of
Applied Sciences

HKA

Institute on Membrane
Tecnology
National Research Council of Italy
ITM

DECLARATION

This dissertation is the result of my own work except where specifically indicated in the text. It has not been previously submitted, in part or whole, to any university of institution for any degree, diploma, or other qualification.

Nov. 2021

_____

Edgardo E. Cañas Kurz

ACKNOWLEDGMENTS

ABSTRACT

The water supply in many coastal regions worldwide is affected by progressive salinization. Here, the use of desalination technologies is a viable solution for obtaining freshwater. In this thesis, two modular concepts for brackish water (BW) desalination by the use of membrane capacitive deionization (MCDI) and low-pressure reverse osmosis (LPRO) were developed and tested at laboratory and pilot-scales with two pilot plants installed in Vietnam. The two concepts were developed by using computer-based calculations (software: WAVE) and evaluated in a socioeconomic and environmental multi-criteria analysis.

The first plant consisting of subsurface arsenic removal (SAR) as pre-treatment and MCDI for desalination was installed in Tra Vinh, in the Mekong Delta for the treatment of arsenic-contaminated groundwater with a concentration of total dissolved solids (TDS) of 1.65 g/L. Results showed the feasibility of the modular concept for producing drinking water (TDS<0.45 g/L) with a specific energy consumption (SEC) of <3 kWh/m^3. The relationship between feed salinity and specific ion removal of the MCDI was evaluated in real environment and compared with laboratory experiments. The use of renewable energies such as solar and wind for autonomous supply was proven feasible for these technologies.

The second pilot plant was installed in a riverine estuary in the region of Cần Giờ, where no access to freshwater is available due to the progressive salinization of river water and groundwater. Here, river water showed TDS concentrations of up to 25 g/L. The combined system consisted of UF pre-treatment, LPRO and MCDI to produce drinking water and product water with TDS of <0.45 g/L and <1.5 g/L, respectively with a total SEC of 5.8 kWh/m^3. Additionally, the performance of the LPRO was compared to seawater-RO (SWRO) in pilot trials, which showed a SEC of 5.5 kWh/m^3. Although the SEC of single-stage SWRO was lower, the separate production of drinking and product water by LPRO+MCDI showed different advantages including a reduced SEC of 5.2 kWh/m^3 for product water and additional 0.6 kWh/m^3 for drinking water. Finally, an optimization of the LPRO+MCDI can be possible by increasing the desalination efficiency of the MCDI, increasing the efficiency of LPRO-pump and the MCDI power supply, and by aiming at feed water qualities with lower salinity.

CONTENTS

LIST OF TABLES

LIST OF FIGURES

NONMENCLATURE

AC	alternate current
CapDI	*capacitive deionisation* – development kit MCDI unit from Voltea B.V.®
CDC	consumer dependant controller
CDI	capacitive deionisation
CP	charge phase / desalination phase
BW	brackish water
DC	direct current
DI	deionized water
DP	discharge phase / regeneration phase
EC	electric conductivity
ED	electrodialysis
EDI	electro deionization
FF	flow factor
FCDI	flow capacitive deionisation
HCMC	Ho Chi Minh City
HFO	hydrous ferric oxides
HKA	Karlsruhe University of Applied Sciences
IEM	ion-exchange membrane
ITM	Institute of Membrane Technology
LPRO	low-pressure reverse osmosis
MCDI	membrane capacitive deionisation
MED	multi-effect distillation
MSF	multi-stage flash desalination
MWCO	molecular weight cut-off
MVC	mechanical vapour compression
NF	nanofiltration
NOM	natural organic matter
PP	pre-charge phase / pre-desalination phase
PV	photovoltaic
RED	reverse electrodialysis
RE	removal efficiency / salt rejection (see variables)
RES	renewable energy sources
RO	reverse osmosis
SAR	subsurface arsenic removal
SEC	specific energy consumption (see variables)
SW	seawater
SWRO	seawater reverse osmosis
TDS	total dissolved solids
TOC	total organic carbon
TSS	total suspended solids
UF	Ultrafiltration
UNICAL	University of Calabria
VGU	Vietnamese-German University
VND	Vietnamese Dong (currency)
WAVE	water application value engine (software)
WHO	World Health Organisation
WR	water recovery (see variables)
ZLD	zero-liquid-discharge

SYMBOLS AND VARIABLES

Latin

I	applied current	A	
J_w	flux	L/(h m²)	flow per unit membrane area
t	phase duration	s	
Q_E	infiltration ratio	(m³/m³)	V_I/V_E
U	voltage	Volts	
$\dot{V}$	flow rate	L/min	
V_E	SAR extraction volume	m³	
V_I	SAR infiltration volume	m³	

Greek

η	efficiency	%
Λ	charge efficiency	%
π	osmotic pressure	kPa

Abbreviations

RE	salt removal efficiency/ rejection	%	
SEC	specific energy consumption	kWh/m³	kWh per volume diluate
SEC_{rem}	SEC for removal	Wh/g	Wh per salt removed
WR	water recovery rate	%	

1 INTRODUCTION

1.1 Motivation

One of the greatest engineering challenges of today is providing safe and reliable drinking water everywhere, most importantly in remote areas, where innovative and sustainable approaches for water treatment are needed the most. This requires not only high-end solutions with sustainable approaches but also innovative engineering that allows making state-of-the-art technologies energy efficient and accessible everywhere.

The availability and quality of freshwater resources like groundwater and rivers in many coastal regions are limited, and are being affected by progressive salinization and threatened by climate change. In order to guarantee the supply of drinking water here, the use of alternative water resources such as saline and brackish water can provide a viable solution in reducing the gap between water supply and demand.

1.2 Scope and goals

The main objective of this study is to evaluate current processes for brackish water desalination, and to develop and test novel combination processes for high energy efficient desalination for drinking water production. This study includes the development of two integrated, energy-efficient concepts for the desalination of low- and high saline brackish water in coastal regions on the example of Vietnam.

The aim is to compare existing and novel technologies and evaluate the desalination process taking into consideration energy efficiency and desalination performance while assessing its applicability, ease-of-use and costs for its development in remote and coastal areas.

The research focuses in the combination of state-of-the-art membrane technologies like reverse osmosis (RO) and nanofiltration (NF) with a new desalination technology called membrane capacitive deionization (MCDI). MCDI is an electrosorptive process for the desalination of low saline brackish water with promising low energy consumption, tuneable desalination performance and higher water recovery rates. The conceptual approach of the thesis is illustrated in Figure 1.2-1.
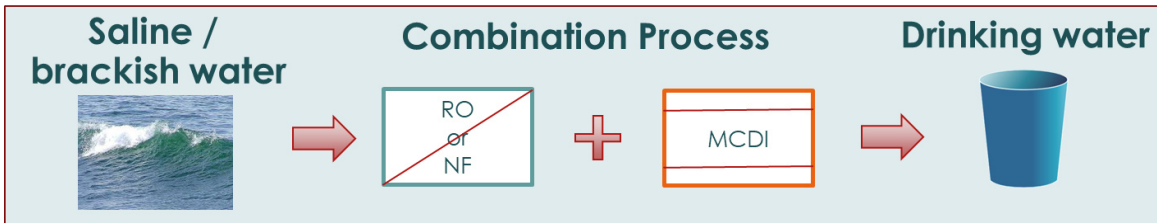
Figure 1.2-1 Conceptual approach of doctoral thesis

The specific objectives of this thesis are:

1. The **development of different concepts** for the optimal system integration between MCDI and state-of-the-art RO or NF. This is carried out with a commercial RO modelling software (Dupont/WAVE) for comparing different RO and NF membranes regarding desalination performance and their energy efficiency. For the MCDI, the use of extensive laboratory experiments is used for the concept development.

2. The **experimental investigation** of the concept at pilot-scale as a holistic, energy efficient system regarding energy consumption, salt rejection and water recovery. The testing is carried out through lab-scale experiments and the testing at pilot-scale. The pilot concepts for this work are tested on-site in Vietnam with two pilot plants installed in Tra Vinh City and Can Gio Province. The first pilot plant demonstrates the desalination of arsenic contaminated brackish groundwater with MCDI powered by renewable energies (solar and wind) in Tra Vinh. The second pilot plant showcases the desalination of high saline brackish river water with a combined system consisting of MCDI and RO in Can Gio.

3. Finally, an **evaluation of the desalination concept** including the use of renewable energy such as solar and wind for its environmental assessment. The evaluation is carried out taking into consideration socioeconomic, technological and environmental indicators.

1.3 Acknowledgments

This research was carried out in a joint collaboration between the University of Calabria (UNICAL), the Institute of Membrane Technology (CNR-ITM) and the Karlsruhe University of Applied Sciences (HKA) in Germany.

2 THEORETICAL BACKGROUND

2.1 Water stress

Water scarcity is steadily increasing as a response to the growing imbalance of rising water demand and diminishing availability of fresh water resources (World Bank Group, 2019). Reports from the United Nations on water stress estimate that the lack of fresh water resources to meet the global water demand leaves over 660 million people without access to an improved water source and 2.4 billion without access to improved sanitation (UN WATER, 2017; UNDP, 2016). The vulnerability of fresh water resources is expected to increase due to exponentially growing populations, expanding industrialization, agricultural activities, water contamination, poor water management and also climate change, which will make the gap for meeting the global water demand even bigger (Giang et al., 2014; IPCC, 2014; Qasim et al., 2019; UNDP, 2006; UNESCO, 2019).

In this first chapter, water stress will be discussed by addressing two issues affecting the vulnerability of fresh water resources: salinization and pollution, specially focusing on the seawater intrusion in estuaries and coastal aquifers, and the contamination of groundwater through naturally occurring arsenic.

2.1.1 Salinization of fresh water sources

Approx. one-quarter of the global population inhabit in coastal regions. However, drinking water supply here faces significant challenges as water sources are being threatened by climate change, raising seawater levels and increased salinization (Green et al., 2011; IPCC, 2014). It is

estimated that around 600 million people worldwide currently inhabit low-elevation coastal zones that are affected by progressive salinization (Dasgupta et al., 2014a; Stein et al., 2021; Wheeler, 2011). By 2050, the sea level rise caused by climate change is expected to worsen approaching one billion people affected increasing the stress on current water supply systems (Acharyya, 2014; Brecht et al., 2012; Dasgupta et al., 2014b, 2014a; IPCC, 2014; Wassmann et al., 2004).

In order to examine possibilities for the safe water supply and to develop sustainable approaches in coastal areas it is important to understand how groundwater and surface water salinization works. This section gives an overview of salt-intrusion and salinization mechanisms.

Aquifer salinization

The geochemical processes governing groundwater salinization and pollution in arid and coastal areas are very complex. They develop according to the natural processes given by the hydrological, climatic and lithological characteristics of each region (Galliari et al., 2021; Rajmohan, 2020) so that groundwater composition is a result of different natural processes including water-rock interactions and the various geological formations. However, it can be also affected by anthropogenic influences such as industrialization, farming and agriculture (Ayers et al., 2016; Colombani et al., 2016; Dasgupta et al., 2014b; Parvaiz et al., 2021; Rajmohan et al., 2021).

In general, the **movement of saline water into freshwater** is called saltwater intrusion. The natural reason for this is the higher hydraulic head of saline water because of its higher mineral content and higher density that exerts a greater liquid pressure in comparison to fresh water.

Salt water intrusion in coastal areas

In many coastal areas where the sea and the groundwater are connected, a natural hydraulic equilibrium prevails at the sloping interface between fresh and saline water within unconfined aquifers beneath the coastal plain. The difference in salinity causes salt water with higher density to flow to the fresh water with lower density (Figure 2.1-1). Salt water intrusion naturally decreases inland when higher elevated freshwater limits the spread of intruding seawater. Certain human activities, however, like excessive pumping and groundwater extraction reduce the hydraulic head of inland groundwater as table drops which leads to increased seawater intrusion (Greene et al., 2016).

In addition, saline water intrusion is intensified by the rising sea level and extreme weather conditions triggered by global warming and climate change (Colombani et al., 2016; Hssaisoune et al., 2020; Prusty and Farooq, 2020; Vu et al., 2018).
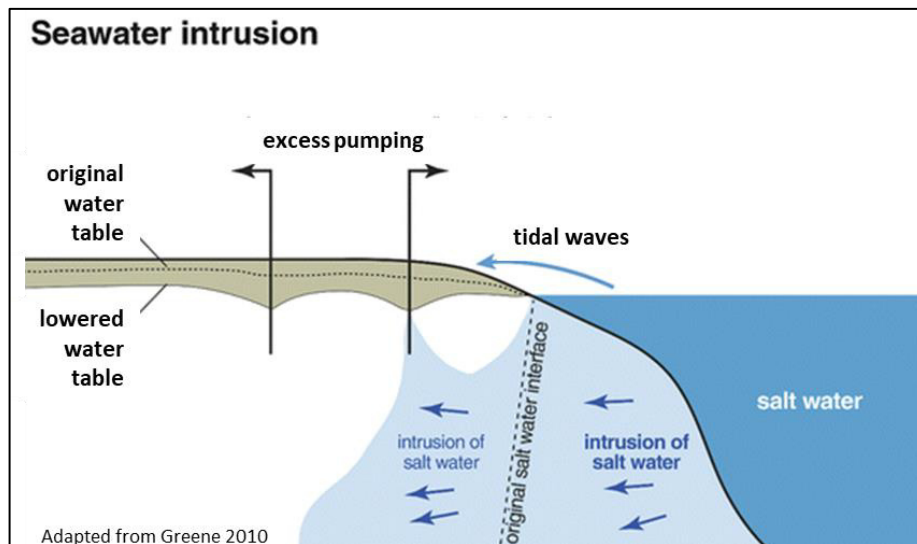
Figure 2.1-1 Seawater intrusion on coastal aquifers

In general, seawater intrusion seems to be the dominant factor affecting coastal aquifers and is becoming a global issue that threatens groundwater utilization and management mostly in arid and semi-arid environments (Prusty and Farooq, 2020; Thu et al., 2020).

<u>Aquifer salinization in Vietnam</u>

In the Mekong Delta, the salinity of the groundwater varies between 1 and > 10 g/L depending on location and distance to the sea (Hien et al., 2009; Ngo-Duc, 2014; Vu et al., 2018; Wassmann et al., 2004). Estimates say that about 60% of the total potential reserves for groundwater in Ho Chi Minh City (HCMC) (2.25 mil. m^3/day) is affected by salinization and are at risk due to climate change (Ky, 2018). Some studies have focused on the effects of sea level rise and the **progressive salinization** in the surrounding of HCMC (Ky, 2018; Ngo et al., 2015; Thanh-Nho et al., 2018) indicating that the decline in groundwater level (39% of total aquifer area) is caused by the long-term abstraction above its recharge capability. These studies suggest that the progressive degradation of groundwater quality is shifting the saline boundary inwards, which already by 2009 had reached values of up to 3 km inland (Ngo et al., 2015).

Effects of salinization have also been studied in the Province of Tra Vinh, at the Mekong-Delta, where groundwater salinization has a great impact on agriculture. A study investigated the **seasonal differences in salinity levels** at four locations of the region. They revealed that maximum concentrations of up to 9 g/L were reached between March and April (end of dry season), which was around four times higher than the concentrations observed during the wet season (Binh, 2015). They indicated a strong correlation for local rainfall and increased freshwater discharge with seasonal fluctuations in salinity in the river branches of the delta (Binh, 2015; Jones et al., 2019; Vu et al., 2018).

Surface water salinization in estuaries

River deltas, estuaries, coastal wetlands, marine mixing areas and tidal channels are distinct ecosystems that connect land and water, for example, where river environments transition to maritime settings. They represent an important source for fresh water with varying salinization. Their salinity is regulated by **groundwater and surface water interactions** and is subject to both seasonal variations during dry and wet periods, and daily tidal variations (Brecht et al., 2012; Colombani et al., 2016; Dasgupta et al., 2014b). Salinization may be also influenced by human activity (Smith et al., 2007).

Estuaries are subject not only to **marine influences** such as tides, waves and the influx of saline ocean water but also to **riverine influences** such as flows of freshwater and sediments. With increasing river output, the marine input and its tidal effects decrease. Therefore the mixing of the interfaces is always varying and the salinity of the river in estuaries is reigned by the prevailing water circulation (McLusky and Elliott, 2004; Mikhailov and Isupova, 2008).

Table 2.1-1 shows a classification of estuaries depending on the interface mixing and water circulation (Kennish, 2018; Pritchard, 1967). In summary, the underlying hydrological characteristics that determine the progressing water salinization in estuaries can be influenced by changes in atmospheric precipitation (drought), river runoff, evaporation and water losses, and tides (Rajmohan et al., 2021).

Table 2.1-1 Estuary classification based on water mixing

Classification	Flow input	Characteristics
Salt wedge	river > marine	river output greatly exceeds marine input and tidal effects have minor importance
Partially mixed	less river more tidal	turbulence causes mixing, salinity varies more longitudinally
Well-mixed	tidal > river	no freshwater-seawater boundary due to intense mixing; salinity vertically homogenous
Inverse	evaporation > river inflow	dry climates, zones with maximum salinity formed
Intermittent	variable	estuary type varies dramatically depending on freshwater input

River water salinization in Can Gio

The Can Gio mangrove estuary is located in the south of Vietnam and connects HCMC, the biggest city in the country, and the Eastern Sea. It covers an area of more than 35,000 ha about 35 km downstream from HCMC. Due to its coastal location, a natural mixing of river and salt water from the Eastern Sea occurs. The salinization effect is greater on the seaside and reduces inwards so that a **concentration gradient** from ca. 2-28 g/L can be observed across the length

of the catchment area (see Figure 2.1-2). The inland salinization is estimated to move 55-110 km inland in coming years, which reached historical peaks in 2015/16 (Tuan and Tran, 2018). Seasonal variations in rainfall, discharge, evaporation and other climatic conditions has also a significant impact on the quality and salinity of surface water (Thanh-Nho et al., 2018; Thu et al., 2020; Tuan and Tran, 2018).
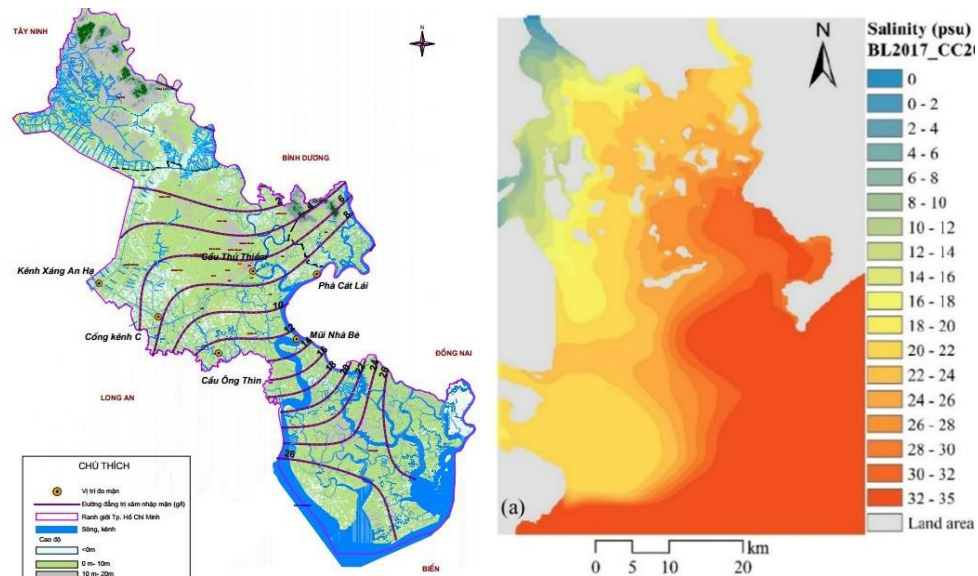
Figure 2.1-2 Saline intrusion warning areas in HCMC and Can Gio, Vietnam (2-28 g/L) (MARD, 2020; Thu et al., 2020)

2.1.2 Arsenic contamination in anoxic aquifers

In addition to saline intrusion many groundwater sources in coastal areas like in South and Southeast Asia have **high concentrations of geogenic arsenic** (As). This includes the groundwater of tidal delta plains such as the Mekong river and Red river deltas in Vietnam (Agusa et al., 2014; Berg et al., 2007; Buschmann et al., 2008; Le Luu, 2019; Stopelli et al., 2020; Winkel et al., 2011), the Ganges-Brahmaputra-Meghna and Bengal delta plains in Bangladesh (Ayers et al., 2016; Chakraborti et al., 2015; Huq et al., 2020; Mukherjee and Bhattacharya, 2001; Natasha et al., 2020; Palit et al., 2019; Sarkar and Paul, 2016), the Irrawaddy delta in Myanmar (Smedley et al., 2002; Wang et al., 2018) and the Pearl River delta in China (Hou et al., 2018).

Arsenic contamination is a natural phenomenon affecting more than 290 million people worldwide and has evolved into a global public health matter with more than 100 countries affected by As levels higher than the **guideline limit value recommended by the WHO of 10 µg/L** (Bundschuh et al., 2012; Chakrabarti et al., 2019; Sarkar and Paul, 2016; Singh et al., 2015; WHO, 2017, 2012, 2011)

Arsenic is considered to be one of the most serious, natural, inorganic contaminants found in groundwater and it is globally recognized as a significant environmental cause of cancer mortality (Chakrabarti et al., 2019; Flora, 2015; WHO, 2017, 2011). In reducing environments, such as in South and Southeast Asia, As exists primarily as the oxyanion of **trivalent arsenite As(III),** which is neutral in charge (H_3AsO_3) in the natural pH range of groundwater (pH 6.5-8). In oxidizing environments, As exists as **pentavalent arsenate As(V)**, which is negatively charged ($H_2AsO_4^-/HAsO_4^{2-}$) (Luong et al., 2018; Smedley et al., 2002). The mobilisation and release of geogenic As into the groundwater in reducing aquifers, such as in most of Southeast Asia, is a result of the reductive dissolution of iron (Fe2+) and manganese (Mn2+) oxi(hydr)oxides from As-bearing sediments (Stopelli et al., 2020; Zhang et al., 2017). Therefore, As is often co-associated with high concentrations of Mn^{2+} and dissolved Fe^{2+} (Cañas Kurz et al., 2020; Sankar et al., 2014; Stein et al., 2021) which might require additional treatment and attention when treating As. In addition, the presence of ammonium nitrogen (NH_4^+) in groundwater is linked to reduced groundwater conditions that in general promote As release (Jia et al., 2018; Kurosawa et al., 2013; Norrman et al., 2015).

Arsenic remediation technologies

A variety of treatment technologies have emerged over the last two decades for the removal of As from water and wastewater (Luong et al., 2018; Nicomel et al., 2015; Sarkar and Paul, 2016; Visoottiviseth and Ahmed, 2008). These include **oxidation and precipitation**, **adsorption**, ion-exchange and membrane processes, which have been extensively studied for As removal from groundwater (Figoli et al., 2020, 2016; Kurz et al., 2021; Shih, 2005). New treatments comprise an array of relatively novel technologies such as As immobilization by sorption like capacitive deionisation, and bioremediation techniques such as phytostabilization, As biotransformation, and hyperaccumulation in plants (Brunsting and McBean, 2014; Bundschuh et al., 2014; Cañas Kurz et al., 2020; Klingel, 2016; Luong et al., 2018; Maier et al., 2017). An overview of remediation techniques is given in Table 2.1-2.

Other mitigation alternatives are **in situ technologies** (e.g. permeable reactive barriers, electro-kinetics, nanoparticles such as zero-valent iron, etc.) which are environmentally friendly and mostly less expensive compared with conventional As remediation technologies. In general, *in situ* processes have the salient advantage of having little to **no toxic waste** production, which is of major importance when assessing the sustainability of As remediation. In *ex situ* processes, As-laden concentrate streams, toxic sludge and/or solid waste are produced, which require often costly treatment and proper disposal. (Clancy et al., 2013; Litter et al., 2014; Luong et al., 2018). However, there is an overall need for long-term experience for *in situ* techniques (Litter et al., 2014; Luong et al., 2018).

Table 2.1-2 Comparison between *ex situ* and *in situ* As remediation techniques

	Ex situ [a]	*In situ* [b]
Remediation techniques	Oxidation + flocculation (Precipitation + filtration) Adsorption (active carbon, activated alumina, ferric hydroxides ...) Ion exchange (synthetic resins, zeolites…) Membrane filtration (NF, RO)	Subsurface arsenic adsorption Bioremediation (Biosorption/-transformation, phytoextraction/-stabilization, hyperaccumulation,…) Permeable Reactive Barrier (ZVI, iron slag, Fe/Al-oxides, multifunctional barriers)
Advantages	High efficiency State of the art Ease-of-use	No liquid waste production Low cost and low maintenance
Disadvantages	Costs Toxic sludge disposal problem Replacement and regeneration of media	Less removal efficiency High dependency on hydrogeological conditions Some difficult to install Arsenic remobilization

[a]Berg et al., 2007; Litter et al., 2010; Mohan and Pittman, 2007; Mondal et al., 2006; POKHREL et al., 2009; Sarkar and Paul, 2017
[b]Bundschuh et al., 2014; Litter et al., 2014; Luong et al., 2018; van Halem et al., 2010; Xie et al., 2015

For this study, an iron-based *in situ* technology was considered for the removal of As called **subsurface As removal (SAR)**. SAR was used upfront the desalination step in the modular treatment of saline brackish groundwater.

Subsurface arsenic removal (SAR)

Subsurface As removal (SAR) is a technique based on a process called subsurface iron removal (SIR), which is a well-established technology for the *in situ* removal of Fe^{2+} and Mn^{2+} in Europe and the United States (Ahmad, 2012; Grischek et al., 2015; Hallberg and Martinell, 1976; Henning and Rott, 2003; Karakish, 2005; Rott and Friedle, 2000; Rott and Kauffmann, 2008). The use of SAR, however, is a novel process that has been investigated in pilot-scale only in a few studies in Bangladesh and in Vietnam, including this work (Cañas Kurz et al., 2020; Grischek et al., 2015; Hellriegel et al., 2020; van Halem, 2011).

The principle of SAR is based on the **adsorption and co-precipitation** of As onto Fe(III)-(hydr)oxides, also referred to as amorphous hydrous ferric oxides (HFO). HFOs are known as the most important sorption materials for As due to their high specific surface area and ability to adsorb both arsenate (As(V)) and arsenite (As(III)) through different mechanisms such as surface ionization, surface complexation and ligand exchange (Farrell and Chaudhary, 2013; Luong et al., 2018; Van Der Laan, 2009).

SAR is carried out **by periodically infiltrating aerated groundwater** into the anoxic aquifer in a process divided in abstraction and infiltration cycles (see Figure 2.1-3) (Cañas Kurz et al.,

2020; Hellriegel et al., 2020; Luong et al., 2018; Rahman et al., 2014). First, groundwater is abstracted and aerated with oxygen (e.g. atmospheric oxygen). Then, the oxygen-enriched groundwater is infiltrated back into the aquifer (infiltration, Figure 2.1-3 left). **Oxidation zones** are formed around the well where dissolved Fe^{2+} can oxidize to Fe^{3+}, precipitating as HFO. During the adsorption or delivery phase (Figure 2.1-3, right) contaminated groundwater flows through the formed adsorption zones where dissolved substances can be adsorbed and then co-precipitated onto the formed HFOs in the edges of the oxidation zone – now **adsorption zone** (Gonzalez et al., 2019; Luong et al., 2018; Rahman et al., 2015).

When more groundwater is extracted in the next abstraction cycle, dissolved Fe(II) is adsorbed onto the Fe(III) coated soil grains forming more HFOs and a clear water zone with lower As concentrations forms around the well (Jeon et al., 2003; Luong et al., 2019, 2018). Finally, water around the well with low Fe^{2+} and As can be extracted from the aquifer until the oxidation zone is depleted and the process is restarted with a new infiltration cycle.
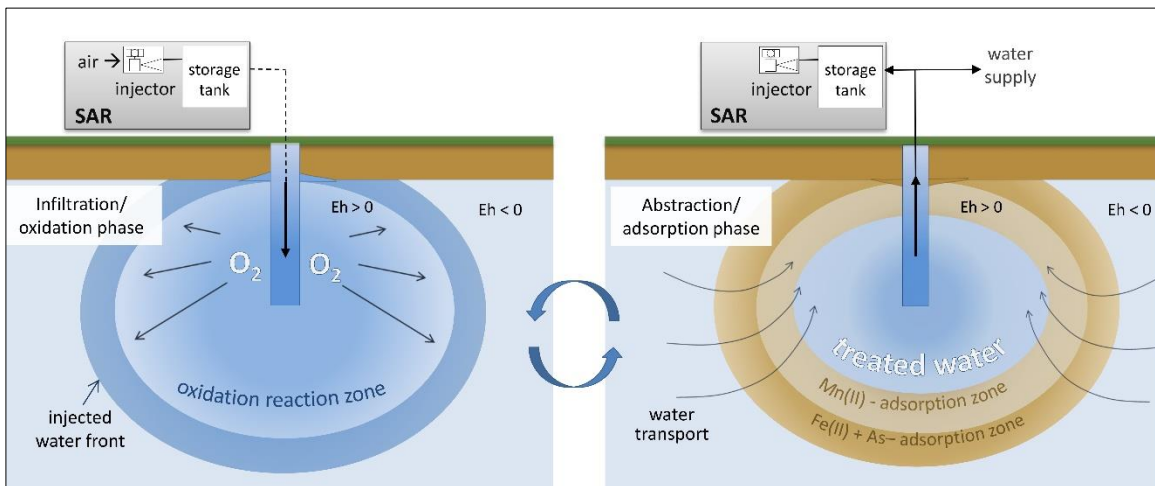
Figure 2.1-3 Schematic principle of subsurface arsenic removal SAR divided in infiltration (left) and abstraction (right) cycles

The most salient advantage of the SAR process over most other technologies is its negligible waste production, simple operation, and low maintenance and operating costs since it does not require any additives or chemicals (Grischek et al., 2015; van Halem, 2011). In the SAR process, As is not eliminated, but transferred from its soluble phase to a less readily, immobile, solid phase as it is bound into the aquifer layer. Both As(V) and As(III) are bound by non-ionic mechanisms through Lewis acid-base interactions, whereas ionic As(V) can be adsorbed by both Lewis acid-base and electrostatic interactions (Huling et al., 2017).

The main reaction for the adsorption of As(V) onto the oxidized Fe(III) can be summarized as follows (Stollenwerk et al., 2007):

$$Fe(OH)_3 + H_3AsO_4 \rightarrow FeAsO_4 \cdot 2H_2O + H_2O$$
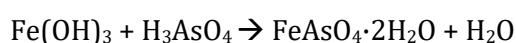
However, the key factors controlling the chemical reactions behind the **As-Fe adsorption and co-precipitation, and its remobilization** into the aquifer are still not fully understood. Still, the long-term experience with SIR show that the no significant accumulation or blockage of the aquifer occurs even after several decades of operating a well with SIR (Grischek et al., 2016; Luong et al., 2019; FERMANOX, 2017). If the aquifer is considered as an infinite reactor with adsorption area, As-waste remains in the underground and no waste stream is produced for the user. This makes the application of SAR especially suitable for **long-term and sustainable treatment option for rural areas** (Cañas Kurz et al., 2020; Luong et al., 2018; Shan et al., 2013; van Halem et al., 2010).

2.2 Desalination

Water scarcity has increased the awareness of the importance of non-conventional water resources such as the use of treated waste water and desalinated water (Pereira et al., 2014; UN WATER, 2017). As a result, desalination plants and the use of **saline water sources for drinking water** production are expected to play a more significant role in narrowing the gap between water supply and water demand in the near future (Ghaffour et al., 2013; Qasim et al., 2019; Voutchkov, 2018).

In this chapter, an overview on state of the art and novel desalination processes is given. The focus lies on current techniques for system performance enhancement and lowering energy consumption and costs. Possible system configurations as best-case examples and pilot-cases were reviewed for evaluating application challenges of desalination systems.

2.2.1 State of the art desalination

Desalination can be defined as the **process for removing salt from water** to produce fresh water, meaning water with a total dissolved solids (TDS) value below 1 g/L (WHO, 2017). Desalination processes can be mainly divided into two categories: thermal and membrane technologies (Greenlee et al., 2009). However, depending on the separation mechanism and type of driving force, there are different categories in which desalination technologies can be classified. A simplified overview is given in Table 2.2-1.

Table 2.2-1 Overview of desalination processes

Thermal	Membrane	Electrochemical/ Electrosorptive	Others
Multi-stage flash distillation Multi-effect distillation Vapour compression	Reverse osmosis Forward osmosis Membrane distillation	Electrodialysis Capacitive deionisation	Ion exchange Solar humidification Freezing distillation

The separation of salts from fresh water in **thermal processes** follows the natural hydrological cycle of water of evaporation-distillation and is driven by thermal energy. Thermal processes are often used in large-scale systems for desalinating high saline water sources.

Membrane separation uses a pressure gradient to drive saline water through a semipermeable membrane which prevent salts from passing, yielding fresh water on the permeate side and a brine stream or discharge on the concentrate side. There are different membrane materials used that showcase different permeability depending on the density of

the membrane. Therefore, membrane processes can be divided in micro-, ultra-, nanofiltration and reverse osmosis, from which only the latter two are able to retain dissolved salts. Other membrane desalination methods use a temperature or concentration gradient such as thermally driven membrane distillation, or osmosis effect such as forward osmosis.

Electrodialysis uses ion-exchange membranes to separate the ions but is driven by an electrical potential so it can be regarded as an **electrochemical process** (Varcoe et al., 2014). Another electrochemical or electrosorptive process is a novel separation technique called capacitive deionisation (CDI) which is used in this study for the desalination concepts. The basic principles of this technology is explained in section 2.3 Membrane capacitive deionisation (MCDI).

2.2.2 Reverse Osmosis RO

Principle of RO

Over the last 50 years, RO membrane technology has become the most common desalination technology as materials have improved and costs have exponentially decreased. In RO, the desalination is driven by a hydraulic pressure which is used for firstly offset the osmotic pressure from the feed solution, and secondly to create mass flow transport across the semi-permeable membrane. The permeate flows requires, therefore, applying operating pressures well over the osmotic pressure. The osmotic pressure of a solution π can be defined as:

$$\pi = cRTf \tag{2.1}$$

where c is the molar feed concentration of the dissolved species (mol/L), R is the universal gas constant 8.314 L·bar/(K·mol), T the temperature (K) and f the van't Hoff's factor.

Typically, RO water treatment results in a rejection of dissolved salts that is 95-99 percent or greater, depending on membrane type, feed composition, temperature, and system design. Usually, desalination deals with feed water salinities between 1 and 60 g/L, although two distinct branches of RO desalination have emerged: **seawater reverse osmosis** (SWRO) for TDS concentrations ranging between 20 g/L and 43 g/L, and **brackish water reverse osmosis** (BWRO) for salinities below 20 g/L (Greenlee et al., 2009). Both SWRO and BWRO have similarities and differences but most significant dissimilarities in their development and implementation include fouling behaviour, waste brine disposal options and plant location (Ghaffour et al., 2013; Greenlee et al., 2009).

Usually, SWRO membranes have higher rejection for NaCl but lower flux compared to BWRO membranes being the membrane surface of SWRO more hydrophilic (Zhou and Gao, 2010). Furthermore, inland BWRO plants have, for example, disadvantages for brine disposal while

brine discharge into the ocean can be an easy solution in SWRO. However, in each case, the environmental impacts of a brine discharge should always be considered (Voutchkov, 2018). Recent studies estimate that the global production of drinking water from saline water sources stands at around 95 million m^3/day. This equals to around 15% of the total global water demand, which is supplied by more than 15.900 brackish and seawater desalination plants worldwide (Jones et al., 2019).

Since the energy required in desalination or salt separation is proportional to the salinity of the source water, the energy demand of SWRO and BWRO is vastly different. From this perspective, BWRO is preferable vs. SWRO for the production of potable water. This depends entirely if the water source with less salinity is readily available (Voutchkov, 2018).

Based on Eq. (**2.1**), the osmotic pressure for the desalination of SW (30 < TDS (NaCl) < 43 g/L) and BWRO (1 < TDS (NaCl) < 20 g/L) at 25°C can be calculated to:

$$\boldsymbol{\pi_{SW} = 23.63 - 33.86\ bar} \tag{2.2}$$

$$\pi_{BW} = 0.7875 - 15.75\ bar \tag{2.3}$$

Accordingly, for high saline BW (20 < TDS < 30 g/L) the osmotic pressure ranges between 15.8-23.6 bar. The operational pressure of the system will be affected by operational conditions and desired water recovery rate, so pressures almost double of the osmotic pressure might be applied for the desalination process. Based on long-term testing of a full-scale state-of-the-art desalination systems, the lowest energy use achieved by a commercially available desalination unit (recovery of 42% and average flux of 10.2 L/(m^2·r)) was 1.58 kWh/m^3 (years 2006-2007) (Voutchkov, 2018).

RO design and theoretical calculations

Theoretical calculations for the design of desalination plants are used upfront of manufacturing using different commercially available software. The calculations are used for the determination of the operational parameters, the desalination capacity, suitable membrane selection, selecting pre- or post-treatment, and optimizing the process. Many membrane suppliers provide their software for free.

Mathematical models can be a powerful tool in the operation of RO plants which is often challenged by a varying feed water quality. Novel models aim at unifying full-scale with good modelling practices, in order to have a more practical meaning (Gaublomme et al., 2020). In RO as well as other nonporous membrane methods, the separation process can be described by the solution-diffusion model, which describes the permeability of a fluid through the dense membrane is directly proportional to the product of its solubility (thermodynamics) and

diffusivity (kinetics). Solubility is a measure for the amount of fluid sorbed by the membrane under equilibrium conditions while diffusivity indicates how fast the fluid is transported through the membrane (Mulder, 1996a).

In a calculation software, non-ideal systems must be considered which involve concentration-dependant systems where the solubility and the diffusivity are functions of time and place.

Permeability can be described as flux by Fick's first Law. However, for high flux values the osmotic pressure at the membrane surface is taken into account in the description of the flux, given by Eq. (**2.4**.

$$ J = \frac{\Delta P - \Delta \pi}{\eta \, R_m} \qquad (2.4) $$

where J is the flux in (m/s), ΔP is the hydraulic pressure difference and π is the osmotic pressure in bar, R_m is the hydrodynamic resistance of the membrane in $cm^2 \cdot s \cdot bar/cm^3$ which is material dependant, and η is the viscosity in $Pa \cdot s$ (Mulder, 1996b).The flux will increase with increasing applied pressure but reaching critical flux in RO membranes will be different from e.g. UF. Other important factor considered in calculations is the composition of water (ionic composition) to determine the influence of scaling.

Large-scale and small-scale applications

One advantage of membrane-based systems is the possibility to scale up according to the demand or capacity needed. However, system application of small-scale desalination plants and large-scale facilities require completely different engineering. The total costs in small-sized RO desalination plants in comparison to larger-scale SWRO plants need to be examined thoroughly in order to calculate real specific costs for treated water (cost per cubic metre). One main factor is the use of energy recovery systems in smaller systems where, in contrast to high saline, large-scale plants, the its applicability might be challenging (Avlonitis, 2002; Gude et al., 2010).

A direct comparison of SWRO and BWRO systems is necessary to highlight similarities and differences in process development (Greenlee et al., 2009). New technologies or new system approaches for the application in decentralized, remote areas must consider several different factors such as ease-of-use, applicability, prices and operational costs.

Advantages and disadvantages of membrane technologies

Membrane process showcase overall advantages over other desalination processes since they achieve **higher water recovery** rates, which has significant implications for the overall **desalination costs.** Membrane technologies are also operated at lower temperatures (e.g. than thermal technologies) so scaling is less of a problem, the lifespan of membranes is longer and

maintenance costs are considerably lower since less anti-scaling chemicals are required (World Bank Group, 2019).

However, there are primarily two issues that remain a great challenge and that affect membrane separation efficiency: i) concentration polarisation caused by the increased concentration at the membrane surface and ii) membrane fouling which is strongly related to factors such as feed water quality, pre- treatment options, membrane properties and operating conditions (Goh et al., 2016).

2.2.3 Desalination challenges

Energy demand and desalination costs

There are many elements influencing the overall cost for desalination but principal drivers can be summarized in technology choice and operation, plant size, and location, as well as project delivery and environmental regulatory regimes. In general, costs for desalination decline significantly at lower salinity because less energy is required and costs typically decline as plant capacity increases (Ghaffour et al., 2013; Qasim et al., 2019; Saadat et al., 2018; Voutchkov, 2018).

Hybrid plants and newer plants generally produce water at much lower cost and are generally most cost-effective. In comparison of the biggest plants today (e.g. **Fehler! Verweisquelle konnte nicht gefunden werden.**), the Ras Al Khair plant (capacity over 1 mio. m^3/day) have production costs ranging US\$0.85-US\$0.95 while the plant in Sorek, Israel (624.000 m^3/d) achieve some of the lower costs of US\$0.64. The wide range of costs for similar size plants is also caused by special delivery conditions and subsidies but the total cost of water production ranges between US\$0.49 and US\$2.86 per cubic meter (World Bank Group, 2019).

A typical breakdown of the total costs for water production of desalination systems can be divided in **variable costs** (e.g. energy costs, maintenance incl. materials, replacement membranes, spares and chemicals, and waste stream disposal), and **fixed costs** (e.g. labour costs, amortization (capital recovery), and other operating and maintenance costs) (Qasim et al., 2019; Voutchkov, 2018; World Bank Group, 2019).

The key factors affecting the cost of desalination are:

- o Desalination technology
- o Feed water quality
- o Target product water quality
- o Environmental impact
- o Energy demand
- o Plant capacity
- o Location

While the specific investment costs (per m³) decrease the higher the plant capacity is, the capital recovery or amortization clearly takes the biggest share in the total unit water cost with 41%, followed by power demand and membrane replacement with 19% and 16%, respectively (Ghaffour et al., 2013; Voutchkov, 2018). The price breakdown of product water of a typical RO plant is shown in Figure 2.2-1 (left). With regards to the energy costs, besides the energy usage of the RO system (pumps, etc.) with 71%, the energy share of a typical desalination plant can be divided in intake, pre-treatment and delivery of product water (Figure 2.2-1 right).

Technological advances, especially in membrane processes have led to a significant reduction of the energy demand and desalination costs. However, despite the twofold reduction of the energy required for its desalination over the last two decades, seawater desalination remains the most energy intensive option for production of drinking water today (Voutchkov, 2018). For RO processes, the energy usage for the desalination of seawater (TDS = 35 g/L) can be lowered to **SEC as low as 3-4 kWh/m³** using energy recovery devices while BW (TDS = 1-10 g/L) can vary between 2-7 kWh/m³ depending on the process settings and design (i.e. water recovery, operating pressures, etc.), whether energy recovery systems are applied, and on the overall efficiency and capacity of the plant (Alkaisi et al., 2017; Shemer and Semiat, 2017).

Membrane-based desalination plants today are still using 5 to 25 times more energy than the theoretical minimum work needed (DESWARE, 2018; Gude et al., 2010). The main reason is that the efficiency of older desalination plants was often less than 10 percent. Modern plants nowadays can achieve up to 50 percent efficiency, but still have room left for improvement, with the major efficiency losses still occurring in the pump, motor and the separation units (Cerci et al., 2003; Manju and Sagar, 2017). Therefore, newer SWRO plants generally produce water at much lower costs. However, it is necessary to make desalination processes as energy-efficient as possible through improvements in technology and economies of scale.
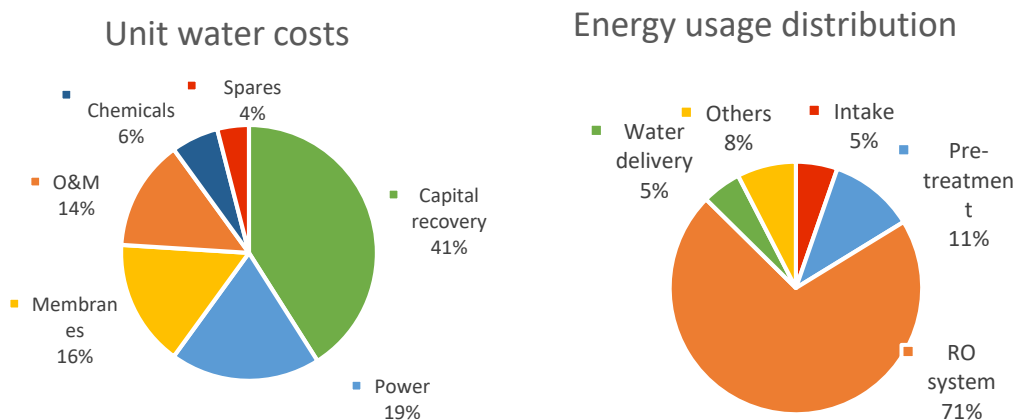
Figure 2.2-1 Unit water cost breakdown (left) and energy usage distribution (right) of typical SWRO desalination plant (values from Voutchkov, 2018)

In terms of **average cost**, SWRO records the lowest costs, but there are many site-specific factors that make comparison difficult. Overall, RO desalination is the most cost-competitive technology for less saline environments, while thermal technologies is more competitive for higher salinity environments. (Voutchkov, 2018; World Bank Group, 2019). An overview on energy requirements for desalination technologies is summarized in Table 2.2-2.

Some drawbacks of thermal technologies like MSF and MED are the costly **material requirements** such as highly anticorrosive materials (e.g. for heat exchangers), whereas RO membranes are made of cellulose acetate or other composite polymers, which are relatively less expensive. Energy costs are also significantly higher for thermal technologies (use of both thermal and electric power), so that plants must generally be located close to thermal energy sources (World Bank Group, 2019; Youssef et al., 2014).

Table 2.2-2 Energy demand of main desalination processes

Treatment technology	MSF	MED	RO	ED
Specific energy consumption kWh$_{el}$/m³	4-6	1.5-2.5	3-7	2.6-5.5
Specific energy consumption kWh$_{th}$/m³	9.5-19.5	5-8.5	-	-
Total SEC	13.5-25.5	6.5-11	3-7	2.6-5.5

Mod. from (Manju and Sagar, 2017)
MSF: Multi-stage flash distillation; MED: Multi-effect distillation; MVC: Mechanical vapour compression; RO: Reverse osmosis; ED: electrodialysis
*Electrical equivalent for thermal energy (kJ/kg)

Finally, the **system configuration** of a plant has also a huge impact on the process and therefore on the final costs of desalination. Production costs of hybrid projects have often proved lower than the costs of single-technology production but the selection of the best technology configuration (or combination) is decisive for a better outcome. Possible system combinations and their application is discussed in Section 2.4 System integration.

Brine disposal

Maybe the biggest environmental issue associated with desalination is the production and discharge of a hypersaline concentrate streams – or brine – into the environment. In order to minimize the negative ecological impacts, brine streams from desalination processes require adequate disposal and/or treatment. With more than 95 mil. m³ of desalinated water a day, estimates suggest that the total brine production is close to the 142 mil. m³/day. These recent estimates double previously calculated quantifications and can be explained by the typically low water recovery of SW desalination plants (< 50%) (Jones et al., 2019).

In inland areas, brine disposal is one of the major limiting factors preventing wider implementation of membrane-based desalination. Various options are firstly, waste

minimization or discharge to wastewater treatment plants but may include discharge to surface water, deep wells, land application, evaporation ponds and wastewater evaporators (Ahmed et al., 2000; Stover and Crisp, 2008).

In coastal areas, the solution is normally just to discharge the brine back to the ocean. However, this might have severe consequences to marine ecosystems since brine contains roughly twice the concentration of seawater, and is therefore denser. As a result, discharged brine naturally sinks towards the seabed severely restricting its mixing and which can result in a hypersaline layer of water that might damage seawater species.

Furthermore, the presence of cleaning agents such as hydrochloric acid, sodium hexametaphosphate, and anti-scalants as well as other hyper-concentrated chemicals such as iron, copper, zinc can severely pollute the ocean and groundwater, if the brine reaches the underlying aquifers (Ahmed et al., 2001; Jones et al., 2019).

Some ways to minimize the impact of brine discharge are:

- o Careful selection of the discharge zone
- o Improve mixing
- o Diluting the concentrate before discharge
- o Concentration or recrystallizing of brine for disposal to landfield
- o Concentrating in evaporation ponds for salt mining
- o Deep-well injection

The alternatives such as deep-well injection can provide a local and permanent disposal solution for brine concentrates (National Research Council, 2010). However, here is important to target naturally saline formations that are hydraulically disconnected from fresh water aquifer in order to minimize the environmental impacts of the brine (Yeboah and Burns, 2011).

Fouling and scaling

Despite the enormous success of membrane desalination technologies, membrane fouling mitigation is still the most critical issue to solve (Goh et al., 2018; Qasim et al., 2019). Fouling refers to the **deposition of particles** on the surface or inside a given host solid material (e.g. membrane, heat exchanger, boiler, condenser, etc.) and is an inevitable phenomenon that occurs in all given surfaces, to different extends, when in contact with water (Khayet, 2016).

Membrane fouling results in elevated operating costs due to the deterioration of permeate flux, increasing transmembrane pressure and frequent chemical cleaning which shorten the membrane's lifespan (Goh et al., 2018).

Fouling can be classified into four groups:

- o **Colloidal fouling:** deposition of colloids or particles
- o **Organic fouling:** deposition and adsorption of macromolecular organic compounds

- o **Biofouling:** adhesion and accumulation of microorganisms and development of a biofilm
- o **Inorganic fouling** (also known as scaling): precipitation or crystallization of sparingly dissolved inorganic compounds such as due to $CaCO_3$, $CaSO_4$, and $BaSO_4$ etc.

In water desalination, especially in membrane technologies, inorganic fouling is exclusively referred to as scaling (Khayet, 2016). Among the three types of fouling, biofouling is considered the most complicated one considering the fact that the foulants are living substances with complex mechanisms.

Organic and biological fouling of a membrane, can be irreversible, which inevitably results in the permanent loss of the membrane's permeate flux. But in membrane and fouling characterization, it is difficult to differentiate between colloidal, bio or organic fouling (Jiang et al., 2017; Khayet, 2016) so that antifouling mitigation strategies should consider all types fouling.

Most important fouling mitigation strategies involve the adequate selection of **pre-treatment**, membrane **surface modification**, optimized **operational conditions** and/or membrane **cleaning** by use of anti-scalant and antifoulant chemical agents. To significantly reduce the rate of membrane fouling, RO elements use crossflow filtration. In essence, crossflow filtration is the result of the high-pressure pump that forces the feed water through the RO membrane, while the separated flow of higher-concentration water moves across the surface of the membrane, carrying away the rejected salts and impurities. The rate between concentrate and permeate is controlled by a valve on the concentrate side. During a typical RO desalination, biofouling of the membranes is typically mitigated by the addition of free chlorine during the pre-treatment of feed solution (Al-Amoudi and Lovitt, 2007; Goh et al., 2018; Khayet, 2016; Landaburu-Aguirre et al., 2016; Mossad and Zou, 2013; Tian et al., 2010).

2.3 Membrane capacitive deionisation (MCDI)

Capacitive deionization (MCDI) is a technology that encompasses a group of different desalination processes based on the electrosorption and desorption of ions while cyclic charging or discharging electrodes (Biesheuvel et al., 2017a).

In this chapter, the fundamentals on membrane capacitive deionisation (MCDI) are illustrated, as the main technology for the study of the desalination concepts in this work.

2.3.1 Fundamentals on electrosorptive desalination

Principle of MCDI

In the CDI desalination process, saline water flows between two porous carbon electrodes. When a voltage is applied, dissolved salt ions are transported from the solution to the electrodes and stored in so called **electrostatic double layers** (EDLs) that form at the surface of the micropores of the electrode (*charge* phase, CP). During this phase, anions are adsorbed in the anode (positive polarity) and cations are stored in the cathode. The concentration in the bulk solution decreases and a stream of treated or desalinated water is obtained (Biesheuvel and Dykstra, 2020; Suss et al., 2015a).

When the electrodes become saturated, meaning, the EDLs are fully charged, the electrodes need to be regenerated. This is carried out by reducing or even reversing the polarity of the electrodes so that adsorbed ions desorb from the EDL into a brine or concentrated stream which is flushed out through the transport channel or spacer (*discharge* phase, DP) (Biesheuvel and Dykstra, 2020; Suss et al., 2015a).

The schematic process of the charge and discharge phases is presented in Figure 2.3-1.
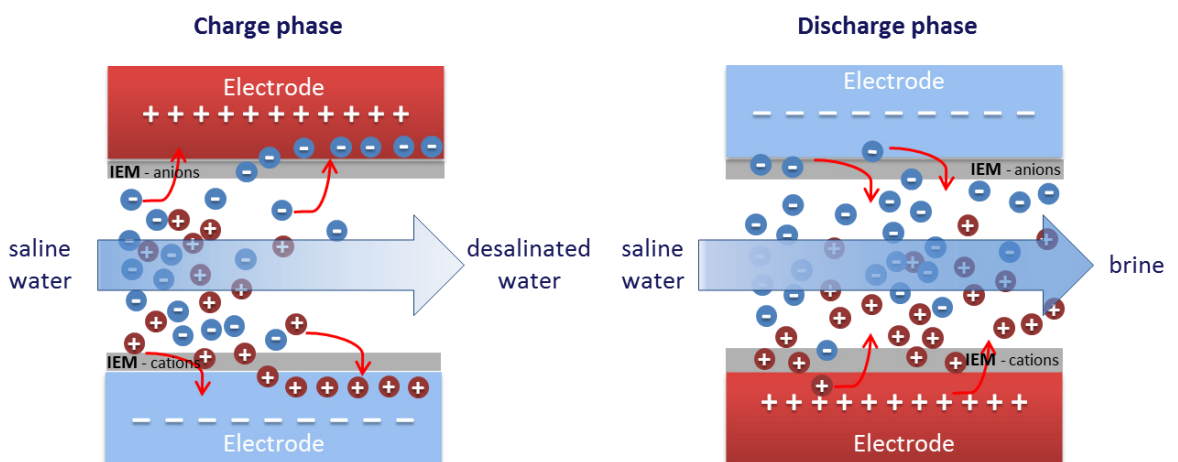
Figure 2.3-1 Schematic MCDI principle for desalination (charge) and regeneration (discharge) phases.

Membrane CDI

In order to enhance the desalination efficiency of CDI, ion exchange membranes (IEM) were introduced to avoid co-ion transport during the *discharge* phase and thereby increasing the charge efficiency and its desalination capacity (Zhao et al., 2013b). This is done by placing ion exchange membranes in front of each electrode, specifically, **cation exchange membranes** in front of the cathode and **anion exchange membranes** in front of the anode. The main benefit of membrane capacitive deionisation (MCDI) is the improvement of the charge efficiency as the membranes block ions with the same charge as the local electrode – or co-ions – from carrying parasitic current. This can also increase the salt storage in electrode macropores which increases overall desalination efficiency (Zhao et al., 2012).

The **charge efficiency Λ** is defined for a 1:1 salt solution as the ratio of salt adsorption by the electrode cell pair divided by the charge stored in the electrode. In MCDI, co-ions that are expelled from the micropores during the CP are inhibited from leaving the electrode structure and remain in the macropores within the electrodes. This allows more counter ions to be transported through the membrane (i.e. ions with the opposite charge as the local electrode), which are stored in the macropores of the electrodes. As a consequence, the concentration of salts that can be stored within the elctrodes during the CP is much higher, which increases the charge efficiency of the process (Biesheuvel et al., 2014).

The **salt adsorption capacity** is the amount of salts (in g) that can be adsorbed by the total mass of the electrodes. By using IEM in the MCDI, the cell voltage between the two electrodes can be reversed during regeneration step without co-ion adsorption, which leads to a shorter duration of the DP and thus an increase of the salt adsorption capacity of the cell in the next cycle. In addition, IEMs may be tailored to have selectivity between different ions of the same charge sign to provide an additional level of tunability for complex multi-ion solutions (Biesheuvel et al., 2017a; Suss et al., 2015b).

Constant current vs. constant voltage

Operation in MCDI can be separated in two modes: **constant voltage** (CV) or **constant current** (CC). In the past, constant electrical potential difference between the two porous electrodes (i.e. V_{cell} = 1.2 V) was preferred during the charge phase (adsorption step), followed by short-circuiting of the electrodes 0 V or reversing the voltage, during the discharge phase. However, operation at a constant cell voltage has as a disadvantage that the effluent salt concentration changes in time (Zhao et al., 2012).

Recently it has been demonstrated that charging and discharging the electrodes at CC can have several major advantages in comparison with CV operation, such as a more stable and adjustable effluent concentration quality (Zhao et al., 2013b) for similar adsorption capacities

(see Figure 2.3-2 a and d). This is attributed to the constant profile of the applied current (Figure 2.3-2 b and e) Furthermore, CC operation consumes significantly less energy than CV for equal amount of charge input and same charge phase duration for similar salt removal efficiency (Qu et al., 2016). The lower energy consumption of CC is attributed to its overall lower cell voltage (see Figure 2.3-2 c and f) (Kang et al., 2014).
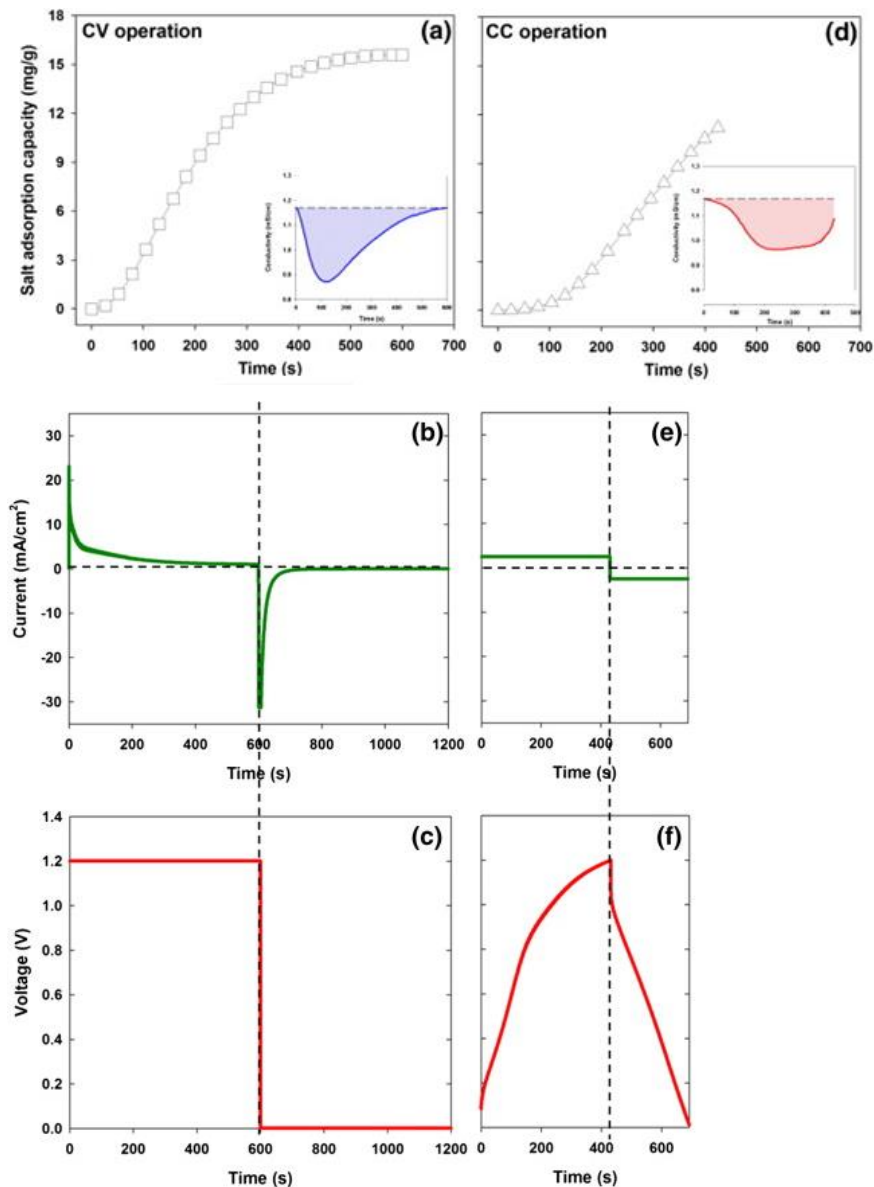
Figure 2.3-2 Comparison of constant voltage (CV) and constant current (CC) modes: adsorption capacities (a, d) with the effluent conductivity during charge phase, the current (b, e), and cell voltage (c, f) profiles. (Adapted from Kang et al., 2014)

2.3.2 State of the art

The concept of CDI emerged in the 1960s with different studies on salt removal on novel porous electrode materials and has been studied intensively since (Suss et al., 2015a). However, despite considerable research, only a few companies produce commercially available CDI modules for domestic or industrial use more than 40 years later. Companies have emerged in the CDI market around the world over the past two decades but only a few remain active in this field, including Atlantis Technologies (US), Aqua EWP (US), Enpar Technologies Inc. (Canada), Green Energy (Australia), Idropan (Italy), Purechem (South Korea), Purelau (Canada), SionTech (South Korea), Voltea (NL) (Chung, 2018; Dash and Weinstein, 2013).

The CDI technology is currently applied in different processes from household units to industrial plants. One of its salient advantages is its **low energy consumption** and **low maintenance** needs compared to pressure-driven membrane processes such as RO. CDI does not require high pressures and has low propensity for scaling, biofouling and organic fouling – and thus a lower energy-related environmental impact (Yu et al., 2016). However, there is only few literature reported on fouling in MCDI and in general, IEM.

Furthermore, the desalination of high saline water by MCDI poses a great challenge and is not yet able to compete with predominant desalination processes due to drawbacks regarding scalability, salinity, efficiencies and cost effectiveness (AlMarzooqi et al., 2014). However, studies showed that CDI can outperform RO at low salinities (Zhao et al., 2013a). For instance, it has been proven that desalination of a 2000 ppm solution by CDI is more cost effective than an equivalent RO process with water production costs of 0.11 \$/m^3 for CDI and 0.35 \$/m^3 for RO (Welgemoed and Schutte, 2005). In order to make the desalination of higher salinities more competitive, capital costs of CDI must be reduced and performance improved.

Cell design

The first and historically most widely used CDI cell design consists of an electrode pair made of porous carbon separated by a spacer in which the feed water flows (see Figure 2.3-1). Here, the feed water flow is perpendicular to the applied electric field, therefore the name "flow-between" or **flow-by electrode**. Since then, new architectural designs for CDI cells have emerged introducing several unique features and novel functionalities. These include flow-through CDI, inverted CDI, hybrid and desalination battery and **membrane MCDI,** which was first reported in the year 2006 (Suss et al., 2015b). A major variation was developed with the use of carbon flow electrodes, or carbon slurry electrodes in so called **flow-through CDI** (FCDI). Here, slurry-based electrodes are used as electrochemical energy storage systems. The two major benefits of FCDI are 1) continuous desalination, since the discharge phase can take place at a separate process downstream and 2) desalination of higher salinity feeds, since the

capacitance available for desalination in FCDI can be effectively increased by continuously introducing uncharged carbon particles into the charging cell (Suss et al., 2015b).

Nevertheless, many of these architectures have been tested so far only at lab-scale so that an application in industry- or real-scale is not yet realized. For this work, MCDI is utilized since it is the most developed CDI cell configuration to this date. The use of membranes in MCDI is explained in following.

Fouling in MCDI

For the investigation of fouling behaviour in MCDI, it is also important to study different fouling mitigation strategies including the fouling behaviour of IEMs. Zhang et al. (2013) studied the **long-term behaviour** of an MCDI pilot plant for the treatment of BW inland in Australia. They indicated that cleaning the MCDI module with a diluted sodium hydroxide (NaOH) solution had the best results. The presence of dissolved iron contributed to the fouling of the electrodes. The MCDI unit with a capacity of 7 L/min at a recovery of 75-80% showed an energy consumption of 1.9 kWh/m^3. However, the system proved to be impractical for the desalination of BW with even low content of inorganic fouling substances as these reduced the desalination efficiency. With higher organic content (TOC) in the raw water, the pores of the activated carbon electrodes are blocked so that the rate of production of the desalinated water was significantly lowered.

Mossad and Zou (2013) also attributed the deterioration of MCDI modules to organic fouling blocking the carbon pores, which increased the energy consumption by 39% at feed concentrations of 10 mg/L of organic matter. Through alkaline solution, the initial flow rate could be recovered by 86%, being more effective than acid or hydraulic cleaning, and suggested that Fe^{2+}-ions accumulate more readily than Ca^{2+} or Mg^{2+} on the carbon electrodes. Wang et al. (2015) reported that cleaning with water was capable of removing protein-like substances, while 0.01 M NaOH was most effective in the removal of humic-like substances from the carbon surface.

Regarding **mitigation strategies for fouling in IEMs**, there are currently different strategies. Coatings or membrane modification for example for increasing the permselectivity and ion selectivity (Golubenko et al., 2018; Khodabakhshi and Asgari, 2018). However, not much is currently being used for anti-fouling properties. Mussel-inspired sulphonated polydopamine coating on anion exchange membranes has been shown to improve the anti-fouling property of anion exchange membranes as well as permselectivity (Ruan et al., 2018). In cation exchange membranes, oxidized multi-walled carbon nanotubes (O-MWCNTs) blended with sulphonated poly (2,6-dimethyl-1,4-phenylene oxide) (SPPO) have enhanced its anti-fouling property (Tong et al., 2016). Physical **cleaning of membranes** like forward or back-washing, air

sparging, or vibration have proven to be effective for pressure-driven membrane processes, but not for dense non-porous such as IEM. For MCDI, chemical cleaning of the membranes is generally preferred (Hassanvand et al., 2017).

Arsenic removal by CDI

Since As(III) is at pH neutral in charge As(III) only As(V) can be removed by the removal of As through CDI processes. Therefore, the As removal through CDI in reducing environments generally involves a **pre-oxidation step** for As(III) to As(V). Most CDI manufacturers report their technology is suitable for the removal of heavy metals and metalloids such as As(V) but only a handful have detailed documentation on As removal. Additionally, reports on As removal is often lacking of detailed information to support the data. Voltea reported an As removal performance for its *CapDI* of 60-65% with a total dissolved solids (TDS) removal of 85% (Voltea, 2016a). Idropan claimed that a removal of up to 100% rejection can be achieved on the datasheet for its CDI test unit module *Plimmer*. In more detailed documentation a removal of 84.2% As and 85% TDS with its *Alfa unit* was reported (Idropan, 2018). A pilot test from Enpar for its *DesEL* system removed 74% As from groundwater (Seed et al., 2006); a removal of up to 97.6% As was achieved and reported later by Hoyos et al. (2008) with the same module. A hybrid CDI-EDI unit from AquaEWP for the purification of BW with 0.039 mg/L was reported to remove 100% of the As with 76% TDS removal (Atlas, 2018).

Some recent scientific publications also documented the removal of As with CDI. Fan et al. (2016) studied the removal of As(III) and As(V) by CDI using $NaAsO_2$ and As_2O_3 dissolved in deionized water (DI) at various concentrations (0.1 to 200 mg/L). The experiments were conducted at equilibrium state in a small lab-scale CDI unit with lab-manufactured activated carbon electrodes to investigate the effect of the initial concentration on As removal. In the case of As(V) removal, no residual As (< 0.0035 mg/L) could be observed for initial concentrations of 0.1 or 0.2 mg/L. The As removal with initial concentrations of 50, 100, and 200 mg/L decreased from 88 to 56.5 and 49.1% respectively. The observed As(III) sorption capacity was lower compared to the As(V) solution. This was explained by the electrostatic adsorption of As(V) due to its ionic charge at neutral pH whereas As(III) is neutral in charge. Adding NaCl or natural organic matter (NOM) also resulted in a decrease of As(V) removal. The lower sorption capacity was attributed to the competition with As(V) to neutralize the surface charge of the electrode and to the substitution of adsorbed As by Cl⁻ ions on the anode.

In a following work Fan et al. (2017) were able to reduce total As by 76% from a multi-ionic solution (As = 0.13 mg/L). They studied the electrosorption behaviour of monovalent and bivalent ions over time showing that monovalent ions are initially better adsorbed than bivalent ions during the charge phase due to their smaller hydrated radius and thus higher size affinity to the electrodes. These ions are then replaced by bivalent ions on the electrode surface

over time, which was directly attributed to the higher valence state of bivalent ions and thus showing an overall better adsorption performance. The energy consumption for the remediation process was calculated as 0.495 kWh/m^3.

Garrido Hoyos et al. (2007) performed treatability tests with real groundwater from the Pajaro Verde Mine in Mexico using a CDI plant model with a nominal treatment capacity of 3.3 L/min. The groundwater had total As concentration 0.21 mg/L, pH = 7.8 and low TDS of 339 mg/L. In a later experiment, tap water was spiked with sodium arsenate up to 0.82 mg/L. The As concentration achieved in the diluate was always < 0.005 mg/L corresponding to 97.6 and 99.4% removal, respectively. The specific energy consumption for adsorption and desorption in the CDI unit was around 0.8 kWh/m^3 and the total energy consumption including pumps varied between 1.37-1.67 kWh/m^3.

2.3.3 Future trends in CDI desalination

Interest in CDI has grown substantially in recent years with currently more than 150 publications reported annually on this topic (Zhang et al., 2018a). However, research on CDI has still a long way to go before reaching the technological maturity needed for the **standardisation and industrialized application** of this technology. Advances have been achieved in many fields but trends in research is focusing mainly on four aspects:

- electrode materials
- electrode modification
- cell design
- system integration

Focus on **electrode materials** and modification is being put on FCDI, which uses an electrode slurry instead of AC electrodes and allows continuous removal. Also faraday electrodes (pseudocapacitive electrodes) that showcase up to 10 times higher removal capacity have become of interest in the research community (Biesheuvel et al., 2017a; Mossad and Zou, 2012). Fewer studies have focused recently on real application and the description of operational parameters based on pilot plant experiments and application.

In general, the selective ion removal of CDI and MCDI cells shows a large potential for specific applications such as water softening (carbonate removal), waste water treatment (bromide, fluoride, oxianions/heavy metals, nitrates, sulphates etc.) (Gaikwad and Balomajumder, 2017; Tang et al., 2017b, 2016a, 2016b), CO_2-capture, and nutrients recovery (P, N) including applications for amine scrubbing, NH_4^+ stripping and protein removal (Zhang et al., 2020, 2018b, 2018c). This study focuses on the **system integration of MCDI** and aims so in contributing to scientific progress in this field (e.g. 2.4 System integration).

2.4 System integration

The term system integration refers to the combination of one or more technologies in one holistic process in order to **increase the overall process performance** of the system. System integration targets improved efficiency and higher purity grades while achieving the highest possible output with the lowest energy requirements and little waste as possible (Singh, 2015a). A hybrid desalination system encompasses the integration of two or more desalination processes or may also involve the coupling with a power plant (Minhas et al., 2014).

This section presents an overview of different successful membrane process integration and the use of renewable energies for process intensification.

2.4.1 Hybrid desalination processes

Process intensification (PI) is defined as the potential for process improvement to meet sustainable production with increasing demands. In general, approaches for PI in membrane desalination focus mostly on material science, physical and chemical properties, and the detailed investigation of the separation process at molecular level e.g. information on concentration polarization (Koltuniewicz, 2017).

One more practical approach for PI focuses on the **design of suitable configurations**, i.e., the selection of different membrane modules and their combinations, in what is called modern hybrid processes. The need to reduce energy consumption in desalination processes such as SWRO has pushed research towards the development of new hybrid systems in which, for example, other membrane processes are used to pre-treat seawater.

Depending on the type of feed and product quality required, a hybrid system can be attainable through combination of conventional membrane technologies or by joining membrane technologies with unconventional (non-membrane) systems. The main goal hereby is to **highlight each individual technology** so that the properties of the integrated design is improved. The optimal success of integrated membrane plants relies highly on the ability to operate various systems together (Singh, 2015a).

For example, the use of ED with RO, NF or ion-exchangers makes the separation of ionic substances from non-ionic possible, and can allow the separation of specific fractions. This is also possible by use of different membranes with narrow size range of particles depending on their molecular weight cut-off (MWCO) (Koltuniewicz, 2017).

The combination of RO and thermal desalination (Calì et al., 2008; Hamed, 2005; Marcovecchio et al., 2005; Qasim et al., 2019) and ED (Li et al., 2013; Pellegrino et al., 2007; Thampy et al.,

2011) has been thoroughly studied in the past. This study focus on **hybrid systems** with membrane technologies (NF, RO) and MCDI as an example for system integration.

Membrane integrated systems

AlTaee and Sharif (2011) investigated the desalination of seawater with a **dual stage system using NF and BWRO** membranes as an alternative approach to RO desalination. They compared a NF-NF system with a NF-BWRO system in terms of overall efficiency. Results showed that NF-NF configuration was more economically feasible considering CAPEX and OPEX but had lower water recovery rates and yielded lower permeate quality. In comparison with a traditional SWRO system it was showed that energy requirements of the hybrid systems were lower than the RO of 4.6 kWh/m^3 with 3.7 and 4.2 kWh/m^3 for the NF-BWRO and the NF-NF configurations, respectively. Same conclusions were drawn by Azhar et al. (2013) when they compared a dual stage NF system and NF-BWRO configuration with SWRO in a theoretical calculation using ROSA (DOW chemicals, simulation software). The BWRO system showed overall lower energy usage and was able to produce a more stable permeate quality over a wider range of feed concentrations (Azhar et al., 2013).

Singh (2015b) described a process design and operation of a low-pressure RO (LPRO) integrated with RO. The **LPRO-RO integrated membrane plant** was used for producing high-purity water from treated seawater. They showed the importance of the pre-treatment in the design of hybrid configurations for the successful implementation (Singh, 2015b). Pazouki et al. (2020) did an economic comparison of medium scale off-grid SWRO, FO-RO and UF-RO configurations. They showed that a FO-RO system was competitive with conventional SWRO at higher water flux >6 L/(m^{3}h) and that both FO-RO and UF-RO had 4–5% lower water unit costs due to energy intensity (Pazouki et al., 2020).

Hybrid system configurations with MCDI

Jeong et al. (2020) investigated the performance of a hybrid system consisting of **NF-MCDI for BW desalination** through experiments and modelling under various operating conditions. The system combination was able to achieve drinking water standards (up to 95% removal) outperforming BWRO systems in terms of energy efficiency for feed concentrations below 10 g/L . The upfront NF consisted of a spiral-wound module (NE90-2540, Toray, Japan) operated at 0.5 and 2 L/min, pressures ranging between 20 and 38 bar and recovery rates of 30-50%. As second stage a commercially available MCDI module (E-100, Siontech, South-Korea) was used with 200 electrode pairs coated with IEMs (Jeong et al., 2020). The MCDI was operated at flow rates 0.1-0.6 L/min achieving SEC from 0.05 to 0.52 kWh/m^3 for the desalination of 2.8 g/L.

The authors suggested the optimization of flow rates depending on system size and operation conditions in order to achieve process optimum. The most important factor hereby was the feed quality, which affected both the SEC and product quality the most. Experiments were also carried out with synthetic SW for NF desalination achieving ca. 50% removal at 38 bar. Overall, the SEC of the hybrid NF-MCDI was ca. 24% lower compared to a typical BWRO for the production of drinking water from BW (< 10 g/L)(Jeong et al., 2020).

Jande et al. (2013) evaluated the combination of a **RO-MCDI integrated system** for the desalination of seawater to produce ultrapure water (TDS < 2 mg/L) and potable water (TDS < 400 mg/L). They calculated a lowest SEC value of 3.17 kWh/m^3 for CV mode for the MCDI, showing the potential for the hybrid system to produce drinking water. Minhas et al. (2014) continued the theoretical study focusing on different operation modes for the CDI and compare CC or CV mode. They showed that CC mode delivered highest removal and recoveries with only minor differences in the SEC compared to the CV mode, which ranged for different experiments between 3.0 and 4.5 kWh/m^3 for the hybrid system. A major difference was identified in the production rate (i.e. WR) of 38% and 5% for CC and CV modes, respectively. Although both theoretical works show the potential of the hybrid system, the results are lacking a validation through practical tests.

Furthermore, Atlas (2018) studied the desalination of BW by use of a **CDI with electro deionization (EDI)** in an integrated hybrid system. The CDI unit was mounted with a semi-permeable coating. The author suggested that the technology had a much smaller footprint and no use chemicals like softeners used for regeneration were needed and 98% desalination at 10 g/L feed with 85% recovery was achieved. Dissolved salts can either diffuse through the semi-permeable coating onto the hybrid electrode or be electrochemically attracted to the electrode by the classical CDI mechanism. In the authors view, the hybrid system also showed faster regeneration times, improved purification and more pure water produced daily at higher recoveries (Atlas, 2018). However, the applicability of this technology is still to be proven.

2.4.2 Renewable energy use in desalination

The use of renewable energy sources (RES) such as solar and wind in desalination are used as an alternative source of energy, for example in remote areas, and to lower the environmental impact of the process. But also, the efficient hybridization of desalination systems with renewable power supply can be implemented to decrease the cost of water production (Garg, 2019; Voutchkov, 2018).

There are different forms RES that can be coupled with desalination, but solar-electrical energy has dominated the market with actually 43% of share of the RES worldwide, while solar-

thermal energy and wind energy contribute to 27% and 20%, respectively (Alkaisi et al., 2017). Coupling desalination plants with RES can be achieved by either direct connection (i.e. off-grid) or by adding the produced power to the grid (i.e. on-grid) to overcome the intermittency of the RES. Direct coupling (i.e. off-grid) of desalination plants to a RES requires variable-speed operation and/or modular operation to match the load to the available power (Mito et al., 2019).

In this study the focus is put in solar-electrical and wind energy, for the on-grid coupling with RO and MCDI desalination processes.

Photovoltaic (PV)

The use of desalination powered by RES is increasingly gaining of interest particularly for the production of potable water from SW and BW in **remote areas and in developing countries**, where the access to grid-electricity and stable energy supply is not always guaranteed (Ali et al., 2018; Aminfard et al., 2019; Caldera et al., 2016; Li et al., 2019; Subiela et al., 2012; Tan et al., 2018). The potential use of photovoltaic (PV) in these regions is even higher since solar energy is typically more abundant here. The cost for PV has also dropped significantly in recent years, making the cost of renewable solar energy highly competitive against fossil fuels (Ettouney and Rizzuti, 2007; Rizzuti et al., 2007; Tan et al., 2018). However, the current contribution of solar energy in desalination is still less than 0.02% (Ali et al., 2018). This can be explained due to the fact that in general, small desalination plants coupled with RES have higher capital cost and show sometimes lower efficiency and productivity than conventional ones. However, the use of small plants with RES is sometimes the **only viable solution for providing access to water**, for example in remote and isolated areas that are experiencing unavailability and inaccessibility of electricity and a potable water supply (Alkaisi et al., 2017; Garg, 2019).

RO has the largest share of use in combination with PV with a 40% share within membrane-based desalination technologies, followed by MD and ED at 16% and 9%, respectively (Ali et al., 2018; Subiela et al., 2012). In terms of **water costs**, RO and ED show currently the most competitive prices amongst solar desalination technologies. In terms of water production cost for hybrid systems, SEC, capacity and the selection of technology have all an influence (Garg, 2019). Generally, membrane-based desalination system are considered as the cheaper and lowest energy demanding technology in comparison to the thermal processes. Also, the water cost for RES-driven desalination strongly depends on battery capacity and nominal power installed, thus hybrid systems play and important role in this regard. Other measures like hybrid pre-treatment, energy recovery devices, and battery-less operation can lower the overall capital costs of the system (Delgado-Torres et al., 2020; Garg, 2019).

Wind energy

The use of wind energy to produce fresh water from desalination process is mostly used in areas with high potential for harvesting such as **islands and higher altitude zones** (Basile et al., 2018; Manju and Sagar, 2017; Tzen, 2012). However, wind energy is associated with unpredictable and intermittent nature, hence desalination using wind energy is a reasonable option when coupled with other RES technologies (Manju and Sagar, 2017)

Numerous studies have focussed on the combination of wind and PV to drive RO plants mostly on a small scale but have not been used to drive large plants off-grid due to the intermittency which may lead to technical challenges such as shortened membrane life and reduced performance of energy recovery devices. Potential strategies for incorporating modular and variable-speed operation is a promising operation strategy to directly operate RO plants with wind and solar power. Some control strategies include model predictive control, neural networks and classical proportional-integral-differential feedback control (Mito et al., 2019).

Implementation or RES and desalination

Garg and Joshi (2014) operated a combined **NF/RO system with PV** for brackish water treatment (TDS = 0.5-4.5 g/L) and conducted a techno-economic analysis. They concluded that the major share of cost was the PV system which contributed more than 50% of overall cost (Garg and Joshi, 2014). Pimentel da Silva and Sharqawy (2020) conducted a techno-economic analysis of **solar BWRO desalination** system (10 m^3/day) for remote communities in the Brazilian semiarid region. The SEC of the proposed system was calculated to 2.8 kWh/m^3 and costs ranging from 1.44 to 1.65 US$/$m^3$ for a 320 W_p PV. Other studies suggest that the cost for SWRO desalination ranges between 3-11 US$/$m^3$ by use of PV and 7-10 US$/$m^3$ for wind while for BWRO the costs range between 5.8-7 US$/$m^3$ for PV and 2-3.25 US$/$m^3$ for wind (Alkaisi et al., 2017; Gude et al., 2010; Manju and Sagar, 2017). These costs can also be significantly be lowered by increasing the capacity of for example the SWRO and wind to >1000 m^3/d to 2.1-5.6 US$/$m^3$ (Alkaisi et al., 2017).

Desalination integrated with RES systems offer a win-win solution to the energy and water problems and its implementation should be supported locally depending on the available resources. The selection of the appropriate renewable energy source depends highly on the local potential of each resource. Among the possible combinations of desalination and RES technologies, solar and wind energy sources have been greatly exploited and found to be more promising in terms of economic and technological feasibility. In general, the construction and operation of desalination plants implies not only technical and economic considerations but also social and institutional issues, which are of particular importance for their implementation in rural areas and in developing countries (Gude et al., 2010; Saadat et al., 2018; Voutchkov, 2018).

3 MATERIALS AND METHODS

3.1 Conceptual approach and computer-based calculations

Computer-based calculations for the RO design and concept evaluation were carried out using the software WAVE – *Water Application Value Engine* (v.1.64) from DuPont® (former Dow Chemicals). This tool is used for the planning and design of water desalination systems based on membrane and ion exchange resins (Dow Chemical, 2018).

The concept development and calculations were separated in following runs:

- o Theoretical approaches for BW desalination
  - ▪ Desalination processes for different salinity ranges
  - ▪ Possible system integration with pre- and post-stage MCDI
- o WAVE calculations for membrane selection with
  - ▪ TDS = 20 g/L
  - ▪ TDS = 16-30 g/L
- o WAVE calculations with XLE membrane

3.1.1 Calculation parameters

In WAVE, desalination processes can be calculated by several input variables. Depending on which parameters are set by the user, the other parameters are set automatically by the calculation results. Design can be based on two variables: the specific water recovery rate as independent variable for the calculation of feed pressure according to membrane type and size, feed flow, etc. Or alternatively, a fixed feed pressure can be defined for the calculations to determine recovery rates according to chosen variables.

In this work, the input parameters for the performed calculations are **feed pressure** (bar), feed **flow** (L/h), **feed concentration** (g/L), and **membrane type** and sizes according to Table 3.1-1. Additionally, a flow factor (FF) is set for simulating aging and scaling of piping and membrane. Following the indication of the manufacturer for new membranes (FF = 1.0) and old membranes (> 3 years, without fouling) factors of FF = 1.0 and FF = 0.8 were considered, respectively (Dow Chemical, 2017).

The software is specific for the modelling of membranes manufactured by DuPont Filmtech™ (former Dow Chemicals) only. Following membranes were considered (Table 3.1-1):

Table 3.1-1 Membrane types considered (DuPont/Filmtec™)

Membrane type*	Application	P (bar)	WR (%)	R (%)
NF270/ NF200/ NF90	Nanofiltration	4.8	15	>97
XLE	Most productive. lowest pressure RO membrane	6.9	15	99
LP	Low pressure RO	6.9	15	99.2
TW30	Industry standard, highest quality water	6.9	15	99.5
LC LE	Commercial applications, low pressure	8.6	15	99.2
BW30	BWRO, light industrial systems	15.5	15	99.5
LC HR	Large commercial application	15.5	15	99.7
SW30[a]	SWRO	55	8	99.4
SWHRLE[a]	SWRO	55	8	99.75

* 4040 Filmtec™ modules; tests conditions: 2,000 ppm $MgSO_4$, at 25°C or specified otherwise
[a]Tests conditions: 32,000 ppm NaCl at 25°C

The most relevant output parameters for the concept evaluations were SEC (kWh/m^3), permeate quality (TDS in g/L) and recovery rate (WR in %) (see 3.6 Metrics and calculations). A maximum limit of 15-20 % WR for single RO/NF membranes was set to comply with manufacturer specifications (Dow, 2018).

The parameters were considered as follow:

1. Lowest SEC, for energy efficient desalination
2. Permeate quality, for direct drinking water production or for further removal by MCDI.
3. Highest WR rate possible, however WR was not as significant, since feed water availability is not limited (seawater, river water) and brine can be discharged back to the source.

3.1.2 Calculation steps

As a first step the technology and type of water was defined. For this study, small-scale RO is utilized and surface water based on NaCl model water and typical raw-water chemistry of brackish water was used. Then the system configurations are input, including number of stages, units and membrane elements per unit, flow factor additionally to operational parameters (temperature, feed flow, etc.), and recovery rate or operating pressure. The defined settings for the calculations with WAVE can be summarized in:

- o Technology: ROSC , (default pre-treatment)
- o Water type: surface water/ seawater
- o Feed water quality: SDI < 5 or >5; pH = 7; design temperature T = 25°C
- o Feed water composition: variable TDS (NaCl, or raw-water composition; see Section 4.2.14.3.1)
- o Pressure vessels: 1
- o Elements per vessel: 1-3
- o Element type: see Table 3.1-1
- o Flow factor FF: 0.8-1.0

Seawater (TDS = 35 g/L) was considered as reference for the feed water composition, which was proportionally lowered to the desired test TDS concentration. After defining all parameters and starting the calculation evaluation, the summary report was generated automatically.

3.2 Lab-scale MCDI

Experiments were conducted to investigate the effect of different operational settings such as flow rate and electric current on the **removal efficiency (R)**, the **specific energy consumption (SEC)** and the **water recovery rate (WR)** (see 3.6 Metrics and calculations).

The desalination target of all MCDI tests was the production of drinking water (TDS <450 mg/L or EC< 850µS/cm), which was monitored by electrical conductivity (EC) and analytical measurements (see Section 3.5).

Three sets of experiments were performed for the investigation of WR, SEC and RE in the MCDI:

i.   Standard experiments with 1 g/L NaCl

for the optimization of the MCDI operational parameters and finding optimum in energy efficiency and WR (see Section 4.1.5)

ii.   Experiments with increasing NaCl concentrations

to study the effect of feed concentration on the SEC (see Section 4.1.6)

iii.   Long-term experiments and with higher capacity

for the evaluation of the MCDI with respects to time and plant capacity (see Section 4.1.7)

3.2.1 Laboratory setup

The laboratory experiments were carried out using a commercial MCDI unit (CapDI, Voltea®) shown in Figure 3.2-1. Two electrode modules were tested: type C3 with 75 electrode pairs and type C5 with 125 electrode pairs. Each electrode pair (16x16 cm), or cell, consisted of symmetrical active carbon electrodes on graphite sheets (current collector) separated by a cellulose spacer (ca. 350 µm). Aminated and sulfonated ion-exchange membranes were used as anions and cations exchange membranes, respectively. The total surface area for the electrode and membrane for the C3 and the C5 modules were 3.7 m² and 6.2 m², respectively. No data on porosity or electrode thickness was given by the manufacturer.

Figure 3.2-1 Lab-scale MCDI (type C5, Voltea®) with a capacity of 0.4-2.6 L/min.

The MCDI lab-unit consisted of:

1. Commercial electrode module (type C3 & C5, Voltea B.V® (NL))
2. Power supply (PSI 880-60R, EA GmbH (GER))
3. Particle filter (cartridge, 1 μm)
4. Feed pump (12 V diaphragm pump, LS243155, LILIE® (GER)).
5. Inlet and outlet EC sensors (SPE-EC100, Supmea (CH))
6. Storage tanks (feed tank; T1)

Model water from the storage tanks (50-120 L) was passed through a particle filter into the module using a diaphragm pump. Sensors measured the EC before and after the electrode module (Figure 3.2-2).

The system was operated with the software from the Voltea CapDI and ran using a DC power supply with a maximum output capacity of 1500 W and a nominal output current of 60 A.
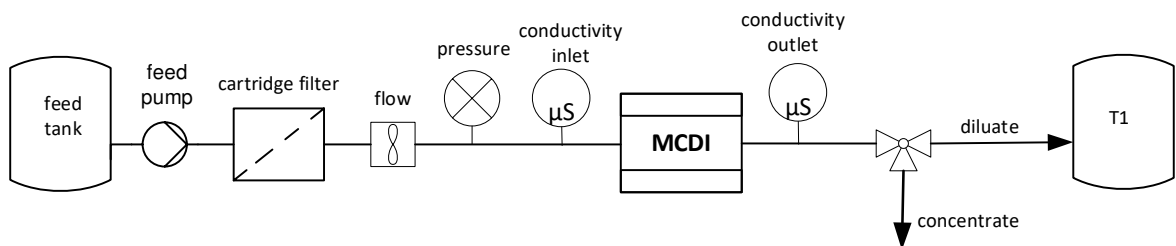
Figure 3.2-2 Scheme of lab-scale MCDI module incl. membrane pump, sensors and cartridge filter (1 μm).

3.2.2 Model water

Model water for the different experiment series was prepared using sodium chloride (NaCl, Sigma-Aldrich®) and DI (EC <10 µS/cm). Experiments carried out used model water with TDS concentrations ranging between 0 and 5 g /L. Depending on the experiment, model water was also spiked with arsenate using an As(V)-standard solution (Merck®), and ammonium (NH_4^+) and manganese (Mn^{2+}) were added in form of ammonium chloride (NH_4Cl, Sigma-Aldrich®) and manganese sulphate ($MnSO_4 \cdot 7H_2O$, Merck®). Fresh model water was prepared every week or depending on usage.

3.2.3 Operation

Experiments were performed in batch-mode unless specified otherwise using 50-120 L feed tank for experiments between 30 min and 4 h depending on the set flow rates (Figure 3.2-3 a). Long-run tests were performed in recirculation mode using the same tank for feed and product water (inlet/feed at tank bottom, outlet on the surface) taking into consideration water mixing through turbulence from product water flow (Figure 3.2-3 b).
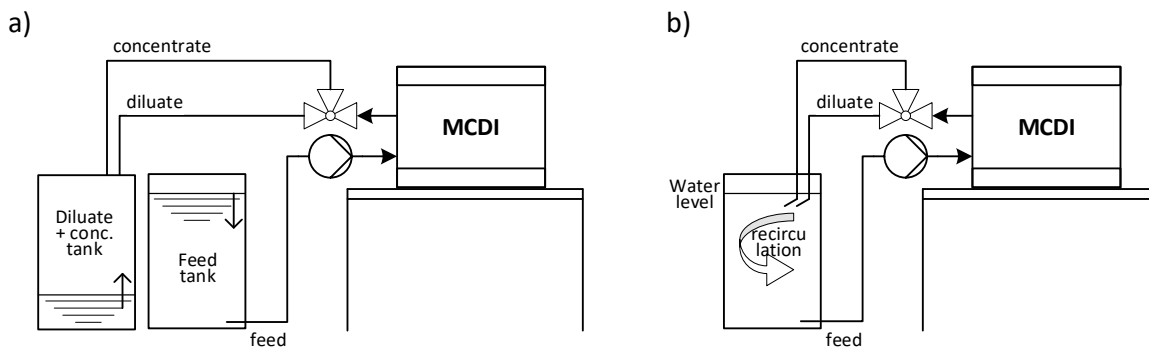
Figure 3.2-3 MCDI operation in a) batch mode with separated feed and diluate/concentrate tanks, and b) recirculation mode (one tank).

Depending on the test duration, each experiment consisted of a number of cycles alternating between charge (desalination) and discharge (regeneration) phases. Each cycle consisted of three phases:

1) <u>Charge phase CP</u>: with positive polarity for desalination generating diluate stream (product water)

2) <u>Discharge phase DP</u>: for electrode regeneration by applying negative voltage generating brine stream (waste)

3) <u>Pre-charge phase PP</u>: for purging the brine out of module before desalination begins

The concentration evolution in the MCDI over time during a typical experiment is shown in Figure 3.2-4 as an example for the cycle profile over all 3 phases showing a concentration increase during DP (red), and concentration decrease during PP (yellow) and CP (green).
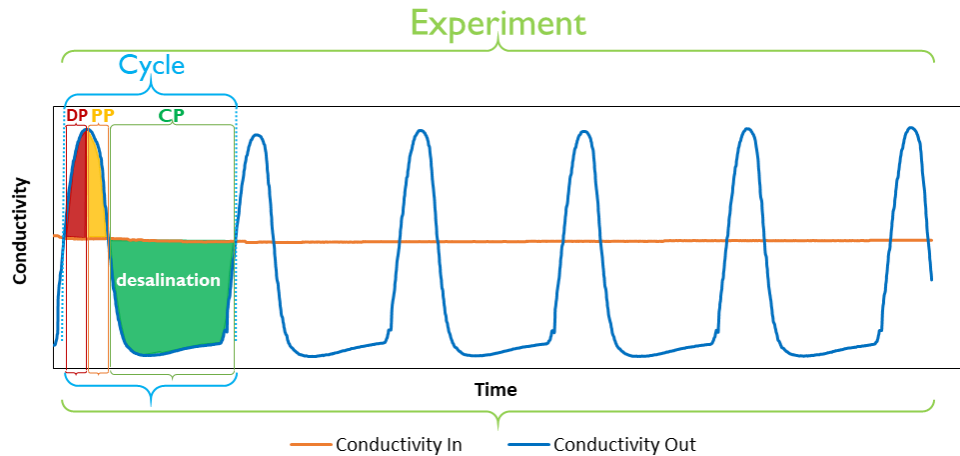
Figure 3.2-4 Concentration profile of typical MCDI experiment: desalination (CP, green), regeneration (DP, red) and pre-charge (PP, yellow).

Desalination with the lab-scale MCDI was carried out in constant current mode, meaning an external current was set for each phase while voltage increased/decreased during the operation. During the DP, the module was run with reversed voltage (negative polarity). For all phases, the maximum potential set was ±2.0 V and the maximum current 60 A.

3.2.4 MCDI settings

The operational parameters for each phase were programmed using the CapDI software (see Figure 3.2-5). Following settings were varied:

 Phase duration t in s:

The processing time indicates each phase length and add up to the total duration of one treatment cycle. The longer the charge phase, the higher the water recovery.

Flow rate $\dot{V}$ in l/min:

The flow rate describes the amount of fluid that passes through the MCDI per second which is set by the membrane pump controlled by frequency.

Voltage U in V:

The system was operated in constant current mode, so the voltage parameter described the maximum applied potential from the power supply in Volts. The max. applied voltage was 2 V.

Current *I* in A:

In constant current operation, the applied current for charge and discharge (incl. pre-charge) are set constant. Desalination is directly proportional to the applied current, so high current intensity leads to a high desalination capacity. In order to maintain constant current, the voltage is increased as desalination advances. The higher the current and voltage, however, the higher the energy consumption.
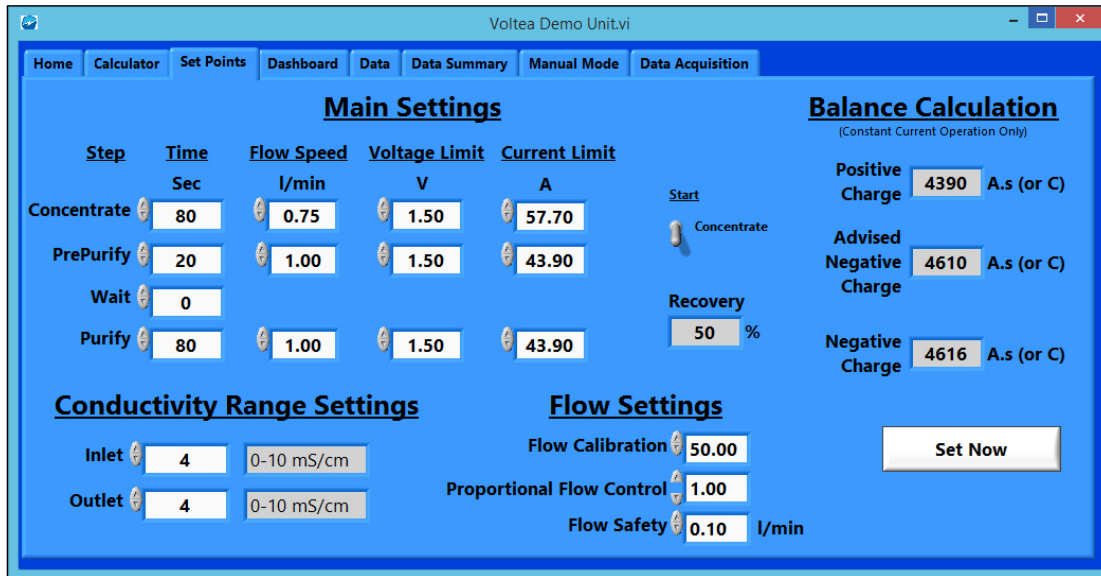
Figure 3.2-5 CapDI - Software (Voltea®) - Lab-scale MCDI settings input.

When defining the operational parameters of the experiment the positive and negative charges (phase duration *t* x current *I*) in Coulomb were balanced (see Figure 3.2-5 "Balance Calculation"). Achieving maximum recovery rates was targeted. The data logging included applied voltage, current, module voltage (directly at the electrodes), EC (feed, diluate, concentrate) volume flow and gauge pressure of fluid for pump speed.

3.3 Pilot-scale SAR+MCDI

3.3.1 Location

The pilot-scale plant SAR + MCDI was installed in the city of Trà Vinh in a coastal region at the Mekong Delta, Vietnam (Figure 3.3-1). It was used for the **desalination of brackish groundwater** and the **subsurface removal of As, Fe^{2+}, NH$_4^+$** and **Mn^{2+}** for wash and drinking water production at a private household. In Trà Vinh, groundwater is facing progressive salinization due to seawater intrusion and tidal conditions, and is affected by naturally high concentrations of As (e.g. Section 2.1.1).

The site selection was based on literature research (Binh, 2015) and upon expert consultation with the VGU and project partners for the installation of the plants (WaKap, 2016). The main criteria considered that Trà Vinh coastal area is affected by salinity intrusion, and showcase diversified livelihood activities, various ecological zones and different ethnic groups.

Trà Vinh
Pilot plant SAR+MCDI
- Brackish groundwater (TDS = 1.65 g/L)
- As, Fe^{2+} and NH$_4^+$ contamination

Source: wiki.commons
CC-BY-SA-4.0

Figure 3.3-1 Location of pilot plant SAR+MCDI in household in Tra Vinh at the Mekong Delta

3.3.2 System set-up and operation

The process scheme of the modular system SAR + MCDI is shown in Figure 3.3-2. The pilot-scale plant was installed in June 2018 and consisted of an MCDI desalination module with upfront As, Fe^{2+}, NH_4^+ and Mn^{2+} removal by SAR. A sand filter was additionally installed for the removal of particulate matter. The system was placed at the rooftop of the house (height approx. 10 m, Figure 3.3-1) and connected to the existing water supply tanks allowing the supply of the treated water via gravity.

The modular concept with SAR+MCDI allowed the production of **two different quality streams**: 1) SAR treated water: As and Fe^{2+} free water, stored in T1 (e.g. for washing purposes) and 2) MCDI diluate: drinking water, stored in T2. The concentrate stream of the MCDI process was directly discharged into the canalisation taking into account that all toxic contents (e.g. arsenic) were previously removed by the SAR treatment.
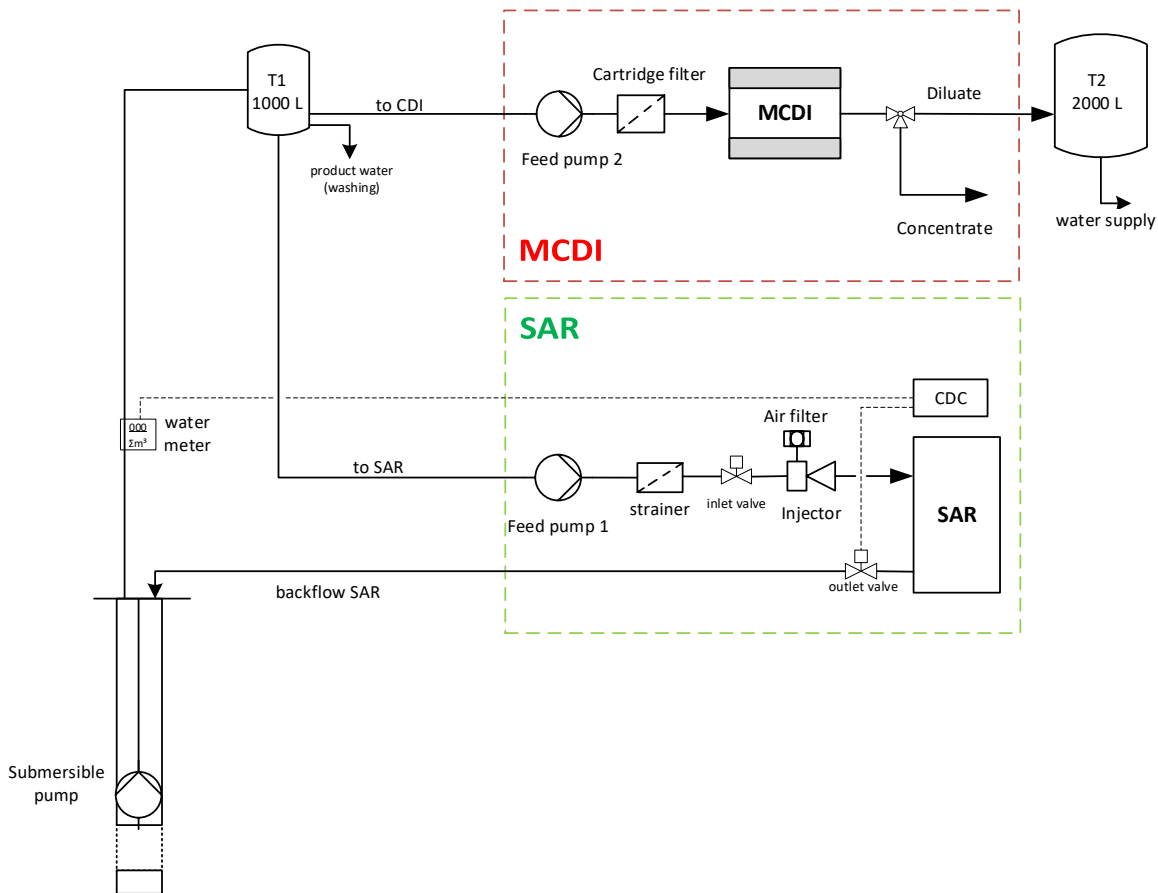
Figure 3.3-2 Scheme of pilot-scale plant SAR + MCDI including supply delivery pump, pretreatment (sand filter) and storage tanks T1 and T2.

SAR set-up

The SAR system (*FERMANOX®-Wasseraufbereitung*, type BV 104) was installed as an upfront stage to the MCDI for the treatment of As laden groundwater and the removal of dissolved Fe^{2+}, Mn^{2+} and NH_4^+ (see Figure 3.3-2). The SAR system consisted of following components:

1. Submersible pump (PENTAX® 4ST 14-8; 2 HP) for the extraction of groundwater
2. Sand filter (1354 FRP Vessel, coarse sand d = 0.5-1 mm;) as pre-treatment for filtering particles
3. SAR aeration storage tank (FERMANOX® 900 L)
4. Injector with air-filter as the aeration device
5. Strainer for protection of injector
6. Feed pump 1 (GRUNDFOS® SCALA2; 550 W)
7. consumption dependant controller (CDC) for automatic aeration and infiltration
8. Inlet and outlet valves actuated by CDC
9. Storage tank T1 (1000 L)

SAR operation

The SAR treatment process was divided into aeration and infiltration cycles.

Aeration: Anoxic groundwater was extracted and stored in T1. Feed pump 1 is used to pass anoxic water through the air injector for oxygenation at a minimum pressure of 2.9 bar. The aerated water is filled in the SAR tank (volume V_{SAR} = 900 L).

Infiltration: After de aeration cycle, the oxygen-enriched water (infiltration volume V_I = V_{SAR} = 900 L) in the SAR tank is infiltrated back into the aquifer by gravity (SAR backflow). Iron oxidation and As-adsorption take place underground following the oxidation/adsorption mechanisms of SAR (e.g. section 2.1.2).

When more groundwater is extracted from the well the infiltrated oxygen is gradually consumed and the oxidation area is depleted. Therefore, aeration and infiltration cycles were repeated 1-2 times per day depending on water consumption which was measured with the water meter and controlled by the CDC in order to maintain a stable oxygenated zone around the well.

In order to avoid leakage of As or any other contaminant, a daily water extraction limit V_E was calculated from the raw water quality as a design parameter based on the previous experience of the manufacturer and fixed for using SAR (Cañas Kurz et al., 2020; Luong et al., 2019, 2018). With two infiltration cycles (each cycle V_I = 900 L), the maximum designed capacity of the SAR

plant was calculated to V_E = 8.3 m^3 per day. This lead to an extraction/infiltration ratio at the pilot site of Q$_E$ = V$_I$/V$_E$ = 0.22 m^3/m^3. Since the oxygenated water was always infiltrated back into the aquifer, another advantage of the process was that no water is lost (WR = 100%) and no waste stream was produced.

Water samples were taken daily at point of use during commissioning, and at least once weekly thereafter (unless specified otherwise) for a period of 181 days. The pilot plant was monitored for several months after the period of research.

MCDI set-up

The MCDI system was installed downstream of the SAR system for the desalination of the groundwater to obtain drinking water (see Figure 3.3-2). The home-made MCDI unit was designed at the HKA and constructed by Tan Vu Luong at the VGU in Vietnam using a commercially available electrode module from Voltea B.V® similar to the one used in the laboratory experiments.

The MCDI is shown in Figure 3.3-3 and consisted of:

1. Commercial electrode module (type C3, Voltea B.V® (NL))
2. DC power supply (HDS 1500 PS12, XP Power)
3. Particle filter (cartridge, 1 μm)
4. Pump 2 (diaphragm pump 8000-243-155, SHURflo® (GER))
5. Inlet and outlet electrical *EC* sensors (SPE-EC100, Supmea (CH))
6. Storage tank (T2)

The MCDI pilot plant included conductivity sensors at the inlet and outlet as well as a pressure sensor to constantly record these parameters. Information provided by the manufacturer indicate a total surface area of the electrodes of 3.7 m^2 for the C3 type, with cation and anion exchange membranes. The used XP power supply had a maximum electrical current output of I_{max} = 100 A and was operated using a self-programmed microcontroller. All operational parameters defined in 3.2.3 were programmable.

MCDI operation

SAR treated water from T1 was passed through the MCDI module using pump 2 in alternate cycles for the charge (desalination) and discharge (regeneration of the electrodes) phases (see Figure 3.3-2). The MCDI was operated at constant current during both phases with reversed voltage in the discharge phase. EC was measured at the inlet and the outlet of the MCDI.

Figure 3.3-3 MCDI pilot plant for desalination including electrode module (C3, Voltea®) (left), electric cabinet (center) and power supply (XP Power HDS 1500 PS12) (right).

The diluate of the MCDI was stored in T2, which was connected to the water supply whereas the concentrate effluent was discharged directly into the sewer, taking into consideration that all toxic constituents have been previously removed by SAR (e.g. As).

3.3.3 Renewable energy supply

Energy module set-up

The pilot-scale plant SAR+MCDI was operated using renewable energy consisting of a 3 kW$_p$ solar PV system and a 2 kW$_p$ wind turbine (see Figure 3.3-4). The energy supply was controlled by an on-grid hybrid inverter to supply the pilot-scale plant while excess energy was fed into the regional power grid (net-metering). The plant was additionally powered by a battery storage consisting of two lithium batteries for a total capacity of 4.8 kWh (Figure 3.3-5). The energy module consisted of:

1. PV panels – 3 kW$_p$ (SUN72M, monocrystalline, SUNERGY (USA))
2. Wind turbine – 2 kW$_p$ (2 KW Windspot 220 V, Hummer (CN))
3. Hybrid inverter (GW-3648, Goodwee (EN))
4. Lithium batteries (2 x 2400 Wh, 50Ah, Sacred Sun (CN))
5. Load dump (Max input: 2.2 kWp; Type HG-2K, Hummer (CN))

Furthermore, a home-made weather station including an anemometer (Davies, 6410) and a pyranometer (Apogee Instr., SP-215) was used to monitor wind direction, wind speed, and solar radiation at the pilot site, respectively.

Figure 3.3-4 Renewable energy supply by PV and Wind turbine.

Figure 3.3-5 Inverter, batteries, charge controller (load dump) and utility meter.

Figure 3.3-6 Wind turbine (left) and weather station installation (right) at pilot site location (centre).

Energy module operation

The pilot plant was supplied directly by PV power. If not enough power was produced and the state of charge (SOC) of the battery was lower than 20%, the plant was directly supplied through the grid. This was controlled by the hybrid inverter. The energy usage and production was registered using a separate net-metering system for the in-going and out-going energy. The power generation from the wind turbine was directly fed into the grid.

3.4 Pilot-scale LPRO+MCDI

3.4.1 Location

The pilot-scale plant LPRO+MCDI for the desalination of **high saline river water** and the production of drinking water was installed in the province of Cần Giờ, a mangrove estuary and natural reservation situated about 60 km southwest from HCMC.

For the selection of the pilot location, important parameters were taken into consideration, including salinity and overall water quality, accessibility (e.g. distance from HCMC, location, permission for research/support from Government, etc.), and if a local contact person for the supervising of the tests was available on site. In discussion with the Vietnamese project partners at the VGU, the proposed location was the **Province of Cần Giờ** (Figure 3.4-1).

**Cần Giờ
Pilot plant LPRO+MCDI**
- High saline river water
- Seasonal fluctuations
- Elevated TSS: UF Pre-treatment
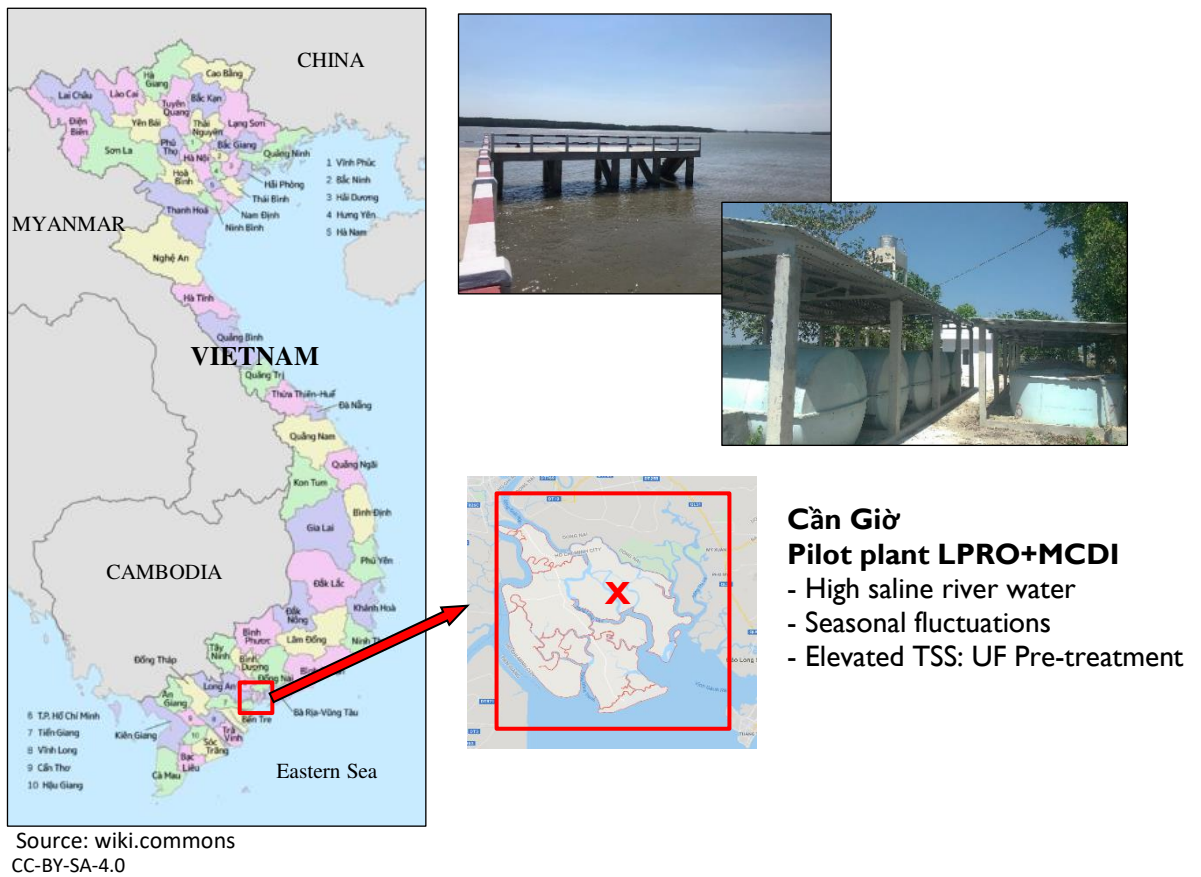
Figure 3.4-1 Location of LPRO+MCDI pilot-scale plant in Thien Lieng, Can Gio

In Cần Giờ, mapping shows a salt concentration (TDS) gradient from ca. 30 g/L at the coast to <6 g/L towards mainland (60 km inland) (see Section 2.1.1). The largest part of the Cần Giờ district is a mangrove reservation area, but also small remote communities, restaurants, etc. where fresh water resources are limited by the **saline intrusion and low water quality**.

The chosen location for the pilot-scale plant was the **commune of Thanh An**, in Thien Lieng hamlet, in the Can Gio district. The commune is located in the heart of the estuary of the Long Tau River and houses around 800-1000 inhabitants in approx. 125 households. Due to its remote location, no centralized water supply from HCMC is possible and because of the groundwater and river water salinization, no fresh water resources are available. Potable water is transported from the mainland to the island by boat.

The costs for transportation by boat range about 24.000 VND/m^3 (€0.85/m^3) and are subsidized by the local government which provides the water on a set tariff of 2.000-4.000 VND/m^3 (€0.07-0.15/m^3). However, the water supply is limited to 3 m^3 per person and month. The shipped water is stored at a pumping station at the island with the capacity of approx. 100 m^3 tanks and is then distributed to the inhabitants of the island.

3.4.2 System set-up

Commissioning

The LPRO+MCDI pilot-scale plant was installed directly at the pumping station on the island about 30 m from the docking station where the fresh water is delivered by boat (Figure 3.4-2). This location was also suitable because the infrastructure (power supply, pipelines, housing, etc.) for the implementation of the pilot system was available here.

Figure 3.4-2 Pier at the Can Gio pilot site (top) and location of the pilot-scale plant LPRO+MCDI (house + blue container) at the pumping station (bottom) in Thien Lieng.

The design of the LPRO+MCDI plant was carried out at the HKA in Germany and the construction of the UF system was done in cooperation with the RO-constructor Spiegl GmbH company, including the set-up of the MCDI module and the power supply system with the control unit.

The system was then sent to Vietnam, where the final assemble and installation on site of the UF, the LPRO/RO and the MCDI was done by project partner SDVICO Company with support of the HKA and the VGU. The commissioning was carried out by VGU and HKA under the coordination from Prof. Song (VGU).

The LPRO+MCDI plant (Figure 3.4-3) consisted of an UF pre-treatment for TSS reduction, the RO system with two parallel membrane units that allowed alternate testing of LPRO and SWRO membranes types, and finally, the MCDI module with power supply.

Figure 3.4-3 Pilot-scale plant LPRO+MCDI in Can Gio: a) storage tanks, b) UF pre-treatment, c) RO system and d) MCDI electrode module incl. power supply.

Plant Scheme

The scheme of the pilot-scale plant is illustrated in Figure 3.4-4, showing the UF pre-treatment, the RO/LPRO system, which was operated using either RO or LPRO membranes, and the MCDI module.
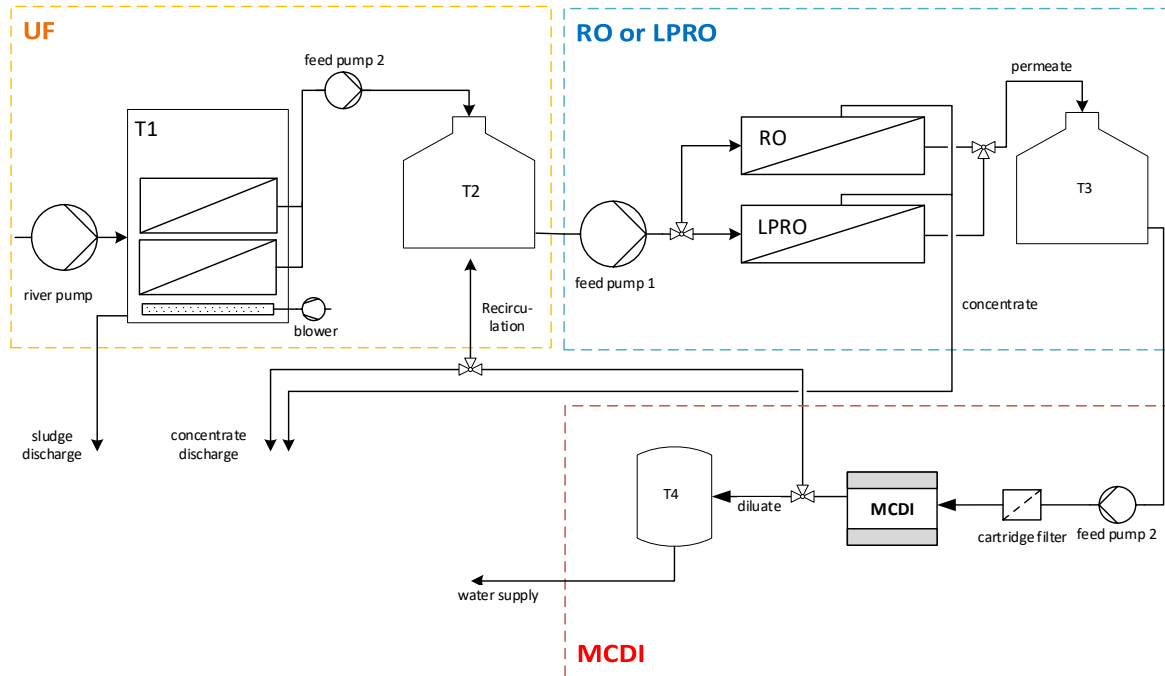
Figure 3.4-4 Scheme of pilot-scale plant in Can Gio consisting of UF-pre-treatment, LPRO or RO system (parallel membrane units), MCDI desalination module and storage tanks.

3.4.3 Plant operation

UF pre-treatment

The UF pre-treatment was used to reduce TSS and turbidity of the river water. The UF system consisted of 2 x 4 m² novel, flat sheet membranes (AQQA8) from Weise Water GmbH (WEISE WATER, 2020).

The **UF-membranes** in the AQQA8 have a modified design compared to other commercial membranes, which allows greater mechanical resistance, so that the modules can be backwashed more frequently and at higher pressures. This enabled a more sustainable operation with low flux but less chemical cleaning processes. The river pump (type 4SDM, NBM Water pumps) for the UF-feed was set-up directly on the river side, below the pier (Figure 3.4-2), and delivered the river water into the UF tank (T1 = 1000 L)) at volume flows 10.8 - 14.4 m³/h. The AQQA8 membranes were submerged in the UF tank and aerated continuously using a blower (enviro® ET 120 SERIES, Charles Austen PUMPS LTD) for air scouring. The designed operating pressure for the UF pre-treatment was -50 mbar using a suction pump (UF

pump) (ET63b-2/Liverani EP Neon, Motek Electric Motors). UF permeate was stored in T2. Backflush was programmed to run every 9 minutes for 60 s by gravity from T2, which was about 1.5 m higher than the membranes, at an average pressure of 120 mbar.

RO / LPRO

The RO/LPRO system (SDVICO, Vietnam) consisted of three spiral-wound membrane units (size 2540, DuPont™, USA) and the pressure pump (AR RC11.11 N, Italy), incl. a cartridge filter (1 µm) for particle filtration. The system was equipped with three spiral wound membrane units in series (3 x SW30-2540 or 3x XLE-2540) from DOW/DuPont™ (see Appendices) for a total membrane area of 8 m² of active membrane (polyamide thin-film-composite). Membrane types were changed by use of a mechanical valve.

 Desalination of pre-treated water (UF) in T2 was done at max. operation pressures of 60 and 40 bar for SW30 or the XLE, respectively. Product water (RO permeate) was stored in T3 for direct usage or for post-treatment with the MCDI, depending on permeate quality achieved.

MCDI

The MCDI system consisted of a commercial electrode module (type C17, Voltea B.V.®) with 425 electrode pairs and a total electrode surface of approx. 21 m². The module used was from the same manufacturer to the modules used for the MCDI laboratory (type C5, Voltea®) and the pilot-scale plant SAR+MCDI (type C3, Voltea®).

In this pilot plant, the system was run in constant current mode using a power supply (TDK Lambda-GEN8-400) with a max. applied current of 400 A. The system was equipped with a pre-filter (cartridge, 1 µm) and the diaphragm pump (Shurflo 5050-1311-H011) for volume flows between 1 and 4.5 L/min.

Automation

The system was programmed to run automatically using a SIEMENS (SIMATIC S7-1200) controller using different flow and pressure sensors as well as relays, solenoid valves and float valves for monitoring and control. A detailed scheme of the electric system is given as supplement in the Appendices.

The modular concept allowed the **production of two different quality streams**: 1) from the LPRO, water with moderate salinity was achieved (e.g. for washing purposes) 2) that could consequently be treated by the MCDI to produce drinking water. From the SWRO stream (stand-alone), ultrapure water could be produced that could be remineralized, if needed, for human consumption.

Brine discharge

In order to follow a **zero-liquid-discharge (ZLD)** approach, the produced brine could be treated in evaporation ponds that are located about 250 m next to the pumping station. Salt production through brine concentration in evaporation ponds is a practiced method in the region. Alternatively, the concentrate stream of the MCDI could also be recirculated back into the RO/LPRO feed (T2) in order to lower feed salinity for the RO process, and increase the water recovery rate and energetic efficiency.

Due to practical reasons, during the course of pilot trials carried out within this study, no brine recirculation was possible. The brine from the LPRO+MCDI pilot-scale plant was discharged directly into the river. The possibility of recirculation and ZLD using evaporation ponds must be, therefore, further investigated.

Figure 3.4-5 Example of salt mining fields located in the commune of Thanh An, Can Gio as an example for brine treatment.

3.5 Analytical methods

Laboratory analysis

Total inorganic arsenic (t-As) was measured with an **atomic absorption spectrometer** (AAS) (ContrAA® 300, Analytik Jena), by means of the hydride technique (HS 55 batch system) Fe^{2+} and Mn^{2+} using the AAS with flame technique (50 mm burner, air/acetylene gas).

Ion chromatography (883 Basic IC plus, Metrohm) was used to analyse ions including measurements of NH_4^+. The concentration of cations was determined with a Metrosep C4-150/4.0 column and of anions with a Metrosep A Supp 5-150/4.0 column according to DIN EN ISO 14911. **Total organic carbon** (TOC) was analysed with a TOC-L Analyzer (Shimadzu).

Electrical conductivity and **pH** were monitored using a portable conductivity and pH-meter (315i, WTW).

All measurements were repeated at least twice, unless specified. Additionally, selected samples were analysed by a certified commercial lab in Vietnam (QUATEST3, Ho Chi Minh City).

Sample taking at pilot site

Sample taking and conservation was carried out following the standard DIN EN ISO 5667-3. Samples were acidified for conservation. Sample analysis was carried out at the VGU lab in Vietnam and at the laboratories of HKA in Germany. Values for pH and EC were measured on site using a portable sensor (WTW Multi-Parameter 3430; see Figure 3.5-1.

Figure 3.5-1 Sample taking and pH and EC measurements on site (WTW Multi-parameter 3430).

3.6 Metrics and calculations

The use of specific metrics and reporting conditions for the evaluation of system performance is crucial for its objective assessment. For the evaluation of RO and common desalination technologies including MCDI systems metrics should include as minimum the specific energy demand (SEC in kWh/m^3), water recovery rate (WR in %), salt removal (R in %) and specific volume flow or water flux per unit membrane area (J_w in L/(h m^2)), which is eq. to the flux J in membrane systems (Hawks et al., 2019).

Furthermore, specific adsorption rates in the MCDI reporting may include salt adsorption capacity (q_a in mg/g AC) of milligram ions per gram electrodes (Huang and Tang, 2020).

In this study, focus was given to the **specific energy consumption SEC,** the desalination performance in terms of **removal efficiency RE** and the **water recovery WR**. Additionally, a rather different metric is proposed in this study for the characterization of the adsorption by the MCDI based on the energy required per gram of removed ions or salts: **specific energy consumption for removal SEC$_{rem}$** in Wh/g.

Removal efficiency (RE):

Salt removal (membrane processes: rejection; MCDI: adsorption) is a measure for the desalination of the test water, which is represented by the formula 3.1. A higher value corresponds to a high desalination of the water.

$$\text{RE} = \frac{(c_{inlet} - c_{outlet})}{c_{inlet}} \cdot 100\% \qquad\qquad (3.1)$$

RE   salt removal in %
c_{inlet} total inlet concentration in mg/L
c_{outlet} total outlet concentration in mg/L

Water recovery (WR):

Water recovery rate refers to the volume of permeate or diluate obtained during desalination to the total volume passed. The higher the value, the more water is available as product water after treatment and the smaller the proportion of water that remains in the concentrate as waste.

$$\text{WR} = \frac{V_{pure}}{V_{total}} \cdot 100\% \qquad\qquad (3.2)$$

WR   water recovery rate in %
V_{total} total volume of treated water (feed volume) in L
V_{pure} volume of product water (permeate/diluate) in L

Specific energy consumption (SEC):

The SEC in kWh/m^3 refers to the total energy consumption as a function of the volume of product water produced (permeate/diluate).

$$SEC = \frac{E_{desalination}}{V_{product}} \qquad (3.3)$$

SEC   specific energy consumption in kWh/m^3
E_{desal} electrical energy in kWh
$V_{product}$ volume of product water (permeate/diluate) in m^3

For the MCDI, the SEC was calculated as following:

$$SEC_{MCDI} = \frac{P_{desalination} \cdot t}{V_{product}} = \frac{U_{MCDI} \cdot I_{MCDI} \cdot t}{V_{product}} \qquad (3.4)$$

P_{MCDI} electrical power input measured at the outlet of power supply in kW
t   time in hours
$V_{product}$ volume of product water (permeate/diluate) in m^3
U_{MCDI} applied voltage measured at the outlet of power supply in V
I_{MCDI} applied current measured at the outlet of power supply in A

Power output P_{MCDI} was calculated from the applied voltages U_{MCDI} and currents I_{MCDI}, giving only the electrical power requirements for the actual desalination performance without considering the further periphery. Voltage U_{MCDI} and currents I_{MCDI} were measured directly at the outlet of the power supply directly.

Specific energy consumption for removal (SEC_rem):

The specific energy consumption for removal gives the total energy required for the desalination of 1 gram of salt. It is given in Wh per gram of removed salts.

$$SEC_{rem} = \frac{E_{desalination}}{\Delta m_{salt}} \qquad (3.5)$$

SEC_{rem} specific energy consumption for removal in Wh/g
E_{desal} electrical energy in kWh
Δm_{salt} mass of removed salt or ions ($m_{in} - m_{out}$) in g

with
$$\Delta m_{salt} = V_{feed} \cdot C_{feed} - V_{product} \cdot C_{product}$$

V_{feed} total volume feed in m^3
c_{feed} feed concentration in g/L
$V_{product}$ total volume of diluate in m^3
$C_{product}$ diluate concentration in g/L

4 RESULTS AND DISCUSSION

4.1 Conceptual approach

In this chapter, different approaches for the desalination of BW are described and the design of a pilot-scale plant is carried out by use of computer-based calculations with the RO- software WAVE from DuPont® and supported by the results of theoretical and preliminary test results.

4.1.1 Theoretical approaches for brackish water desalination

For developing a concept for BW desalination using MCDI, first, a theoretical conceptual approach was developed for evaluating different **scenarios for system integration** with state-of-the-art membrane technologies such as NF and RO.

The use of pressure-driven membrane processes for desalination of low- and high saline water can be divided in LPRO or NF and HPRO (or SWRO) depending on the quality of feed water. Here, the inlet concentration determines the energy requirements of the process. Besides LPRO and HPRO, system integration of different technologies can target desalination with increased efficiency through **process intensification**.

A concept for different scenarios for desalination technologies and their energy requirements for different feed water salinities is illustrated in Figure 4.1-1. For **low saline** water desalination, the MCDI was addressed as single-pass use (concept A), while for **higher salinities**, the concept included typical HPRO. For **medium-range salinity**, the use of MCDI in combination with membrane technologies such as RO, LPRO and/or NF as pre- and as post-stage desalination (concept B) was proposed as innovative alternative to single-pass LPRO or single-pass NF.
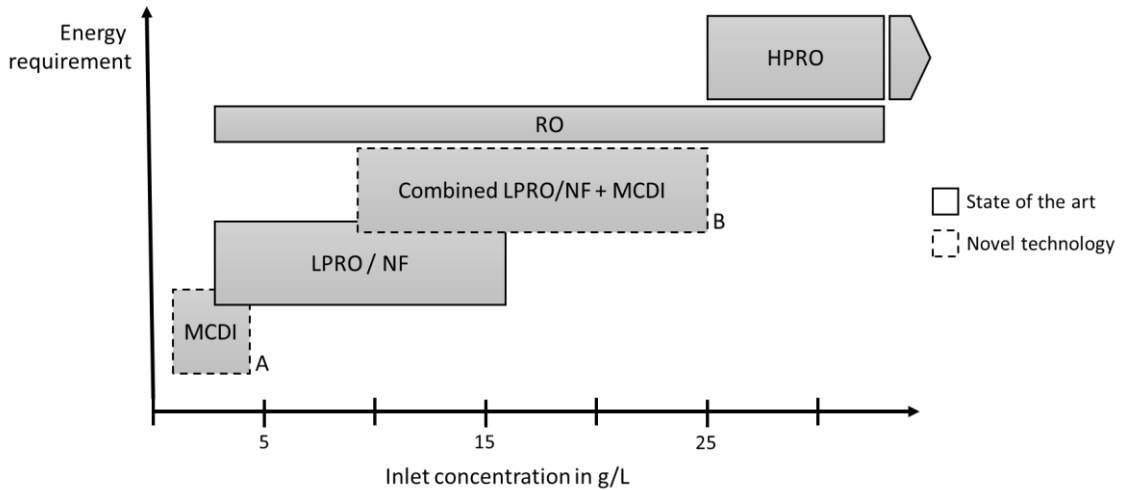
Figure 4.1-1 Qualitative concepts for brackish water desalination by use of state of the art technologies and novel processes (concept A: MCDI, B: LPRO/NF+MCDI).

The technologic advantages of the concepts for low and high saline streams can be summarized as follow:

High salinity: TDS > 20 g/L (State-of-the-art)

State-of-the-art technology RO is used for a wide range of feed water quality including the desalination of high saline BW. The use of HPRO allows the desalination of higher concentration ranges (TDS>25 g/L) with greater energy demand.

Low salinity: TDS < 5 g/L (Concept A)

Energy-efficient desalination of low-brackish water with feed concentrations in the range of ca. 1 g/L to 3-5 g/L is possible with the MCDI with an energy demand below 3-4 kWh/m^3 (Concept A). This was previously investigated in literature studies and shown in preliminary tests with the lab-scale MCDI that showed that the desalination of NaCl model water could be achieved with SEC<1 kWh/m^3. These results and the desalination of higher concentrations by use of the MCDI-technology are investigated in in Section ⬚.

Medium salinity: 5 < TDS < 20 g/L (Concept B)

The desalination of BW with concentrations higher than 5 g/L is possible with both RO and LPRO with pressures raging between 10-40 bar. For TDS concentrations of up to ca. 25 g/L, the LPRO can be operated at pressures of below 21 bar depending on the LPRO/NF-membrane used. LPRO showcases the main advantage of high permeate flux with relatively low SEC and energy requirements compared to other desalination technologies.

Due to relatively low operating pressures, the system setup and pump can be dimensioned accordingly, thus resulting in lower capital expenditures (CAPEX). Pressures below 21 bar allow, therefore, an easy system setup and easy operation which is particularly advantageous in developing and newly industrialized countries. For example in the Vietnamese market there is a wide range of pressure pumps available for this pressure range, which allows additionally cheaper CAPEX and OPEX costs. The operation at max. pressures of up to 16 bar for the LPRO allows additionally easy set-up and construction (e.g. PVC vs. stainless steel) which significantly reduces CAPEX costs. In addition, pricing for pumps increase considerable for operating pressures above 16 or 21 bar, because dry priming rotary vane pumps do not withstand corrosion due to higher chloride concentrations and the cost of materials increase. For pressures up to 21 bar, there are reasonable priced cast iron fittings and valves on the market, also in Vietnam.

Additionally, the combination of LPRO/NF membranes with MCDI technology is also a possible concept for the desalination of high-brackish water that could not be treated by a single technology (process intensification: Concept B). For the desalination of varying TDS concentrations, such as in estuaries and delta plains, an integrated process of LPRO+MCDI can, in addition, allow a flexible operation as well as the production of different quality streams for an efficient and sustainable operation. Based on actual technology operation, power demand for the desalination of 15 to 18 g/L TDS should remain below 5-6 kWh/m^3 (Garg, 2019; Qasim et al., 2019).

The evaluation of desalination **Concept A** was carried out with the lab-scale MCDI laboratory tests included in Section ⬚, while **Concept B** was developed based on theoretical RO-calculations with WAVE-Software (DuPont®) and supported by the results of preliminary tests in Sections 4.1.2 and 4.1.3. Furthermore, Concept B is used for the design of the pilot scale-plant (Section 4.3). The design is carried out in 4.1.4.

4.1.2 System integration LPRO/NF+MCDI

The system integration of LPRO/NF with MCDI (Concept B) can be separated in two approaches consisting of pre-stage and post-stage MCDI. The aim of the concept evaluation was to identify the most efficient configuration for the desalination of medium-range to high-range salinity BW.

Approach I: Pre-stage MCDI

The first approach for the combined treatment of BW considered the upstream desalination with MCDI to lower the energy requirements for the membrane process downstream. The scheme of the upfront MCDI system is shown in Figure 4.1-2. In this concept, the desalination

of feed water with high TDS concentrations (up to 25 g/L) must be provided by the MCDI, which has proven challenging for flow-by cell MCDI-architectures. Over the past two decades, some CDI companies emerged in the market worldwide but only a handful remain competitive in the current industry and only few of these remain active in the field of high saline BW desalination. When compared to RO, different studies have shown that the MCDI can be more energy efficient for the desalination of BW with TDS concentrations below ca. 3 g/L (AlMarzooqi et al., 2014; Welgemoed and Schutte, 2005; Zhao et al., 2013a). The critical factor for this concept is, therefore, the desalination performance of the MCDI module within economically feasible energy consumption. For that reason, new system approaches and an optimization of the process must be investigated.
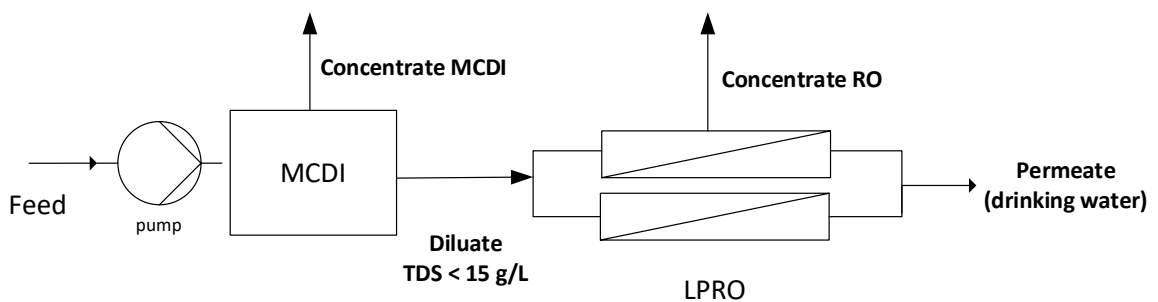
Figure 4.1-2 System configuration upfront MCDI with downstream LPRO.

An approach for the desalination of high saline water with the MCDI follows a low-voltage desalination with low flow rates during charge phase, which lowers the energy requirement for the adsorption. However, the decrease in cell voltage results in low charge efficiency (Biesheuvel et al., 2017b, 2014), while the decrease of flow rate can affect the water productivity and WR. The use of lower flow rates during electrode regeneration can significantly increase WR but can also affect the desalination performance due to limited regeneration, mostly for high saline feed. A combined short-circuit followed by reverse voltage desorption with shorter discharge times can also be effective for high TDS desalination (Dorji et al., 2020). In addition, novel cell architectures such as FCDI show promising desalination efficiency for BW with high concentrations and even seawater (Jeon et al., 2013; Suss et al., 2015a). However, practical experience in this field is still needed.

Approach II: Post-stage MCDI

The second approach for the desalination of high saline BW consists in the upfront treatment with RO or NF and a downstream desalination with the MCDI (second-stage polisher). The process scheme is presented in Figure 4.1-3.
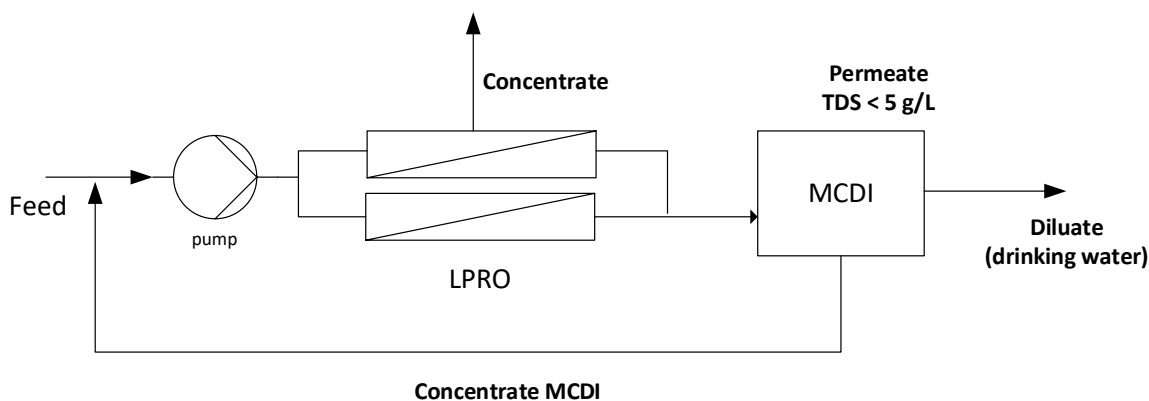
Figure 4.1-3 System configuration LPRO with downstream MCDI.

The approach focused on using "loose" membranes, such as LPRO or NF, over "dense" RO membranes. The advantage herewith is that the membranes can be operated at lower pressures than by use of SWRO membranes, which operate at pressures >60 bar. Achieving drinking water standard was aimed at by using the MCDI downstream instead of a second stage NF or RO configuration as it has been investigated in other studies (e.g. AlTaee and Sharif, 2011; Singh, 2015b) (e.g. Section 2.4.1). The LPRO+MCDI configuration could therefore validate theoretical concepts for the combination of MCDI as second stage to RO as proposed by Jande et al. (2013).

Pressure limitations below 21 bar were also applied for this concept, targeting BW desalination with inlet concentrations of up to around 20 g/L. An inlet concentration ranging from 15 to 25 g/L was regarded as a viable option depending on the salt permeability of the RO/NF membrane. However, higher salt permeability results in higher inlet concentration for the downstream MCDI process. For the energy efficient production of drinking water (TDS<0.6 g/L), the inlet concentration for the MCDI module was aimed as low as possible, while targeting an SEC lower than that of a single-pass SWRO. The practicability of the concept and the choosing of adequate salinity ranges to fulfil this were evaluated with computer-based calculations including membrane selection and plant design (see Section 4.1.3).

Furthermore, preliminary tests with lab-scale RO showed that the energy demand for producing drinking water (TDS < 0.8 g/L) from BW lies between 1.4 kWh/m^3 and 26 kWh/m^3 for the desalination of 10 and 20 g/L, respectively. The large differences in the obtained SEC can be attributed to the increased feed salinity, along with applicability of the membranes (pressure vs. recovery) and the needed rejection for achieving drinking water quality.

4.1.3 Computer-based calculations

In order to investigate the technical feasibility of different membranes for BW desalination and the production of drinking water, the use of LPRO-membranes and NF-membranes in contrast to SWRO-membranes (high rejection, less permeability) was considered. For this, computer-based calculations with WAVE (DuPont® v1.64) were carried out for the evaluation of salt removal performance and SEC of different commercially available membranes (Section 3.1).

Membrane selection-TDS = 20 g/L

The calculations were initially divided in two runs: first, the membranes were tested with 20 g/L NaCl at 21 bar and 1000 L/h feed flow and WR<20%, which is the operation limit given by the calculation software. The aim was to compare the performance of several membranes and evaluate the suitability of each membrane type for its application for BW desalination as process integration with MCDI (Concept B). For the simulation, membrane types were chosen following Table 3.1-1 using 4040-sizes and a flow factor of FF = 1.0 (new/unused membranes).

The calculated parameters SEC and permeate salt concentration are summarized in Figure 4.1-4 and Figure 4.1-5. The x-axis shows the membrane types NF, LPRO and RO positioned from left to right. Results show lower salt permeability and increasing SEC from NF membranes towards RO. In order to select adequate membranes for concept B, a maximum permeate salt concentration of 2 g/L and a SEC of <8 kWh/m^3 was considered, based on the optimum desalination performance given by the MCDI manufacturer (Voltea, 2016b) and on average literature values for state-of-the-art desalination (e.g. Table 2.2-2).
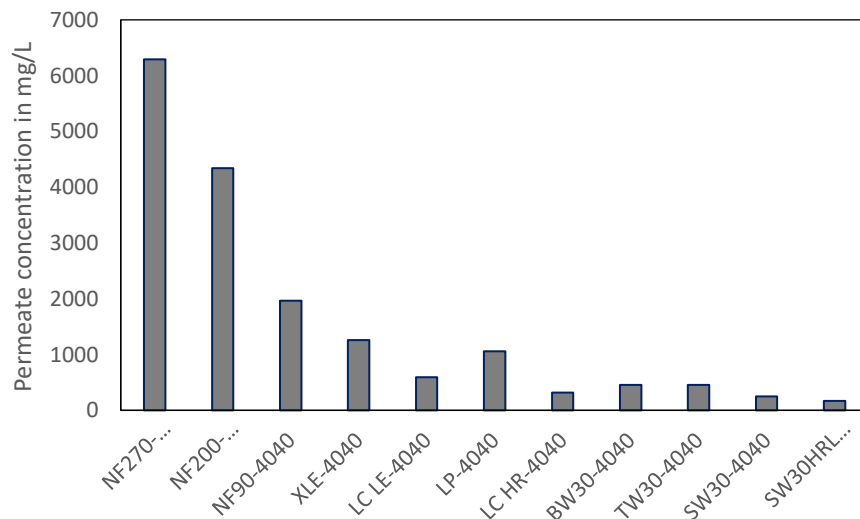
Figure 4.1-4 Permeate concentration of different membranes-calculations at 21 bar and 1000 L/h with inlet concentration of 20 g/L.
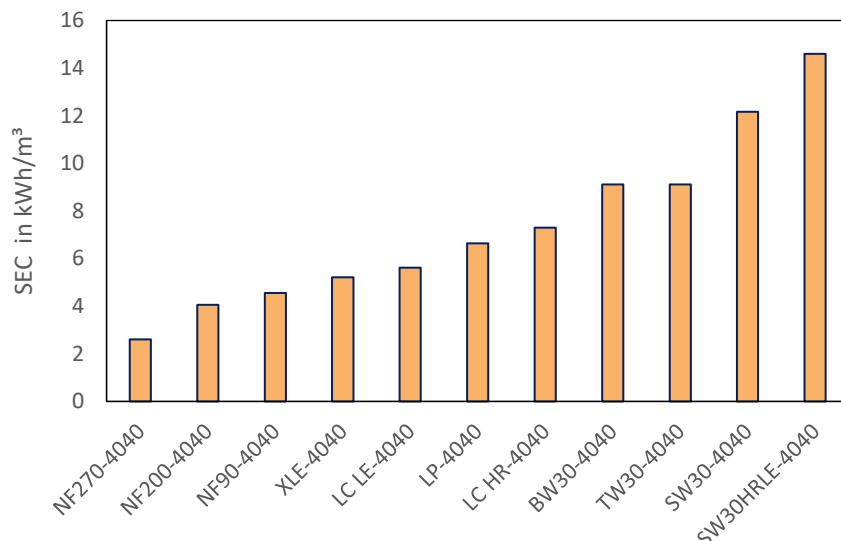
Figure 4.1-5 SEC of different membranes-calculations at 21 bar and 1000 L/h with inlet concentration of 20 g/L.

Based on the defined criteria and the performance results in Figure 4.1-4 and Figure 4.1-5, the selected FilmTec™ membranes included NF90, XLE, LC LE and LC HR (DuPont, 2020). The membrane type LP 4040 was excluded since both SEC and permeate conductivity calculated were poorer than of LC LE.

Membrane selection-TDS: 16-30 g/L

Secondly, calculations with the selected NF/LPRO membranes were carried out with increasing NaCl concentrations (16 g/L < TDS < 30 g/L) at 16 and 21 bar, and 1000 L/h feed flow in increments of 2 g/L. The results for FF of 0.8 and 1.0 were averaged.

Calculation results showed that increasing inlet salinity reduces RE. The results of the permeate conductivity across the TDS range is shown in Figure 4.1-6. Here, the limit value for drinking water quality (TDS<600 mg/L) shows which membranes are able to produce drinking water at an operating pressure of 21 bar and increasing inlet concentrations.

The XLE-4040 membrane is able to produce drinking water up to an inlet concentration of approx. TDS = 19 g/L, while the LC HR-4040 up to a TDS = 26 g/L. However, the difference in SEC is significantly higher between the LC HR-4040 and the other membranes, the latter, consuming at least 1 kWh/m³ more over the whole feed concentration range. The behaviour of the SEC over increasing inlet concentration is shown in Figure 4.1-7. Calculation results suggested that the most suitable membrane of the selected types for concept B is the XLE.
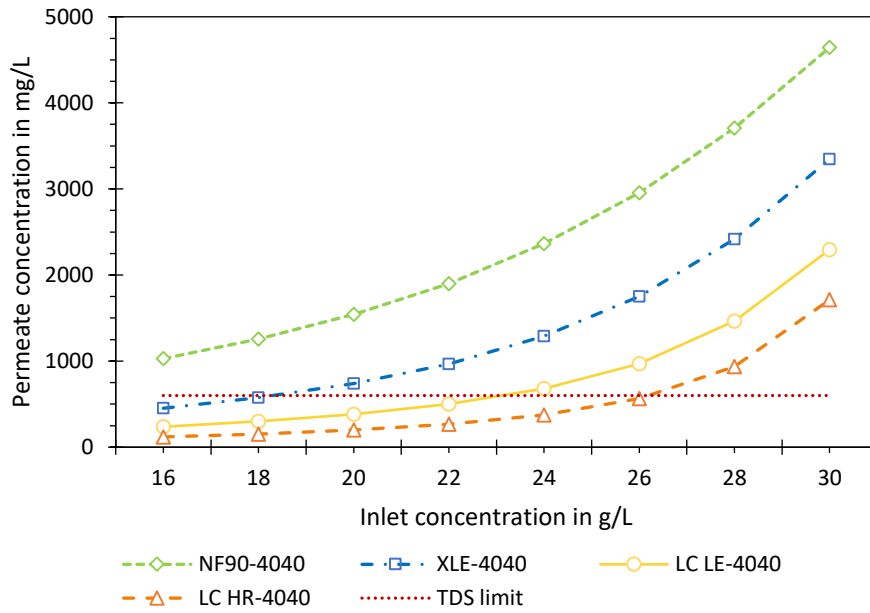
Figure 4.1-6 Calculated permeate TDS of selected membranes-(at 21 bar; 1000 L/h).
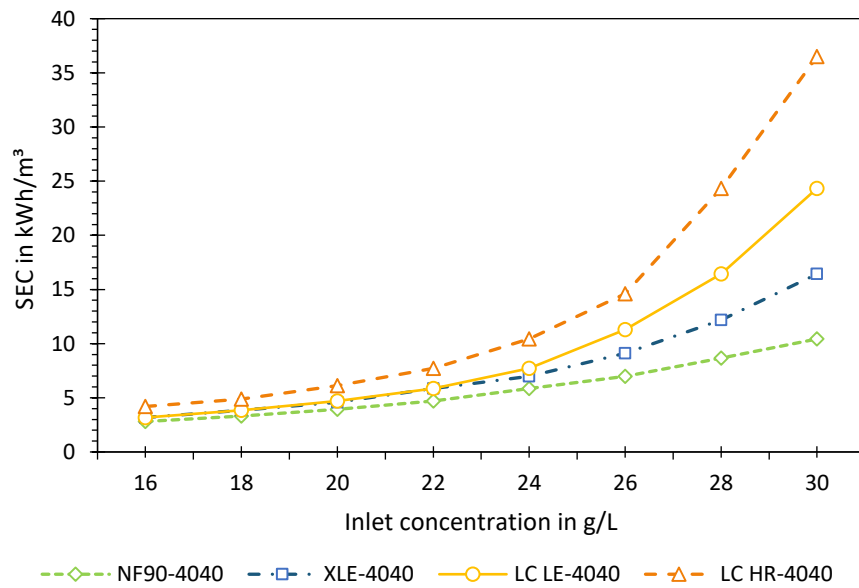
Figure 4.1-7 Calculated SEC of suitable membranes-(at 21 bar; 1000 L/h).

XLE-Membrane-operation

A comparison between operating pressures (16 vs. 21 bar) and module sizes (2540 vs.4040) for the XLE-membrane was carried out to determine the optimum parameters for plant design. Both FF of 1.0 and 0.8 were calculated for inlet concentrations of 5, 10 and 15 g/L. Calculations for 2540-module size were carried out with a feed flow of 500 L/h, while 4040-module was calculated with 1000 L/h. The results for SEC, RE and WR are shown in Figure 4.1-8.
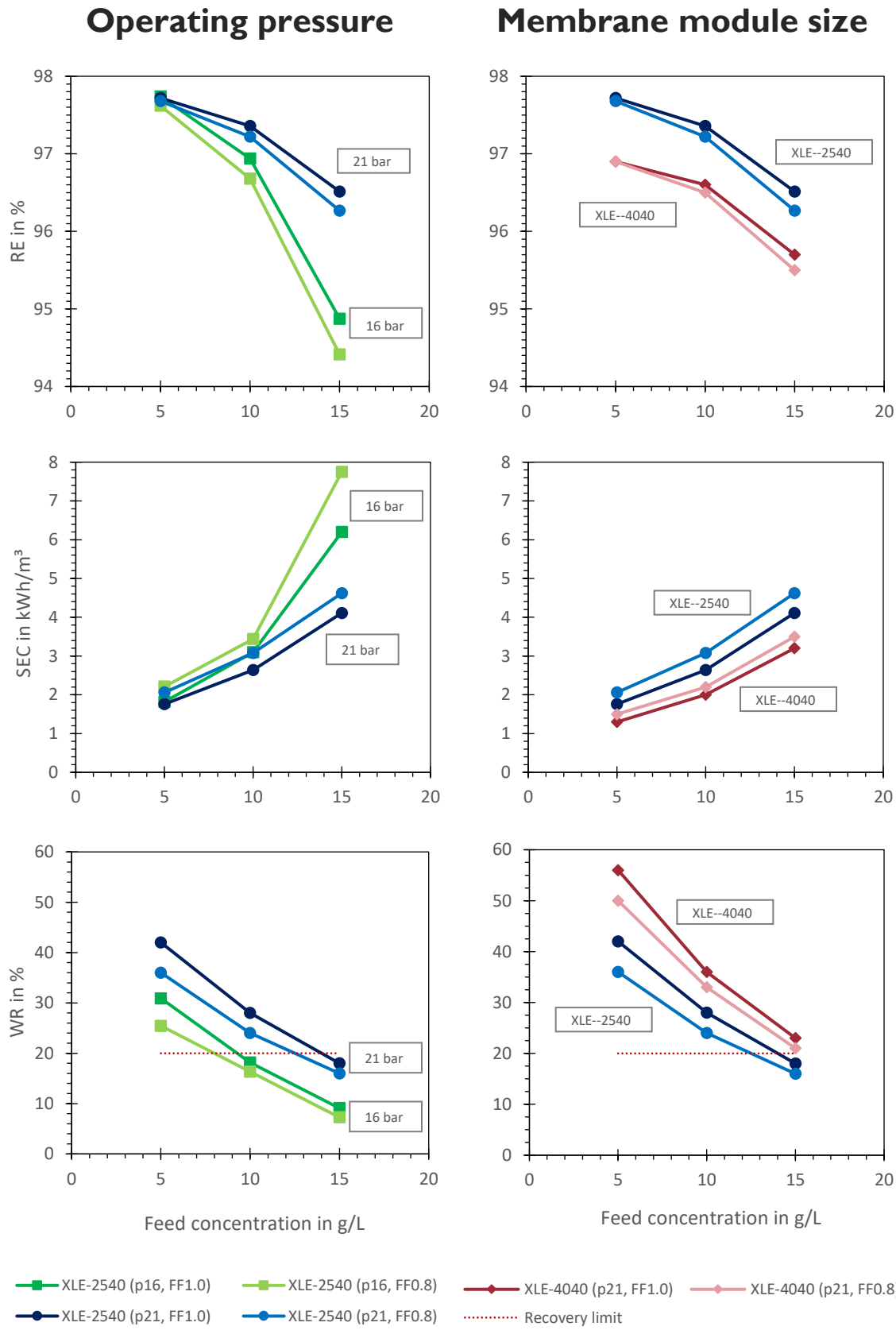
Figure 4.1-8 Comparison of rejection, SEC and water recovery of XLE-membranes. Left: operating pressure (p =16 vs. 21 bar), right: membrane sizes (2540 vs. 4040).

Calculations for both **operating pressures** showed better results at 21 bar with higher RE and WR, in addition to lower SEC values than 16 bar. Particularly, the calculated SEC at 21 bar increased slighter with higher inlet concentrations. While the SEC and the RE are rather similar at 5 to 10 g/L, a greater difference in the operation at the different pressures was observed at 15 g/L. Results suggested that desalination of salt concentrations of 15 g/L or more at 16 bar is not viable due to higher osmotic pressure and an approach with operating pressure of 21 bar should be followed for concentrations above 15 g/L. Additionally, calculation results of **membrane size 4040** at 1000 L/h showed very promising results with higher WR and lower SEC than 2540-elements at 500 L/h feed flow. However, for lower concentrations at given pressure, the calculated WR exceeded the WR limit of 20% for membrane unit, hence operation parameters (e.g. lower pressures or higher inlet concentrations) must be taken into consideration for the final plant design.

4.1.4 Conclusions for concept design

Situation analysis

Due to seawater intrusion, mostly during the dry season, groundwater and surface water salinization is an increasing problem, mostly in coastal regions. By comparing the calculation results presented in the previous sections and analysing the current situation of water sources and the water market in Vietnam as a typical newly industrialized country it was estimated that river water with salinities between 15 g/L and 25 g/L has the biggest potential and attractiveness for local drinking water production. In comparison to groundwater, surface water poses, however, a greater challenge due to its lower quality and its higher vulnerability to anthropogenic and seasonal fluctuations.

The concept for the combination of MCDI and upfront LPRO for desalination of BW from river in estuarine regions is a feasible option for WaKap (WaKap, 2016).

Pilot-scale plant design

Taking into consideration the energy requirements of the process, the combination of the MCDI with the different selected membranes was also simulated at different scenarios. Results are illustrated in Figure 4.1-9 and showed that the high-rejection LC HR have the highest SEC in comparison to the other membrane types for the simulated inlet concentrations. Membranes NF90, XLE and LC LE showed similar values, whereas the latter two presented the lowest SEC.

When comparing both membranes, results showed that above 24 g/L inlet concentration the XLE outperforms the LC LE with 1 kWh/m^3 less energy consumption (see marked section in Figure 4.1-9). Regarding the target SEC of 8 kWh/m^3, drinking water quality is obtained up to an **inlet concentration of up to 24 g/L**.
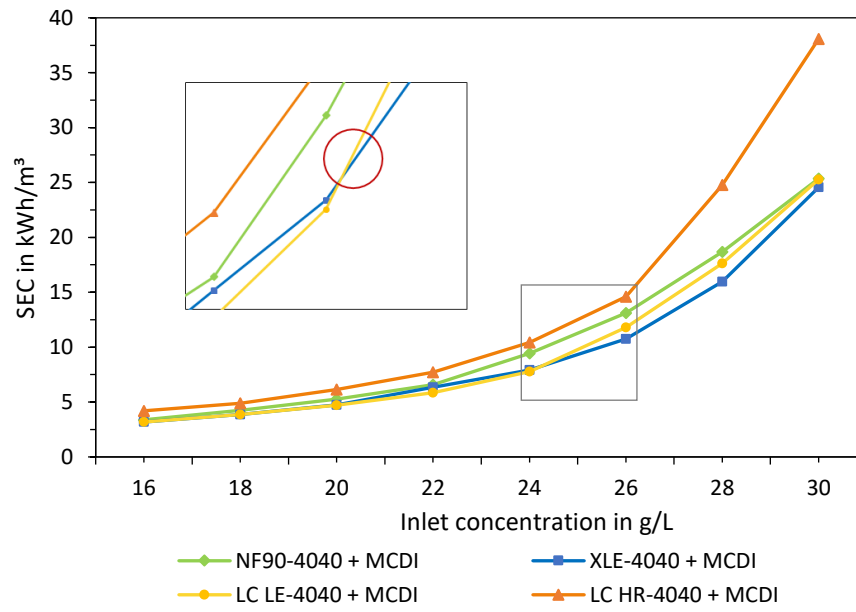
Figure 4.1-9 SEC of different selected membranes in combination with MCDI for increasing inlet concentrations. Marked section: LC CE and XLE turning point.

Concept proposal-summary

- "Loose" membranes (NF/LPRO) were chosen for lower SEC and lower removal, in contrast to denser membranes (RO) which showed higher removal but high SEC.

- Operation at higher pressures (21 bar) and larger membrane sizes (4040) showed the better results.

- The XLE membrane showed the lowest SEC for the desalination of medium-saline BW at given operational parameters.

- In combination with MCDI production of drinking water is only possible up to an inlet concentration of ca. 24 g/L for SEC values below 8 kWh/m^3 (SEC of conventional SWRO up to 7 kWh/m^3).

- The pilot-scale plant should provide a comparison of the XLE+MCDI process with state of the art RO (e.g. SW30 membrane).Lab-scale MCDI

This section presents the results of the laboratory tests for the study of the MCDI technology and the investigation of WR, SEC and R. The lab-scale experiments were carried out over the course of three years. Investigated parameters included volume flow (V), current (I) and phase duration (t) while cell voltage (U) was regarded as a constant parameter (i.e. constant current operation; see. Section 3.6).

The tests were divided in:

i. Standard experiments with 1 g/L NaCl

ii. Experiments with increasing NaCl concentrations (1-7 g/L)

iii. Operational evaluation of MCDI

4.1.5 Standard experiments

MCDI standard experiments with 1 g/L and 2 g/L NaCl were performed in order to investigate the effect of different operational parameters in the process efficiency, and to find the optimum energy efficiency for the production of drinking water (TDS < 0.45 g/L).

The test results of 1 g/L experiments with the lab-scale MCDI (C3 and C5 modules) are shown in Figure 4.1-10 (left). The results show **SEC values between 0.5 and 2.75 kWh/m³** for R>50% varying subject to WR, which ranged between and 40 and 90%. The relationship between the SEC in dependence on the RE and WR revealed that the choice of the operational parameters to target a specific RE had a direct effect on energy efficiency.
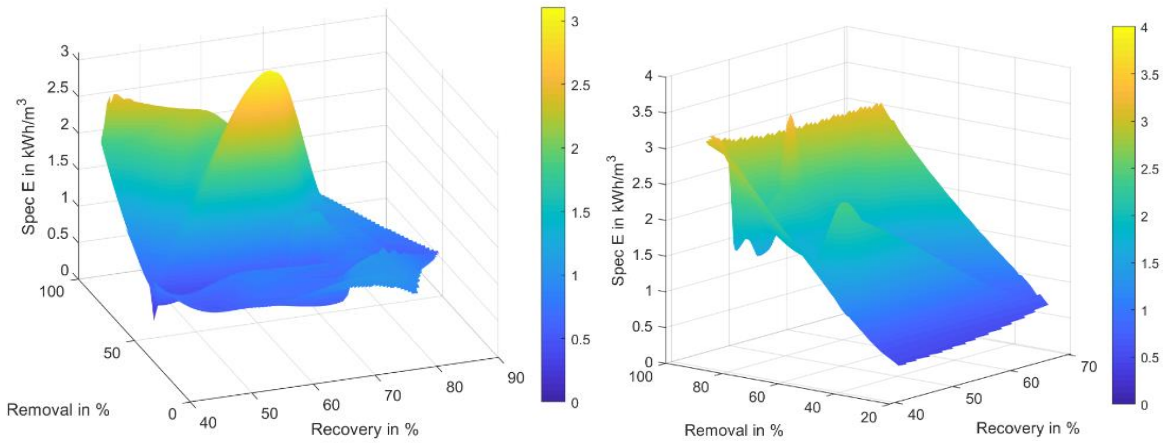
Figure 4.1-10 Relationship of RE, WR and SEC of lab-scale experiments with the MCDI at 1 g/L (left) and 2 g/L (right) inlet concentration.

The test results of 2 g/L in Figure 4.1-10 (right) indicated that **SEC values varied between 0.5 and 3.5 kWh/m³** for RE between 20-90% and WR between 50-70%. It is evident that the higher the salt removal RE, the higher the SEC. However, the increase in WR yielded different SEC values for equivalent removal efficiency rates RE as it is seen in the experiments with 1 g/L. This indicated that the operational parameters set can be adjusted to increase or decrease the overall efficiency of the MCDI and that the relationship between SEC, RE and WR is very complex.

The main objective of the laboratory tests included therefore, the finding of the optimum operational settings of the MCDI for the desalination of 1 g/L NaCl (EC ≈ 2000 µS/cm) and the production of drinking water quality (EC<850 µS/cm). The target was to achieve WR>50% and SEC<1 kWh/m³. From Figure 4.1-10, the best results achieved for a total RE of 54% and a WR of 71% were SEC_{C3} = 0.61 kWh/m³ and SEC_{C5} = 0.72 kWh/m³ with the C3 and the C5 modules, respectively. The MCDI settings of the optimum experiments are listed in Table 4.1-1.

Table 4.1-1 Lab-scale MCDI optimum operational parameters for feed TDS = 1 g/L

Phase	Phase state	Flow rate (L/min)	Cycle time (s)	Applied current[*] (A)
DP	Discharge	0.25	115	57.6
PP	Pre-charge[**]	1.0	40	18.1
CP	Charge	1.0	310	18.1

[*]Constant current operation with voltage limit: 1.5-1.9 V
[**]Pre-phase phase to ensure water quality at beginning of charge cycle

The experimental settings in Table 4.1-1 showed that desalination in constant current mode with low flow rates during the DP for high WR yielded the best experimental results. The relationship between each individual parameter on the desalination efficiency is discussed in the following section.

The concentration and current-voltage profiles over time are illustrated in Figure 4.1-11a and Figure 4.1-11b. These profiles can be used for the evaluation of the set parameters and give an insight of the stability of the desalination. The **concentration profile** shows the constant inlet concentration at 2 mS/cm while the outlet concentration increased and decreased over the three displayed cycles. During the CP, brine salinity rises to a concentration of 5.7 mS/cm while during DP the diluate drops to a constant concentration between 0.8-0.9 mS/cm throughout the 310 s phase length. The concentration profile follows the current profile, set in constant current. This indicated that the operational parameters were set correctly.

The **constant current** operation is visible from Figure 4.1-11b, which shows the linear profile of the applied current at 18 A and 57.5 A for CP and DP, respectively. The drop of the current from 57 A to ca. 37 A at the end of the DP can be attributed to the applied voltage limit of the power supply of 1.7 V. When reaching this limit, the increasing electric resistance in the module causes a drop in the current - shifting the operation to a constant voltage mode. The maximum voltage is set in order to avoid water decomposition (E° = 1.26 V) and other possible parasitic reactions (Faradaic reactions) that may occur if there is a potential build-up in the cell (Dykstra et al., 2017; Tang et al., 2017a; Zhang et al., 2018a).

The potential of the electrodes in the MCDI module – or **cell voltage** – is displayed together with the current profile (Figure 4.1-11b), showing that the min./max. voltages were (-)1.2 and (+)0.56 V during regeneration and desalination, respectively, and that there was no risk for water decomposition. The shape of the voltage profile (semi-linear, peak-formed towards phase end) is a typical voltage behaviour during sorption and desorption. The applied voltage reaches its upper and lower limits towards the end of each phase and its shape remains constant in every new cycle, which also indicates that the set parameters are right and that no potential overload or shift over time can occur.
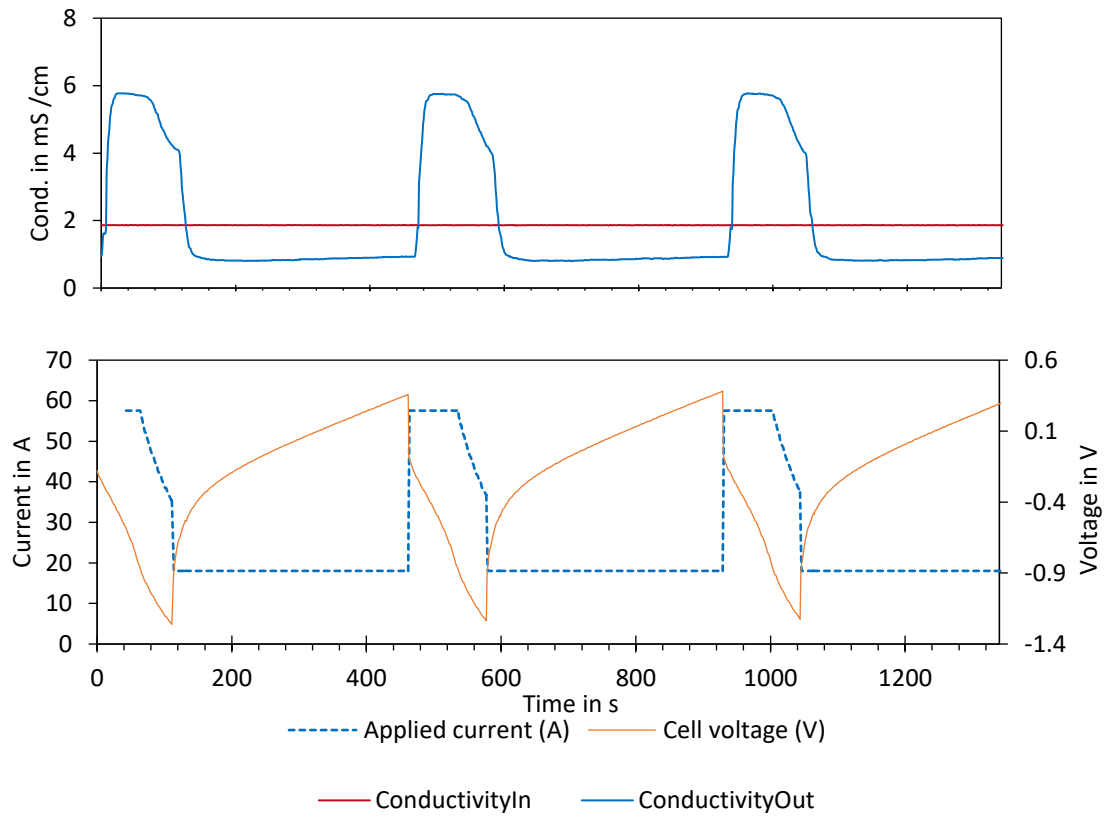
Figure 4.1-11 Concentration (top) and voltage-current (down) profiles over three desalination cycles for optimum experiment (TDS: 1 g/L).

4.1.6 Experiments with increasing TDS

Experiments with increasing NaCl concentrations were performed in order to study the effect of feed concentration on the SEC and salt rejection RE of the MCDI system. Depending on the inlet concentration of feed water, the operational parameters (e.g. currents and flows) were changed systematically to find out the best settings. Experiments were based on previously experimentally determined configurations with the MCDI unit for optimum SEC in standard experiments with 1 g/L (Section 4.1.5). In these experiments, applied current and volume flows during the CP and PP were respectively increased and lowered to improve total removal.

Desalination performance: SEC, WR and R

Experiments were conducted for the evaluation of the desalination performance of the C3 and C5 modules. The SEC values for both MCDI modules with increasing NaCl concentrations (EC: 0.7-7.4 mS/cm; TDS: 0.35-4 g/L) is illustrated in Figure 4.1-12.
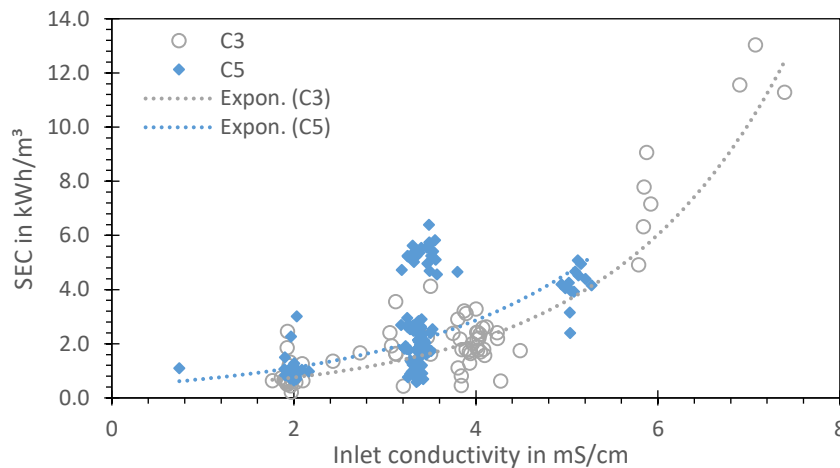
Figure 4.1-12 SEC of MCDI modules (C3 & C5) for the desalination of model water (NaCl) with increasing feed salinity.

While the increase in SEC with increasing TDS was expected, the vertical variation of the SEC at a given inlet concentration was an indication that the **operational parameters** had a great influence on the process efficiency. Results in Figure 4.1-12 showed that for the desalination of 1 g/L (2 mS/cm), a SEC between 0.65 and 2.0 kWh/m^3 was needed while for 2 g/L (4 mS/cm) results showed values from 0.8 to up to SEC>6 kWh/m^3, depending on the target rejection.

For this reason, the experiment results were used to investigate the factors influencing the output parameters and the achieved energy requirements for both modules. The **relationship between SEC and both RE and WR** are shown in Figure 4.1-13 and Figure 4.1-14. Results showed that higher removals required greater SEC, whereas increasing the WR reduced the energy consumption, as seen in previous section. Interesting was the difference between both
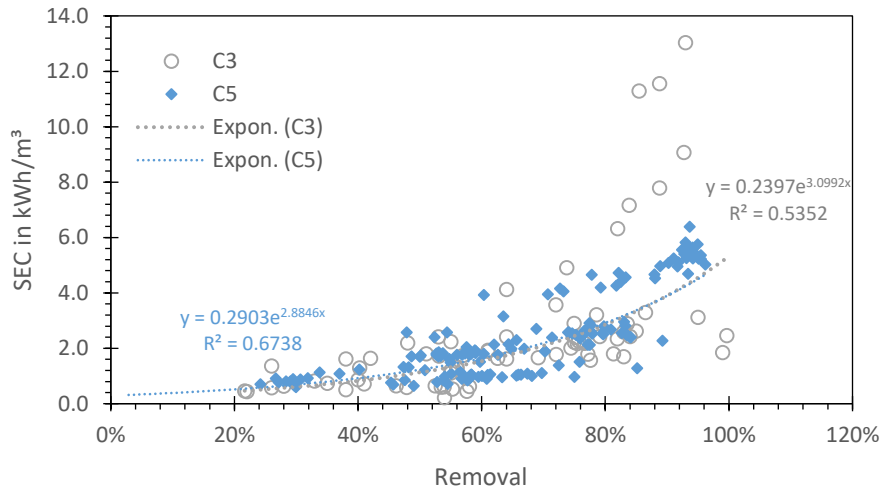
Figure 4.1-13 Relationship between removal RE and SEC for MCDI (C3 & C5).
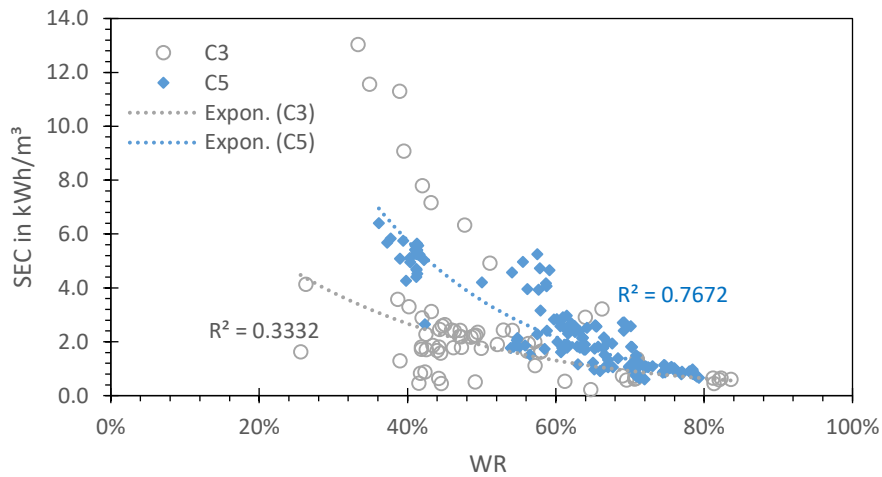
Figure 4.1-14 Relationship between recovery WR and SEC for MCDI (C3 & C5).

modules. In Figure 4.1-13, the exponential trend line for both data sets are nearly identical for C3 and C5 (R=0.55; R=0.67) suggesting the relationship between SEC and RE is not dependant on module size.

Additionally, the relationship of SEC in dependence of WR in Figure 4.1-14 for both C3 (R=0.33) and C5 (R=0.76) could be used to compare the efficiency of both modules regarding size and WR. Results showed that C5 module had higher SEC for the same WR in comparison to C3 even though the C5 module was expected to have a better performance due to bigger size and higher capacity. However, the C3 module showed better results in the reduction of the SEC when increasing the WR. This could be explained, however, by the fact that the operation of the C5 with a higher capacity required higher volume flows (>0.4 L/min)-and currents-than the C3 module, which weren't always given. Due to the limited power supply output of the CapDI of 60 A, both C3 and C5 were operated at similar operating conditions, with volume flow rates as low as 0.25 L/min for increasing salt concentrations.

Furthermore, the exponential approximation for C3 only fitted the scattered data partly (R<0.5) suggesting that the relationship between WR and SEC is affected by more parameters and that the electrochemical behaviour of the desalination is more complex. The direct correlation of increasing inlet concentration and WR on the growing SEC is shown in Figure 4.1-15. Results showed clearly the higher inlet concentrations increases the SEC of the desalination process.
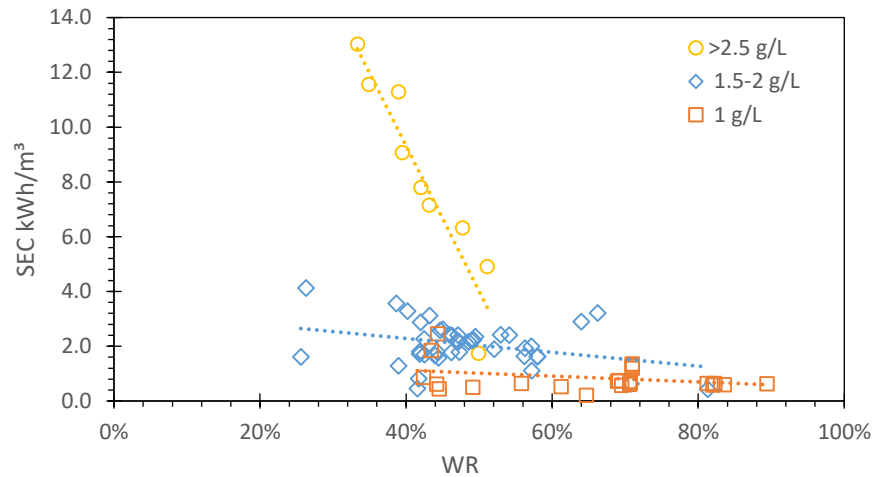
Figure 4.1-15 Relationship between water recovery WR and SEC of MCDI (C3 module) at different inlet concentrations.

Current, flow and phase duration

In general, ion adsorption is directly proportional to the **applied current** and desalination can be simply improved by higher currents. However, the required amount of energy will depend greatly on the thermodynamic efficiency through appropriate electrode regeneration and the relationship between current efficiency and electrosorption. The laboratory tests revealed that the SEC is highly dependent on the set of operating parameters not only for the desalination phase (i.e. CP), but also of the regeneration phase (i.e. DP).

For this reason, tests with similar desalination performance RE could show different SEC values. This could be explained by the relationship between WR and the power requirement during each individual phase (CP, DP, PP). By changing, for example, only the **water flow rate** during the DP, the WR was directly increased while the energy required for the desalination remained mostly unchanged. The relationship between power output (P) and WR over diluate flow is shown in Figure 4.1-16a. Through the linear slopes of WR (m = 60.8) and P (m = -26.4) it is evident that the effect of the flow rate is more significant over WR. As a result, higher diluate outputs yielded lower SEC improving the overall process efficiency as shown in Figure 4.1-16a.

Alternatively, adjusting the **phase duration** of the DP affected both the WR and the SEC. This is illustrated in Figure 4.1-16b, where longer CP yielded lower SEC. Additionally to these parameters, intermittent flow operation in MCDI reduced the energy consumption of desalination by reaching high salt rejection and water recoveries without an energy penalty. Recent studies have also shown the effect of the DP on the overall performance of the MCDI (Porada et al., 2020; Ramachandran et al., 2019).
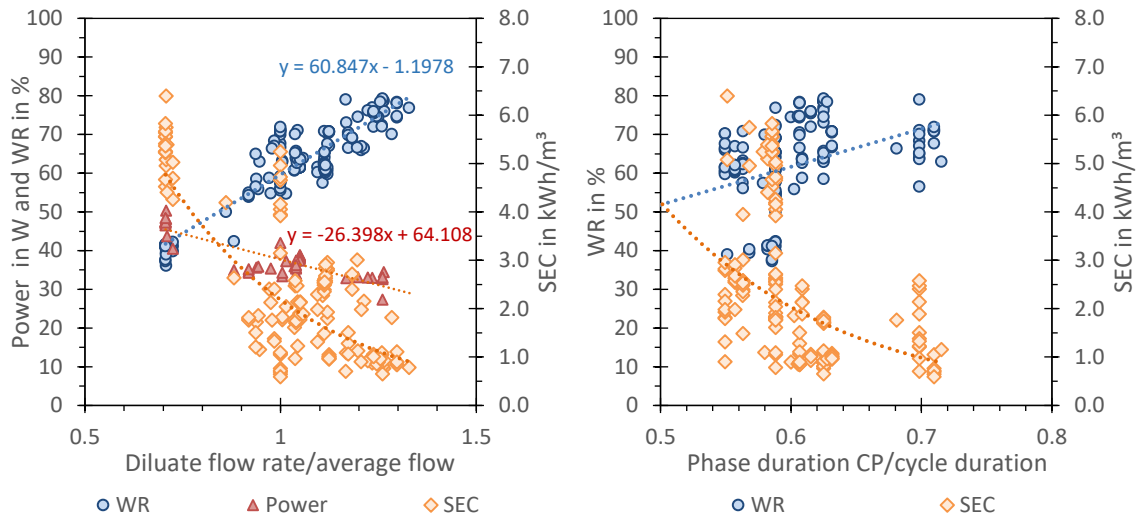
Figure 4.1-16 Effect of a) diluate flow rate and b) phase duration on power output of MCDI, WR and SEC.

Charge balance

If the **applied charge** between the positive (CP + PP) and negative (DP) phases is unbalanced, there is a shift of the polarity window between the electrodes over time. With longer DP (negative polarity) than CP and PP together (positive polarity), more negative charge is applied as positive charge and vice versa. The charge balance can be calculated using Eq. (4.1):

$$q = \int_{t_i}^{t_f} I \cdot dt \qquad (4.1)$$

with

q	charge in C (A·s)
I	net outward current in A
dt	change in time in s
ti	time

Additionally, during the regeneration of the electrodes (DP), the salt ions desorb from the electrodes and are released into a concentrated brine. Too low water flow rates during this phase showed decreased efficiency due to the **inefficient salt regeneration**. Thus, the flow

rate should provide enough time for the released salts, or the majority of them, to be flushed out of the module.

The effects of an unbalanced experiment is illustrated in Figure 4.1-17a - Figure 4.1-17c showing a concentration, voltage and current profile over the course of each cycle (e.g. Figure 3.2-4) for an experiment with poor desalination performance.
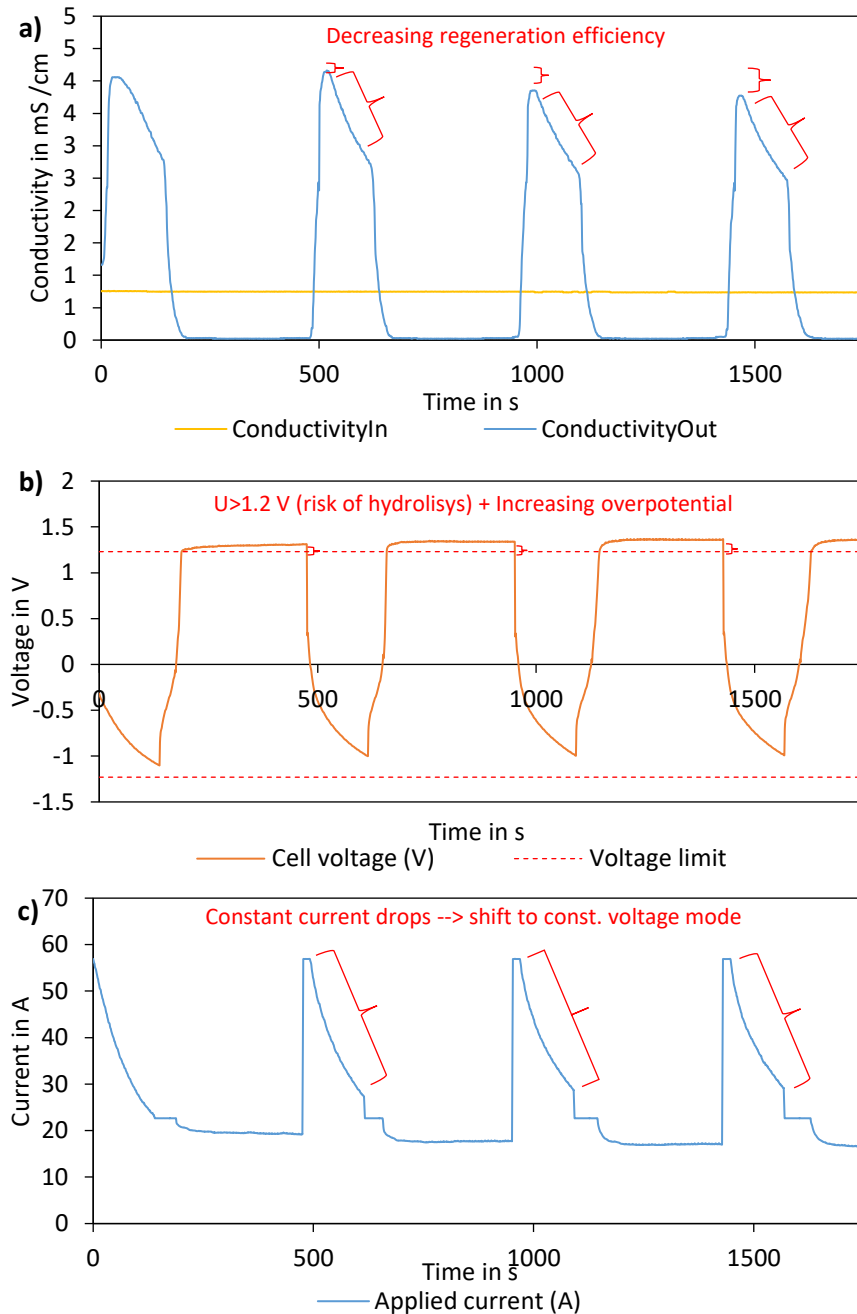
Figure 4.1-17 Effects of unbalanced settings on the concentration (a) voltage (b) and current (c) profiles over time (DP: 58 A, 175 s; PP: 29 A, 35 s; DP: 29 A, 290 s).

When the combination time of DP and PP were not selected properly, the desalination efficiency of each subsequent cycle declined (Figure 4.1-17a). This was a result of the

electrodes that were not regenerated properly when the DP was either too short or the volume flow to low.

The development of the voltage in these experiments indicated that the currents selected (constant current) are set too high and cannot be sustained with the increase of electric resistance within the module during the desalination. When the **voltage limit** of 1.2 V is reached during DP, operations then shifts to **constant voltage** mode (Figure 4.1-17b), and the current declines together with the desalination performance of the MCDI (Figure 4.1-17c).

In conclusion, the concentration and current profiles can be used to identify if the experiment settings are chosen properly and if any limitations in the voltage development can occur.

4.1.7 Operational evaluation

Setting of parameters

A summary of the most important MCDI operational parameters and their effect on the efficiency are illustrated in Table 4.1-2. The setting of the operational parameters were based on their effect on the charge balance, which is mandatory for a sustainable long-term operation, and their effect on their efficiency for improving operation at different scenarios, "low removal"-poor diluate quality; "high removal"-high energy demand, and "low water recovery".

Table 4.1-2 Relationship between operational parameters in the MCDI and their effect on the charge balance

Situation	Changes _without_ effect on charge balance	Changes _with_ effect on charge balance[*]
LOW SALT REMOVAL	$\downarrow \dot{V}_{charge\,(+)}$ $\uparrow \dot{V}_{discharge}$	$\uparrow I_{charge}$ AND $\uparrow I_{discharge}$ $\downarrow t_{charge}$ $\uparrow t_{discharge}$
TOO HIGH SALT REMOVAL[#]	$\uparrow \dot{V}_{charge\,(+)}$	$\downarrow I_{charge}$ AND $I_{discharge}$
LOW WATER RECOVERY	$\uparrow \dot{V}_{charge}$ / $\downarrow \dot{V}_{discharge}$	$\uparrow t_{charge\,(+)}$

[*]Positive-negative charge must be balanced as Eq. 4.2
[#]With regard to drinking water standards
(+): most effective

The balance of the positive q_+ and negative q_- charges in a cycle can be visualized in Eq. (**4.3**) and (4.4), where a positive charge is applied during the CP and PP phases, and negative during the DP phase.

$$q_+ = q_- + 5\% \tag{4.3}$$

$$I_{CP} \cdot t_{CP} + I_{PP} \cdot t_{PP} = I_{DP} \cdot t_{DP} \qquad (4.4)$$

Therefore, the adjustment of phase time and current for the MCDI experiments was based on the charged balance.

Different operational parameters were chosen for the different setups. To obtain reasonable WR rates, the DP times have to be set as short as possible. Thus, the constant current in the DP was always set higher than the constant current during the charge phase.

Module cleaning and performance decline

Deterioration of the MCDI performance was expected due to electrode material degradation and fouling. In order to minimize the fouling effect, mitigation strategies were implemented following the manufacturer's recommendations. The cleaning of the modules was carried out regularly depending on usage and performance decline.

Chemical cleaning consisted in the recirculation (60 min) with 3% hypochlorite (NaOCl) against bio- and organic fouling, and with 5% citric acid for scaling mitigation. Since most experiments were run with model water (DI+NaCl), cleaning with NaOCl was carried out more frequently. When both methods were used, caustic cleaning was done first followed by acid cleaning with thoroughly water flushing in between.

Mechanical cleaning consisted in the flushing of the modules with saline solution or DI water at higher flows (>2 L/min) for short intervals alternating between the two inlets of the module. Additionally, scouring with air-water mix was implemented for the mechanical release of organic materials inside the electrode module.

Pressure drop was monitored continuously during all experiments over the period of at least 2 years operation, which was in average 0.30±0.2 bar for the C3 module, 0.10±0.08 bar for the C5 module depending on the volume flow.

In general, mechanical cleaning showed the best results for **improving the removal efficiency** and decreasing the pressure drop in subsequent runs. After several months of operation (>12 months) chemical cleaning seemed to affect the performance of immediate tests after the cleaning showing sometimes removal efficiencies well below average. However, after flushing and operating the module for 60 -120 min with tap water, this effect disappeared, which suggest the chemical cleaning (caustic and/or acid) affected the IEM's performance, as it is known from literature (Hassanvand et al., 2017; Mossad and Zou, 2013).

In order to study the **long-term effect** of harsh and frequent cleaning, standard experiments with 1 g/L were repeated throughout 2 years of investigation (April 2017 and June 2019) to evaluate the MCDI performance over time. Results of the SEC, RE and specific energy

consumption for removal SEC_{rem} over time are shown in Figure 4.1-18. Here, the WR remained constant ($\Delta WR = 1\%$), indicating that the standard tests were repeated under the same parameters and conditions.

Results show that the SEC increased by 12% and the desalination RE dropped by 46% in the investigated period. The comparison of the SEC_{rem} over this period also showed a linear increase from initially 0.66 Wh/g adsorbed to 1.0 Wh/g, which corresponds to a 51% more energy demand.
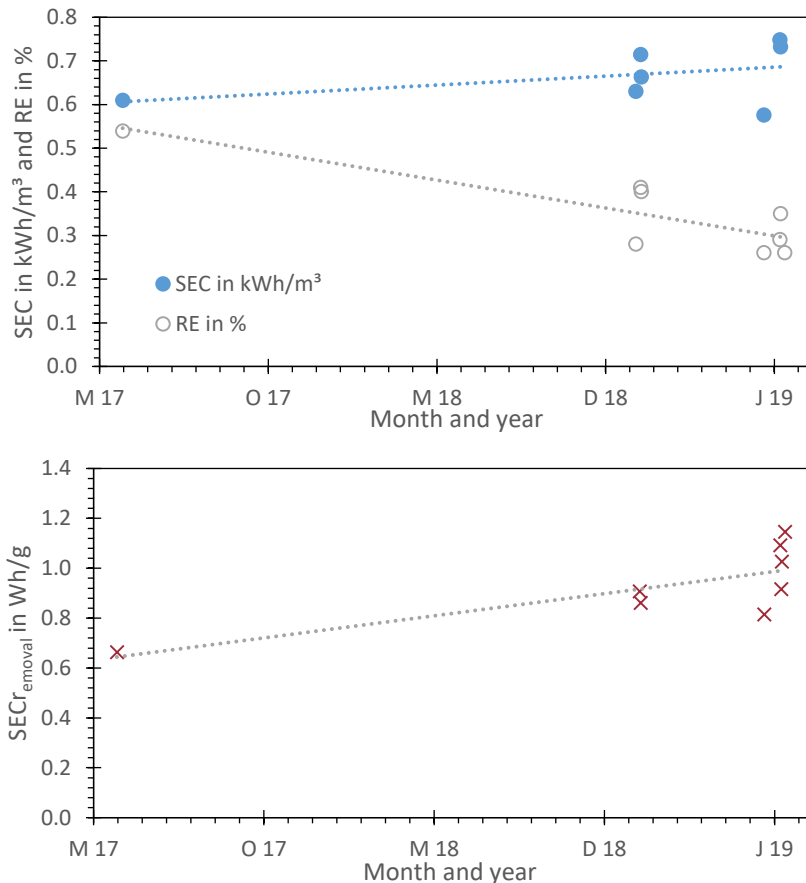
Figure 4.1-18 Long-term performance of MCDI (C3): SEC and RE (top) SEC$_{rem}$ (bottom) over time.

There were many factors that influenced the long-term deterioration of the performance of the MCDI modules (C3 and C5) over the course of this investigation. **Irregular usage** and **long idle periods** could have contributed to increased fouling potential of the membranes and electrodes although the electrode modules were stored in preservation solution during idle, and cleaning was performed frequently before and after experiments. Studies in literature have shown that the performance decrease of the MCDI is linked to carbon electrode deterioration and membrane selectivity decline after increased module usage and intensive chemical cleaning (Zhang et al., 2018a). However, it is not clear what the effect of irreversible fouling in the long term is (AlMarzooqi et al., 2014).

In this study, the wearing out of the IEM's and carbon electrodes in the MCDI modules was mainly attributed to the extensive laboratory usage and experimentation with **variable feed water quality** (iron, total hardness, TOC, etc.) in addition to the **frequent chemical** cleanings (caustic/acid), rather than to a typical fouling behaviour response. The laboratory usage of the MCDI modules (e.g. not in a household or standard industrial application) included experiments with increased iron (Fe^{2+}) content which increases the scaling potential of semi-irreversible Fe scale deposits on both the IEM (Wang et al., 2020) and the electrodes (Tang et al., 2017a; Zhang et al., 2018a). Additionally, increased cleaning intervals enhanced electrode and membrane deterioration. Therefore, a slower deterioration of the MCDI module was expected for the pilot-scale plants during the pilot-trials.

Up-scale experiments

Furthermore, standard experiments with 1 and 2 g/L were repeated with an industrial module with higher capacity to evaluate the MCDI performance at higher flow rates. The aim of the experiments was to compare the energy consumption and the power output with different volume flows. Three experiment sets were carried out with initial volume flows of 1.85 and 0.9 L/min as shown in Table 4.1-3 The tests were repeated for the desalination of 1 g/L (E01) and 2 g/L (E02 and E03) with increasing volume flows (factor 4 and 6) between approx. 1 and 11 L/min and currents of up to 220 A. Outlet target concentrations were fixed to 45%, 32% and 48% for experiments E01-E03, respectively.

Table 4.1-3 Operational parameters for the desalination of 1 and 2 g/L

Experiment nr.	Concentration (g/L)	Flow rate CP (L/min)	Applied current CP (A)
E01	1.0	1.85	36.7
E02	2.0	1.85	31.9
E03	2.0	0.9	31.9

Results of the SEC at increased volume flow of the three experiment sets are shown in Figure 4.1-19. Results showed that the desalination performance of the MCDI system could be improved with increasing volume flows. It was shown that the SEC of the lab-scale MCDI could be reduced by >65% (e.g. E03) through the optimal setting of operating parameters when using larger systems (larger modules or several modules connected in series).

Due to the interdependence of various MCDI operating parameters (see previous sections), when setting different volume flows, all other parameters must also be adjusted (several independent variables). Therefore, a direct comparison of the experiments E01-E03 was not possible. However, the results in Figure 4.1-19 show that a reduction in the specific energy requirement was possible for similar desalination targets, which is a promising result speaking for the up-scaling and implementation of larger pilot plants.
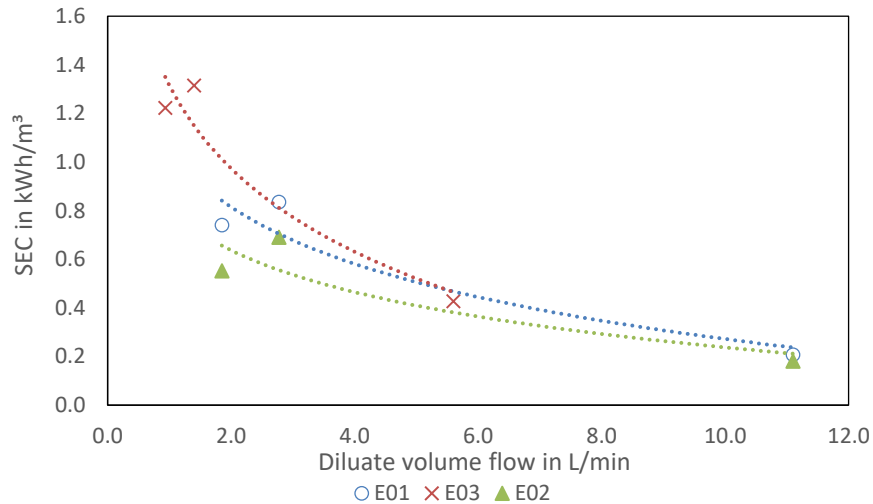
Figure 4.1-19 SEC over diluate volume flow for three up-scale experiments with lab-scale MCDI.

4.1.8 Lab-scale MCDI tests: summary

The laboratory tests and calculations were used for the designing of the pilot-scale plants in Sections 4.2 and 4.3. A summary of most important findings includes following points:

- By choosing different operating parameters, products of different quality can be produced and the SEC can be reduced if necessary

- Lower SEC was achieved by optimizing the operational parameters. This included using low volume flows during the regeneration phase and increasing the WR.

- Higher water flows with the use of larger modules lower the SEC value.

- The MCDI only showed lower SEC values than conventional RO in the range below 2 - 3 g/L NaCl.

- Additional improvement was achieved by up-scaling the MCDI system.

- The desalination concept for BW by use of LPRO+MCDI was defined for salinities in the range of 20-25 g/L.

- A comparison of the results of the laboratory tests and the pilot-scale tests in Vietnam with real water to investigate the dependency of the WR and the energy consumption is shown in Sections 4.2 and 4.3.

4.2 Pilot-scale MCDI (Concept A: low salinity)

The pilot-scale SAR+MCDI was installed for the **desalination of low saline brackish groundwater** (concept A) in a modular operation. The pre-treatment of the groundwater was carried out by means of the SAR subsurface removal process for As and Fe^{2+} removal (see Section 2.1.2). The plant was installed in the city of Tra Vinh, in the Mekong Delta, Vietnam.

4.2.1 Raw water measurements

The raw groundwater from the well was analysed at different times before commissioning in order to evaluate the changes in its quality and assess if any seasonal fluctuations occur. The results of the water analysis are summarized are in Table 4.2-1 showing an increased salinization with an EC value of 3.3 mS/cm, which corresponds to concentrations of TDS = 1.65 g/L.

Table 4.2-1 Analysis of raw groundwater at pilot site in Tra Vinh

Parameter	Unit	Sampling 2/8/2017[a]	Sampling 7/3/2018[b]	Vietnamese standard[c]
pH	-	7.2	6.9	6.5-8.5
EC	mS/cm	3.3	3.3	NA[d]
Cl^-	mg/L	858	955	250
NO_3^-	mg/L	11	NM[e]	50
SO_4^{2-}	mg/L	96.5	138	250
PO_4^{3-}	mg/L	BDL[f]	BDL[f]	NA[d]
Na^+	mg/L	342	374	200
K^+	mg/L	12	10	NA[d]
Ca^{2+}	mg/L	174	NM[e]	120[g]
Mg^{2+}	mg/L	111	110	NA[d]
NH_4^+	mg/L	2.3	2.1	3
t-As	mg/L	0.011	0.0026	10
Fe^{2+}	mg/L	1.7	1.8	0.3
Mn^{2+}	mg/L	0.68	0.26	0.3
TOC	mg/L	16.2	NM[e]	NA[d]

[a] Average from own measurements and certified commercial lab QUATEST3 (HCMC, Vietnam)
[b] Measurements at VGU lab
[c] Vietnamese national technical regulations on drinking water QCVN 01: 2009/BYT
[d] NA: not applicable
[e] NM: not measured
[f] BDL: below detection limit
[g] Calculated from $CaCO_3$ = 300 mg/L

Chloride and Na^+ maximum concentrations measured were 955 and 374 mg/L, respectively, which were almost four and two times higher than the established Vietnamese limit values for drinking water (QCVN:01, 2009). Measurements also showed elevated concentrations above the drinking water standard for Fe^{2+} = 1.8 mg/L, Mn^{2+} = 0.68 mg/L, t-As = 11 μg/L and

Ca^{2+} = 174 mg/L. The largest difference between the two sampling measurements was for As concentration, which could be attributed to naturally occurring fluctuations with possible levels above the WHO guideline value of 10 µg/L. The elevated TOC and NH_4^+ concentrations indicated human or animal contamination. These values were examined individually during the pilot.

A detailed overview on the parameters analysed and the results of the pilot trials were reported in Hellriegel et al., (2020).

4.2.2 Results SAR pre-treatment

The pre-treatment was necessary to lower the high dissolved Fe^{2+} concentrations that could damage the MCDI electrodes, and to lower the As content in order to allow the sustainable discharge of non-toxic brine.

The efficiency of the SAR process for the treatment of As was evaluated in two steps. First, the impact of **groundwater extraction** on the water quality was monitored during daily abstraction before SAR start (pre-commissioning, without infiltration cycles) for a period of 34 days. Afterwards, the SAR process started with daily abstraction and infiltration cycles. The **As removal efficiency** of the process was monitored during a period of 181 days. The long-term performance was studied over a period of two and a half years.

Pre-commissioning

For a period of 34 days, groundwater was extracted and its quality was monitored. Water samples were taken daily during the pre-commissioning stage (10 days), and finally on day 34 before starting the SAR process.

The results of the water analysis for relevant parameters are shown in Figure 4.2-1. During the 34 days extraction, the concentration for all dissolved salts remained relatively stable with the exception of t-As that increased to 4.8 µg/L by day 34. The 71% increase in t-As was a result of the influence of groundwater extraction and the natural As distribution/mobilization in groundwater. However, due to the small concentrations in µg-range, natural fluctuations and measurement uncertainty cannot be discarded. The As concentration was also linked to the rise in Fe^{2+}, which showed a slight increase to 2.2 mg/L only by day 10 (11% increase). However, no measurement for Fe^{2+} for day 34 was provided. It was assumed, that there was also a slight increase of Fe^{2+}.
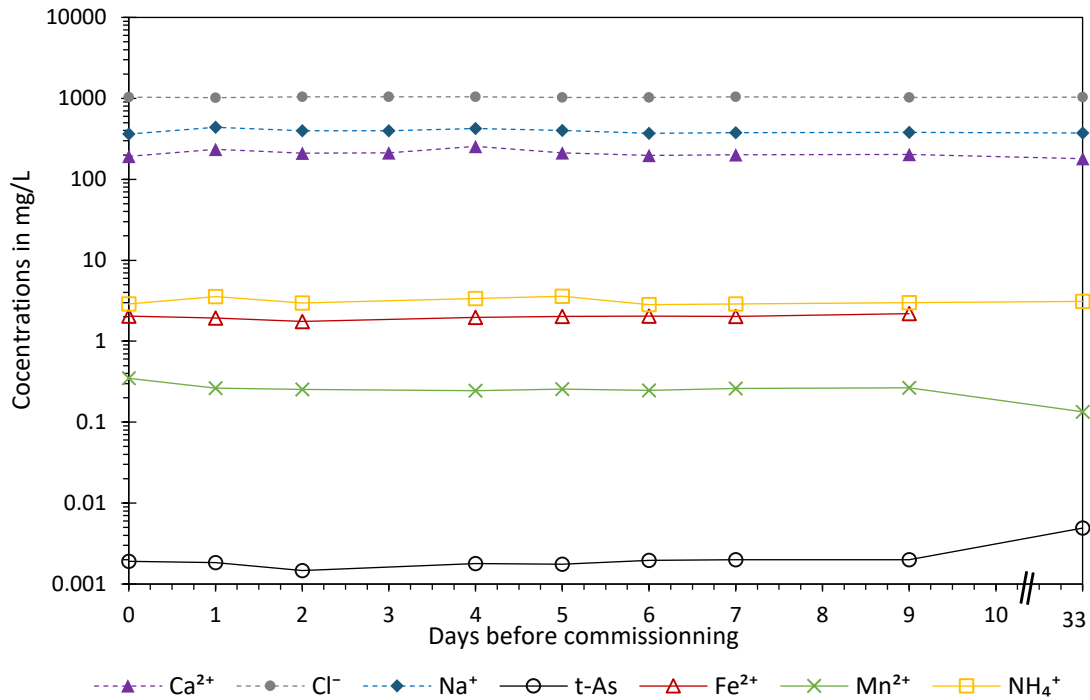
Figure 4.2-1 Groundwater monitoring before commissioning with daily groundwater abstraction (2-4 m³)

The concentrations measured during the 34 days before commissioning were averaged and considered as the **initial concentrations for the evaluation** of the SAR process which is explained in the next section.

Iron and As removal

The results for the first 181 days of operation of the SAR plant for the removal of Fe^{2+} and t-As including the pre-commissioning stage (days -34 to -1; Figure 4.2-1) are shown in Figure 4.2-2. Initial concentration of $c_{0,Fe}$ = 1.8±0.7 mg/L and $c_{0,As}$ = 2.3±1 µg/L were averaged from this period and are respectively indicated in the y-axes.

After the start of the SAR process (day 0), results show an **immediate decrease in Fe²⁺** within the first day of operation achieving a concentration of 0.05 mg/L by day two. This indicated that Fe^{2+} is effectively oxidized to Fe^{3+} already after the first infiltration cycles. However, Fe-concentrations spiked irregularly within the first 30 days and constant values below 0.1 mg/L were achieved only after day 37.

The irregular increases in the Fe^{2+} concentrations can be explained by minor technical problems during the operation of the pilot plant that caused incomplete infiltration (marked in red. The CDC controller automatically initiated the SAR infiltration cycles based on water consumption. By not maintaining a correct extraction/infiltration ratio, oxidation zones provided by the infiltrated oxygen cannot maintain the adsorption required for the amount of

extracted water (Luong et al., 2019). Over-extraction can not only lead to contaminants leakage but also to iron-incrustations and blockage on well and pump.

Some technical failures during the course of the pilot trials included feed pump failure due to corrosion and groundwater extraction above the plant capacity of $V_E = 8.3 \text{ m}^3$ (over-extraction). Additionally, the water meter was blocked due to particles coming from the well. This is a common feature seen from constructed wells that are not properly sealed.
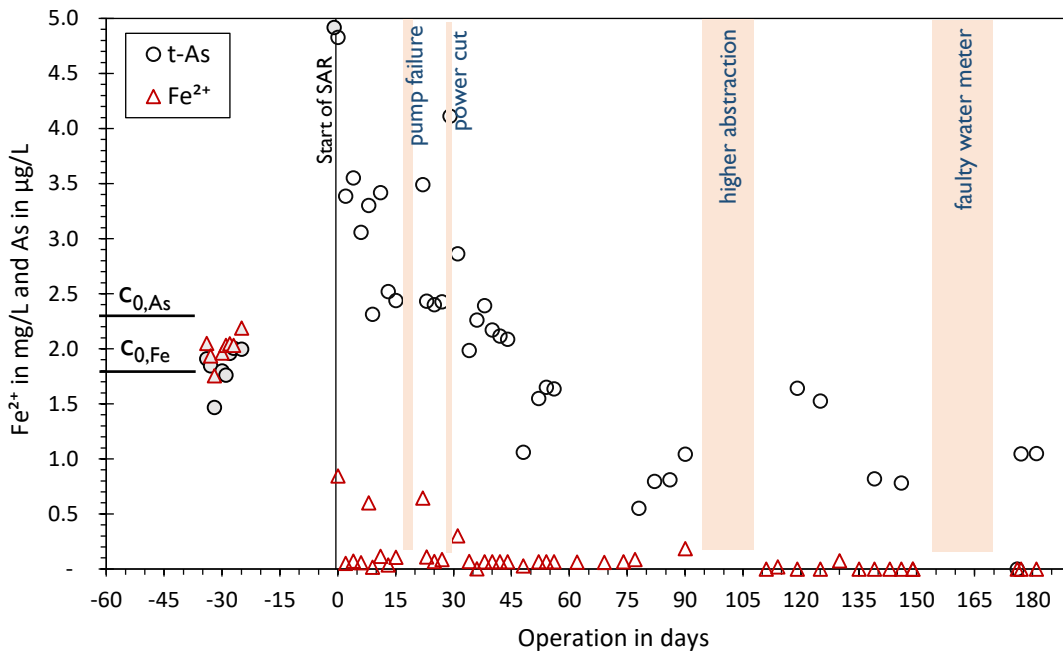
Figure 4.2-2 Arsenic and Fe²⁺ groundwater concentration development during SAR operation (infiltration/abstraction stops marked in pink)

The As concentration was lowered slowly but continuously following the removal of Fe^{2+}. Values of 0.55 µg/L were reached on day 78, corresponding to **As elimination rates of 76%**. Increases in Fe^{2+} caused the leakage of As with the highest t-As concentration increase from 1.0 to 1.6 µg/L measured from day 91 to 120, until normal operation restarted from day 120.

Arsenic levels remained low thereafter with a concentration of 1.0 µg/L measured on day 181 corresponding to a removal of 54%. Elimination rates for t-As achieved by SAR were acceptable for an already significantly low background concentration of $c_{0,As} = 2.3$ µg/L. Previous studies carried out also in South Vietnam showed that a removal of concentrations of $c_{As} = 80$ µg/L to below 5 µg/L was also possible by means of SAR (Cañas Kurz et al., 2020).

Manganese and NH₄⁺ removal

Manganese and NH_4^+ are also present in groundwater of Southeast Asia, and are important reducing agents in the water and therefore, important oxygen consumers in the SAR process.

For that reason, it was of peculiar interest to study the removal of Mn^{2+} and NH_4^+ from the water to assess the efficiency of SAR.

Results for Mn^{2+} and NH_4^+ removal are shown in Figure 4.2-3. The initial concentration of Mn^{2+} of $c_{0,Mn}$ = 2.4 mg/L dropped linearly to below 0.06 mg/L within the first seven days of operation, indicating a **Mn^{2+} removal of 75%**. However, increases in Mn^{2+} were observed throughout the first 70 days of operation. The spikes in Mn^{2+} first followed the rises in Fe^{2+} (three spikes on days 8, 22 and 31) with the latter peak (day 31) resulting in a concentration increase for Mn^{2+} on following days (34 and 38). Subsequently, rises on Mn^{2+} continued but not exceeding the initial value of $c_{0,Mn}$ = 2.4 mg/L even though the concentrations of Fe^{2+} were stable from day 36. The **slower decrease in Mn^{2+}** was associated to the oxidation mechanisms in groundwater, which are fundamentally driven by microbial activity and only partly driven by chemical oxidation. The first decrease seen in Mn^{2+} concentrations was related to a chemical oxidation of Fe^{2+} and Mn^{2+} through the SAR process, which was given by the unusual high temperatures of ca. 28-30°C, and the adsorption onto the soil grains and coating of oxides.
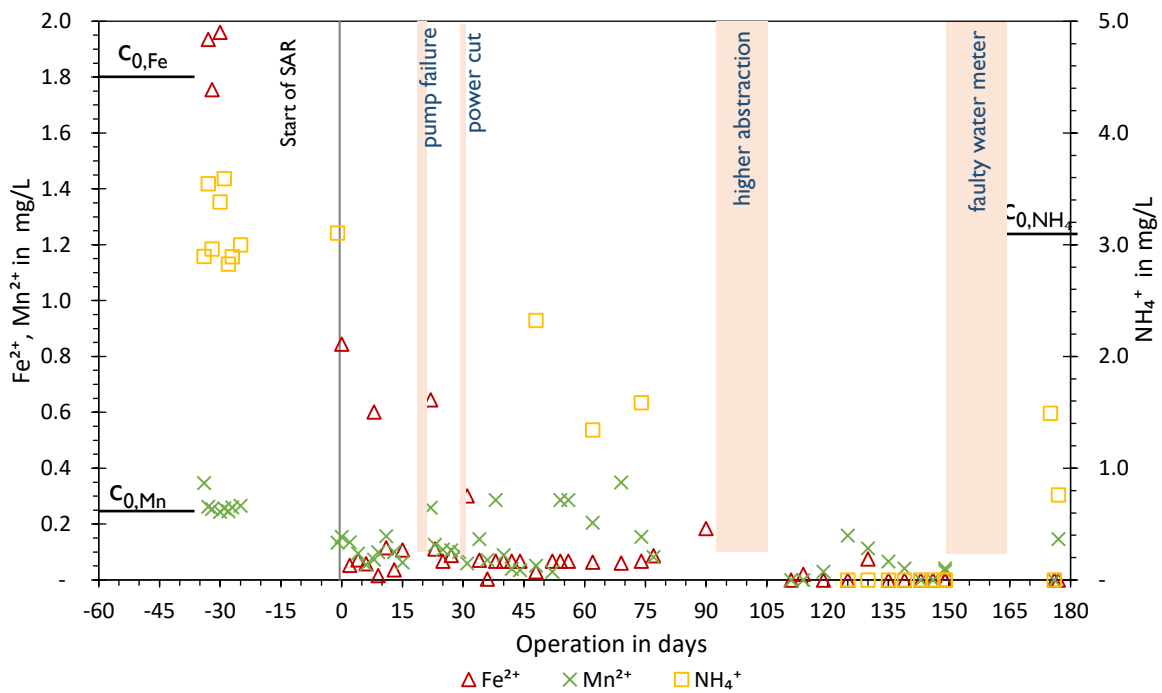
Figure 4.2-3 Ammonium, Fe^{2+} and Mn^{2+} groundwater concentration development during SAR operation (infiltration/abstraction stops marked in pink)

The initial concentration of NH_4^+ in the raw groundwater was lowered from initial concentrations of $c_{0,NH4+}$ = 3.1 mg/L to an average of 1.2 mg/L by the end of the trials (days 175- 81) corresponding to a **NH_4^+ removal of 65%**. Concentrations below detection limit of 0.05 mg/L were achieved in operation days 125-150. However, after the technical failures

between days 155 and 170, the concentration of NH_4^+ rose to levels above 1 mg/L, but below initial raw water concentrations due to over-extraction.

Results showed that **the removal of NH_4^+ was considerably slower** than the removal of Mn^{2+}. Similar to Mn^{2+}, ammonium mitigation through SAR is based on its biological oxidation to nitrate (NO_3^-). Generally, the oxidation of Mn^{2+} can only take place after complete nitrification due to the necessary evolution of the redox potential (Gouzinis et al., 1998; Luong et al., 2018). However, the slow NH_4^+ mitigation could be associated to the unfavourable Eh-pH conditions given by the natural anoxic hydro-geological settings.

The removal of Mn^{2+} and NH_4^+ was also investigated in a previous study on SAR (Cañas Kurz et al., 2020). Results were not included in this dissertation but showed that after the microbiological build-up the oxidation reactions were much shorter and a mitigation, even after concentration rises or leakage due to process interruption, was feasible. This indicated that once the removal of Mn^{2+} was established, the microorganisms responsible for the oxidation remained active and can drive the mitigation process.

In general, the results showed an exceptional removal rate for Fe^{2+}, and a slow but continuous removal for t-As, Mn^{2+}, and NH_4^+ after 181 days of operation. Furthermore, **no breakthrough above the limits for drinking water standard** was observed for any species even though technical failures occasionally interrupted the SAR process. This shows the feasibility and stability of the As remediation through SAR.

Further research on the behaviour of the ammonium-oxidation is needed to critically evaluate the role of microbial oxidation in the long-term during SAR.

4.2.3 Results MCDI desalination

Desalination of groundwater at pilot location was carried out by use of the MCDI pilot-scale plant. The general goal was to achieve drinking water quality with a diluate concentration < 450 mg NaCl/L or < 600 mg TDS/L, respectively (WHO guidelines for "good" drinking water; WHO, 2017).

The desalination with the MCDI started after the pre-treatment with SAR was running steady on day 112 (e.g. Figure 4.2-2). This also ensured that the concentration of Fe^{2+} in groundwater was in compliance with the recommended permissible inlet concentrations of $Fe^{2+} < 0.5$ mg/L provided by the manufacturer (Voltea, 2016b).

Specific adsorption and salt removal efficiency RE

Results showed an overall **desalination efficiency of 75%** TDS removal to produce diluate of 188 mg/L on average. The desalination was tested with different operational parameters based on the laboratory-experiments with feed water quality 3.3 mS/cm (see Section 4.1.6).

Additionally, the adsorption efficiency for selected ions was evaluated. The results are summarized in Figure 4.2-4, which shows the elimination rates for ionic species at their given averaged inlet concentrations (MCDI inlet after SAR treatment). Samples of the MCDI feed and diluate were taken between operation days 112 and day 181.

Results showed that the **electrosorption of the bivalent ions** was higher than monovalent ions with specific ion removals for Cl^- and Na^+ of 90% and 75%, respectively while adsorption of up to 97% were achieved for Ca^{2+} and Mg^{2+}, indicating a stronger selective adsorption of bivalent cations as shown in literature (Suss, 2017).

However, lower sulphate (SO_4^{2-}) mitigation was observed with only 54% adsorption. The lower SO_4^{2-} removal was explained by the increasing hydrated radius and decreasing permeability of SO_4^{2-} in comparison to bivalent Ca^{2+} and Mg^{2+} cations (Li et al., 2016; Tansel et al., 2006). Yet, the high incertitude in measurements particularly in the outlet concentrations (average concentration inlet: TDS = 111±19 mg/L, and outlet: TDS = 51±21 mg/L) indicated a larger averaged removal was possible and further evaluation of the measurements is needed.
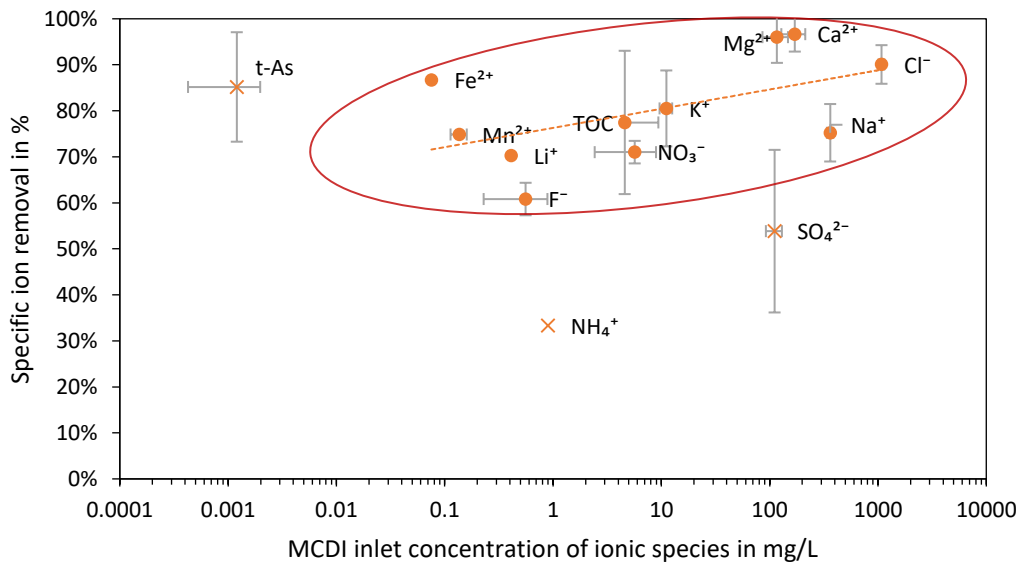
Figure 4.2-4 Average specific removal of MCDI for different ionic species and TOC in dependence of inlet concentration. Dotted line gives the logarithmic approximation for selected ions (circled in red). Error bars show the standard deviation of the averaged values.

The t-As concentration of averaged 1.2 μg/L after the SAR treatment was lowered with the MCDI desalination to below 0.18 μg/L, indicating an **additional As removal of 85%**. Although no speciation between As(V) or As(III) was carried out, the high t-As removal may indicate that the oxidation after the SAR process was successful and As(V) prevailed. Iron adsorption was of Fe^{2+} 87% while 75% Mn^{2+} was removed.

Model vs. real water

The MCDI pilot-scale plant was tested both in the laboratory with model water (NaCl) and at the pilot site. A summary of the operational parameters and the results of both tests is given in Table 4.2-2.

Table 4.2-2 Evaluation results of MCDI pilot-scale plant at pilot site and laboratory

	Parameter	Unit	Pilot site	Lab-tests
Operational parameters	Constant current (charge phase)	A	50	12.3
	Constant current (discharge phase)	A	66	54.1
	Voltage limit	V	1.3	1.3
	Water flow (charge phase)	L/min	1	0.4
	Phase time (charge phase)	s	45	440
	Cycle time	s	135	630
Performance indicators	Feed EC	mS/cm	3.12	3.29
	Feed TDS concentration [a]	mg/L	1560	1645
	Diluate TDS concentration [a]	mg/L	188	410
	TDS reduction	mg/L	1372	1235
	Product rate	L/d	477	400
Evaluation results	SEC [b]	kWh/m^3	1.75	0.97
	Water recovery WR	-	33%	65%
	TDS removal RE	-	88%	75%
	SEC for removal SEC$_{rem}$	Wh/g	0.39	0.46
	Charge efficiency	-	75%	77%

[a] TDS Calculated from EC (NaCl, K = 0.5)
[b] Power consumed by desalination module only

Energy requirements SEC

A comparison of the SEC of both tests showed a higher energy consumption at pilot site with SEC_{MCDI} = 1.75 kWh/m^3 versus SEC_{MCDI} = 0.97 kWh/m^3 achieved in the laboratory. However, a higher salt rejection of 88% vs. 75% was achieved at pilot site. In total, the average energy consumption for the operation of the SAR and MCDI module was 11.6 kWh per day.

The SEC was calculated considering only the required power for the desalination module. However, an analysis of the energy consumption in total revealed that the component with the

highest energy requirement was the power supply. Due to inefficiency in energy conversion, the energy efficiency of the power supply was as low as $\eta = 20\%$ (power supply inlet vs. power output). In larger commercial modules, higher energy efficiency η is achieved by a design that allows a more efficient AC to DC conversion from 230 V (grid) to a specific low voltage <2 V and high ampere range for the MCDI operation. Experiments with larger modules have shown an efficiency of the power supply conversion of $\eta > 0.75$ is possible.

Water recovery WR

The pilot-scale plant was able to produce more (477 L/d) and better quality water (TDS = 188 mg/L) in comparison to the laboratory tests, so that an optimization of the operational parameters (higher diluate flow rate) should allow the increase in WR while still achieving drinking water quality. Following the results of the lab-scale MCDI tests at HKA (e.g. Section ▯) the increase in WR would lead to an increase in diluate salinity but also to the reduction of the SEC. However, the variation of the operational parameters at pilot site after commissioning was very limited and an extensive optimisation of the operational parameters was not possible.

The comparatively low WR of 33% at pilot site vs. 65% achieved in lab-scale showed that the operational parameters on the pilot site could be still optimized for a more efficient MCDI operation (see also) Additionally, the size of the module could be increased to treat the water under pilot conditions with higher WR and lower SEC.

Specific energy consumption for salt removal SEC$_{rem}$

Additionally, the evaluation of the specific energy requirements for removal SEC$_{rem}$ revealed that the operation of the MCDI at pilot trials yielded a more efficient desalinisation with in average 0.39 Wh per grams removed, while the tests with model water showed a SEC$_{rem}$ of 0.46 Wh/g.

In general, the comparison of the pilot-scale plant performance with the lab-scale MCDI, the pilot plant achieved higher desalination RE and a better efficiency for SEC$_{rem}$. This gave further evidence to prove that **larger plants yield better performance results**, as well as emphasized in the importance that operational parameters must be adjusted individually to obtain the best results possible.

4.2.4 Renewable energy supply

The SAR+MCDI pilot-scale plant was supplied with renewable energies by use of solar PV (3 kW$_p$) and a small wind turbine (2 kW$_p$). The PV production, and the power demand of the plant were used to evaluate the efficiency and autonomy of the power supply including the local data obtained with a weather station.

Weather data

A weather station assembled at the HKA was set up on the rooftop of the household to monitor wind direction, wind speed, ambient temperature and solar radiation at the pilot site location. An overview of the recorded data gives Table 4.2-3 showing that monthly radiation averaged at 338±53 W/m^2 while the maximum radiation values ranged between 990-1215 W/m^2 (average = 1122±69 W/m^2). Additionally, wind data showed average speeds of up to 16 m/s. All measurements were in agreement with literature values (AHK Vietnam, 2019) and gave a specific insight to the exact site location.

Table 4.2-3 Average monthly weather data at pilot site for the period from May 2018 to December 2019

Parameter	Jan	Feb	Mar	Apr	May	Jun	Jul	Aug	Sep	Oct	Nov	Dec	Ave.	Std. dev.
Ave. temp. (°C)	26	27	27	30	30	29	28	29	27	29	28	27	**28**	**±2.7**
Max. temp. (°C)	32	31	33	37	40	39	37	36	37	37	38	35	**36**	**±2.9**
Min. temp. (°C)	22	24	22	25	23	23	23	24	23	23	11	22	**22**	**±5.3**
Ave. radiation (W/m²)	286	406	426	395	333	295	306	394	252	385	318	271	**339**	**±53**
Max. radia. (kW/m²)	1.12	1.02	1.19	1.17	1.17	1.11	1.15	1.14	1.21	1.00	1.11	1.09	**1.12**	**±0.7**
Ave. wind speed (m/s)	7.4	4.6	4.1	3.6	3.3	3.9	4.0	4.5	2.5	3.6	3.9	3.9	**4.1**	**±1.1**
Max. wind speed(m/s)	15.6	11.3	11.1	9.5	16.2	14.6	11.4	13.3	10.1	9.8	13.6	13.5	**12.5**	**±2.2**
Wind direction (°)	W	NW	S	S	E	E	E	E	E	W	W	W	**E**	**-**

Power generation with PV

Measurements of solar radiation at the pilot plant location and the results of the PV panels for the acquisition period between May 2018 and December 2019 (monthly averages) are shown in Figure 4.2-5. Additionally, the difference to the maximum theoretical energy production of the PV modules was calculated from the mean daily irradiation measured by the weather station of 135 kWh/d and the module efficiency of 18% specified by the manufacturer for standard conditions (T = 25°C; 1000 W/m^2). With an average of 339 kWh/m^2 radiation a theoretical production of 24.0±5 kWh/d was calculated. The **average daily power production** by the PV panels resulted in **11.2±1.3 kWh/d** which resulted in an average energy loss of 53% with respect to the theoretical value and an efficiency of the PV-system of 8.5±2%.

The efficiency losses due to high ambient temperatures of 30°C and a considerable increase in surface temperature of the modules above standard conditions are caused by ohmic losses, which can be estimated to -0.48%/K above 25°C (26% at 80°C). The lower efficiency (-20%)

could be attributed to PV orientation and inclination, and soiling (accumulation of dust, dirt, etc.) but also due to possible parasitic resistances due to module quality (Vidyanandan, 2017).
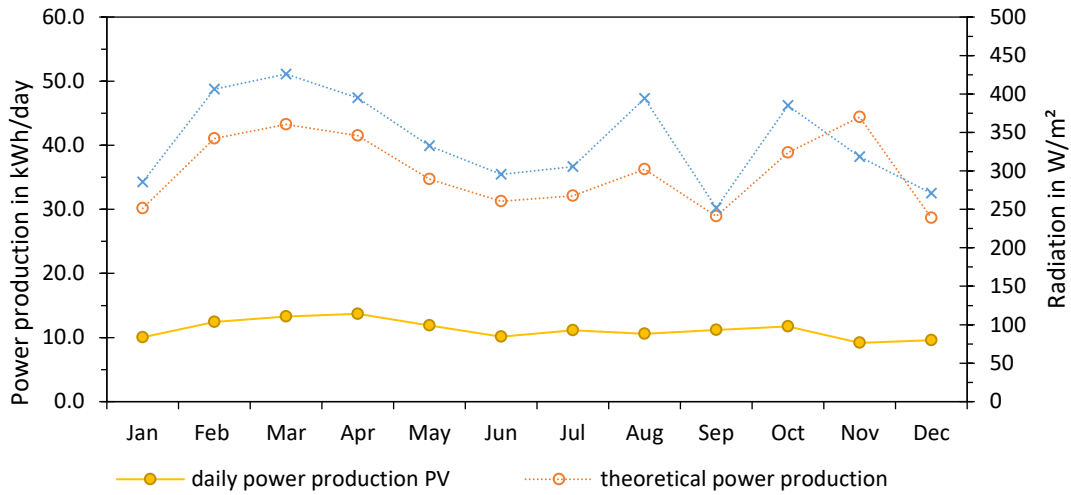
Figure 4.2-5 Daily averaged solar energy PV production (solid circles) for each month in 2019 vs. theoretical supply (dotted, circles) calculated from mean solar radiation at pilot location (dotted, cross; measurements taken from May 2018 to Dec 2019).

Power generation with wind turbine

Additionally, the wind turbine produced in average during the tested time only 142±14 W which was a result of the low average wind speed of 4.1±1 m/s. The typical power generation of the small wind turbine during four different measurements is illustrated in Figure 4.2-6.
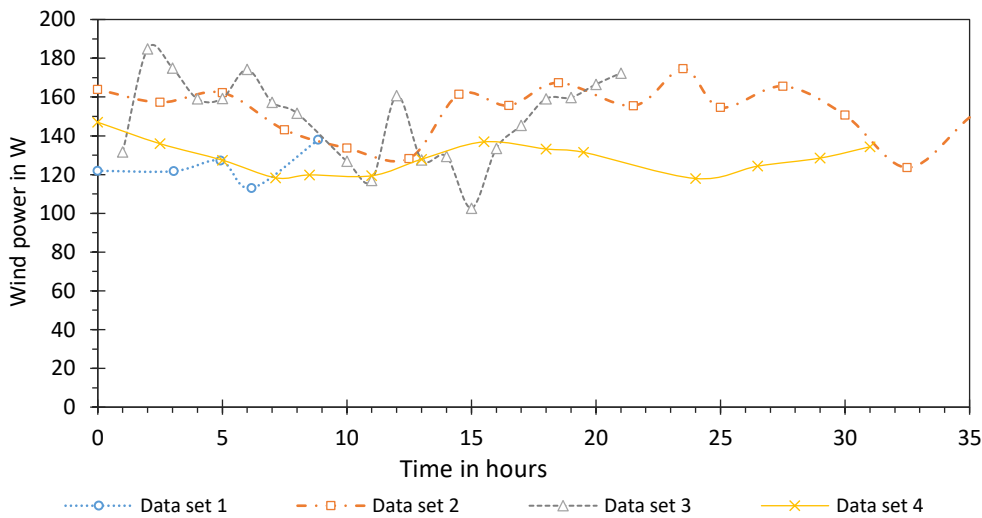
Figure 4.2-6 Measurements of power production from wind turbine at pilot site.

In comparison to the expected power curve from the wind turbine (Hummer, 2020) the output values obtained for the 4.1 m/s wind speed are in line with the data sheet so that the total energy production from wind was 3.4±0.3 kWh (Figure 4.2-7).

A detailed analysis of the average power production over wind speed revealed that stronger wind speeds of up to 20 m/s did not yield the theoretical increase of power. However, this might be due to the low average and irregular occurrence and speed. The wide range of average wind speed is shown in the error bars of the measurements in Figure 4.2-7a.
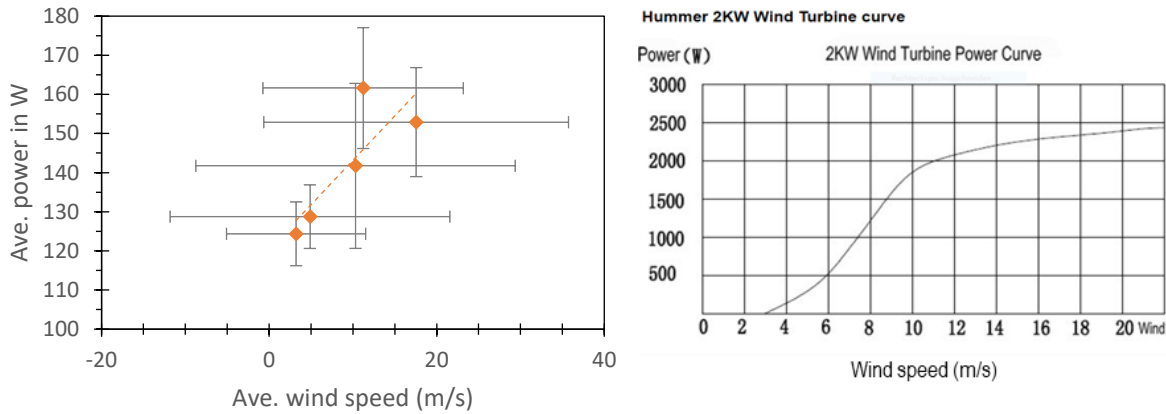
Figure 4.2-7 Relationship between power production and wind speed: measured (left) and theoretical (right) values.

In general, the wind turbine could not be operated continuously due to noise complaints from neighbours and the power generation of the 2 kW$_p$ wind spot was very low. But the weather station registered max. wind speeds of more than 12 m/s which corresponded to a power of over 2000 W according to the 2 kW wind turbine power curve (Hummer, 2020). While the potential was much higher than the actual average power output of 142 W, the use of wind energy in residential areas is still in need of improvements regarding energy production, noise protection, and lowering investment costs.

Energy supply and demand at pilot site

The daily PV power generation and power consumption is shown in Figure 4.2-8a-d for four different scenarios. Figure 4.2-8a shows the **typical power production** of the PV panels (blue line) on a clear-sky and sunny day with no power consumption or load (purple line; load = 0).

The power production stretched from 5:30 to 18:00 to a total of 12-13 hrs per day with an average peak power output of P_{peak} = 2060 W. When there was no power consumption, the generated power was fed to the grid (net-metering), which is shown by the yellow line.
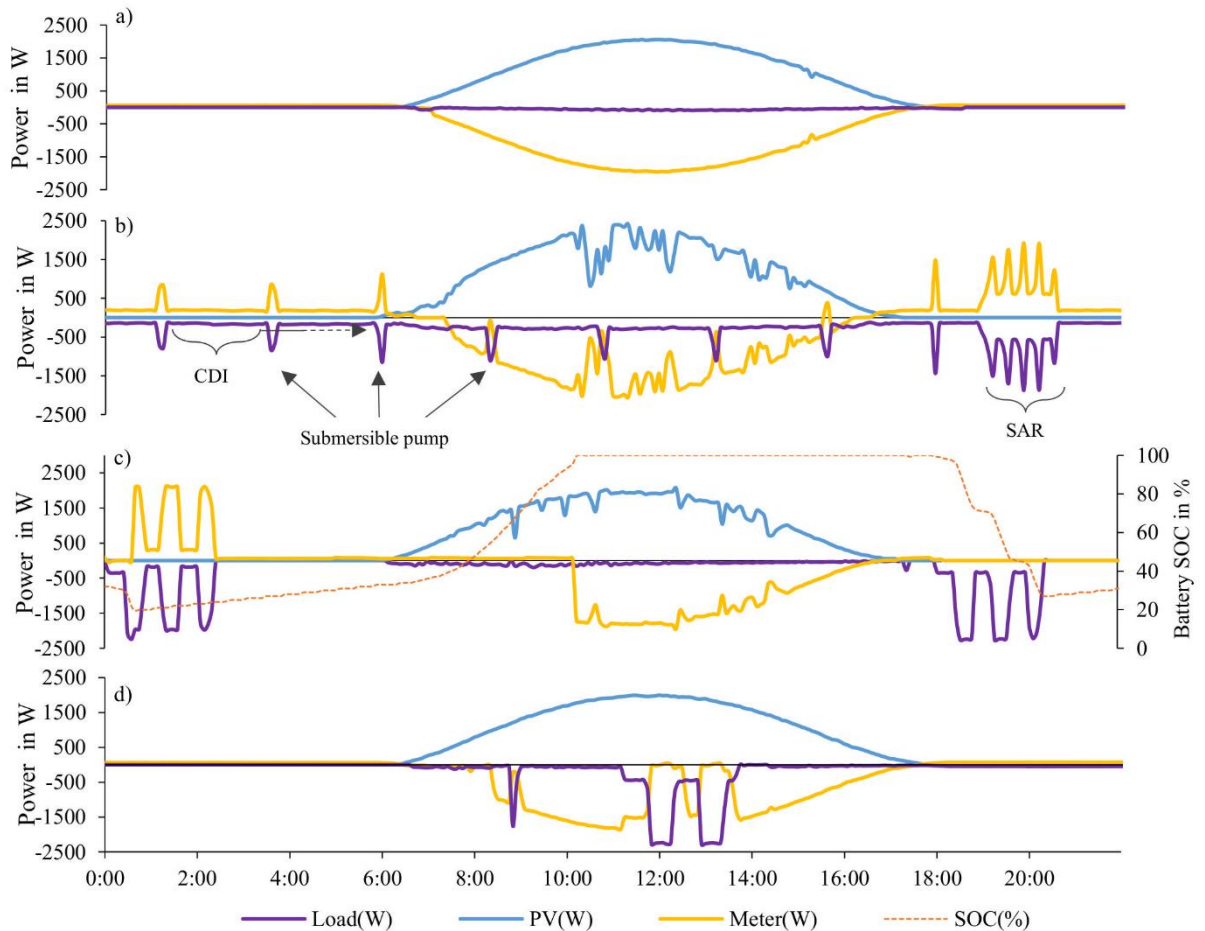
Figure 4.2-8 Typical solar power generation (PV, blue line) at pilot-scale plant for four different scenarios: a) without consumption and feed onto grid (yellow line); b) with typical consumption (Load = *MCDI + pump + SAR*, purple line); c) using battery for semi-autonomous supply (dotted line); and d) autonomous supply for one SAR cycle operation during day time.

Figure 4.2-8b shows the **on-grid operation** of the SAR+MCDI plant. The supply of the pilot-scale plant is given by the purple line, which shows the load of the SAR and MCDI at a typical daily operation. Results showed the power consumption of the MCDI desalination (24 hours operation) with averaged P_{MCDI} = 190 W, the SAR process including abstraction and infiltration cycles with the SAR pump, P_{SAR} = 390 W (beginning at 18:00), and the submersible pump for feeding T1 with averaged $P_{feed\,pump}$ = 1290 W (periodically during the day, more frequent during SAR operation). Here, the load was supplied by the grid during night time (yellow line: positive) and by the PV after sunrise (06:00).

The addition of the power production (blue line, positive) and the load (purple line, negative) equals to the amount of energy supplied by or fed into the grid (yellow line, positive or negative, respectively). Figure 4.2-8c shows the **semi-autonomous supply** for the SAR when using both battery (orange line) and grid for two infiltration cycles during the night at 18:00

95

and 00:00. Following the discharge of the battery (orange line) after the first SAR cycle (18:00), the second SAR cycle (00:00) was supplied directly from the grid (yellow line). Battery recharge for the next cycle was powered by the PV and completed around 10:15 (state of charge SOC = 100%). After this, the energy produced was fed into the grid (net-metering: yellow line decreasing) following the absolute values of the power production (blue line).

In Figure 4.2-8d, the **autonomous operation** of the SAR process was tested. For this, the operation of SAR was shifted during day time (one infiltration cycle) in order to use the solar energy production more efficiently and minimize battery capacity.

The operation of the combined plant MCDI+SAR (two infiltration cycles) during the day could enable an off-grid operation without battery and 100% autonomy. However, the operation of MCDI in 10-12 hours instead of 24 h would yield less product water, which was not an option tested within this pilot.

Total energy consumption

An analysis of the power requirements and the SEC of the SAR + MCDI process including pumping is shown in Figure 4.2-9. The feed pump had the highest power demand (P_{Pump} = 1.29 kW) followed by the SAR (P_{SAR} = 390 W) and the MCDI with around 190 W ($P_{MCDI,PS}$ = 130 W and $P_{MCDI,pump}$ = 60 W). The actual SEC of the four components is divided in Figure 4.2-9b showing a different breakdown of the energy usage for the production of 1 m^3. With an average of 0.9 kWh/m^3 the SAR process and the water delivery with the feed pump had the lowest energy requirements, followed by the MCDI with 2.2 kWh/m^3. The difference in the SEC can be attributed to the different capacities (maximum) which each plant or component was run at. The SAR process including the feed pump delivered 3.64 m^3 in average per day (maximum capacity 8.3 m^3/day), while the MCDI produced in average only about 0.5 m^3 desalinated water per day.

In total, the average SEC for the operation of the SAR and MCDI module was 3.97 kWh/m^3 with a power consumption of 11.6 kWh per day. By use of PV supply only, a **97% degree of autonomy** was achieved with a total energy production of 11.2 kWh. The energy deficit was supplied by the electricity grid. By adding the power generation of the wind turbine, the degree of autonomy increased to 126% and a surplus of 3.0 kWh/d of electrical energy was fed into the grid to increase the electricity revenue and decrease amortisation time.

In general, the **off-grid operation** showed the great technological potential for the use of PV in Vietnam. In order to achieve higher degree of autonomy and pursuit an off-grid operation, desalination and treatment consumption not only need to be as efficient as possible, but also, the work-load and operation times (load profile) must be planned in such way, that peak-loads can be minimized.

a) Power output (W)

b) SEC (kWh/m³)

21%

3%

7%

69%

■ Feed pump ■ MCDI
■ Pump CDI ■ SAR

22% 23%

11%

44%

▨ Feed pump ▨ MCDI
▨ Pump CDI ▨ SAR
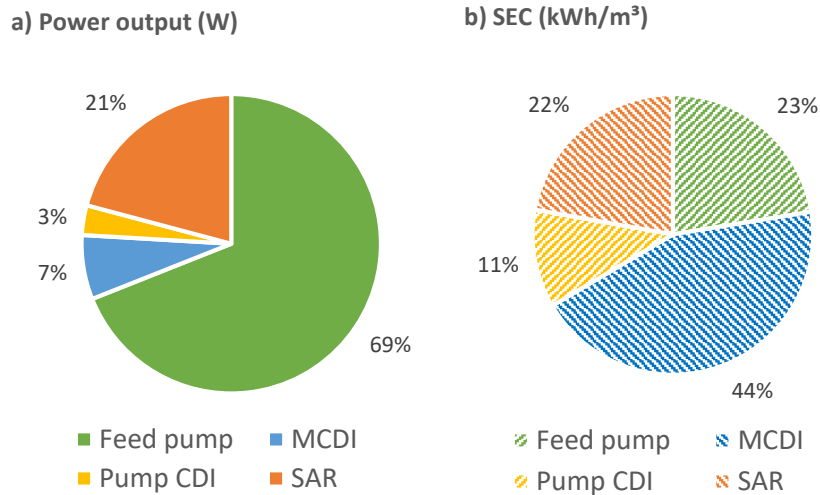
Figure 4.2-9 SAR+MCDI pilot-scale plant: a) power requirements breakdown (total = 1870 W$_p$) and b) averaged SEC distribution (SEC$_{total}$ = 4.0 kWh/m³).

4.2.5 Performance evaluation SAR+MCDI system

The operating parameters of the pilot-scale tests were based on the settings of the lab-scale MCDI system. However, desalination phases were shortened and current used was increased in order to comply with the drinking water limit values. These measures reduced the yield of the system from 64% to WR = 33%.

In contrast to the laboratory tests at the HKA, the MCDI plant showed higher RE but higher SEC = 1.75 kWh/m³. Optimizing parameters included reducing the volume flow in the regeneration phase, showed increase of WR. Desalination with the MCDI module powered by only the PV system was possible at a high degree of autonomy. The total energy consumption of the SAR+MCDI system including the pump was SEC = 3.0 kWh/m³.

Favourable ambient conditions and the low pressure loss in the MCDI module (<500 mbar) could allow a construction without the use of a pump by using a gravitational flow or the remaining kinetic energy of the water through the well pump. The SAR+MCDI plant was able to successfully produce 0.48 m³ of drinking water and 3.16 m³ of washing water (of a potential 8.3 m³ treated underground) per day. By use of the 3 kWp solar PV system, a theoretical degree of autonomy of 97% was achieved for the entire treatment process (SAR + MCDI). A degree of autonomy of 127% is possible when using the wind turbine. However, the noise pollution caused complaints in the neighbourhood and the turbine had to be switched off.

4.3 Pilot-scale LPRO+MCDI (Concept B: high salinity)

The LPRO+MCDI pilot-scale plant was installed for the **desalination of high saline river** water (24 g/L) and followed a modular concept: the combination of both technologies LPRO+MCDI was used to produce drinking water while the LPRO yielded product water for household or other purposes. The pilot-scale plant was designed based on the concept developed in 4.1 (Concept B), the lab-scale results in ▯, and the conditions at pilot-site in the Thien Lieng Commune in Can Gio.

4.3.1 Raw water quality

The river water quality at the selected pilot are shown in Table 4.3-1. Water analysis were taken from the surface (0 m) and at a depth of 2 m. In addition, the river water was characterized hourly over the course of a whole day, especially with regard to TSS and salinity.

The analysis results showed an average conductivity of the river water of EC = 38 mS/cm, (TDS = 24 g/L; with K = 0.64). Compared to seawater (30-42 g/L), the relative salinity of the river water at the pilot site was was about 60-80%. Also high TSS of up to 345 mg/L with a large fluctuation range (145-345 mg/L) were identified, which was an important parameter for the later design of the pre-treatment.

When examining the water quality at different depths, the analyses showed that solids accumulation occurred in greater depths of the river with TSS values doubling from 63 to 140 mg/L already at a shallow depth of only 2 m. Figure 4.3-1 shows the quality of a shallow river side stream.

Can Gio Biosphere reserve (CC-BY-SA-3.0)

Thien Lieng river, side stream (03-2020)
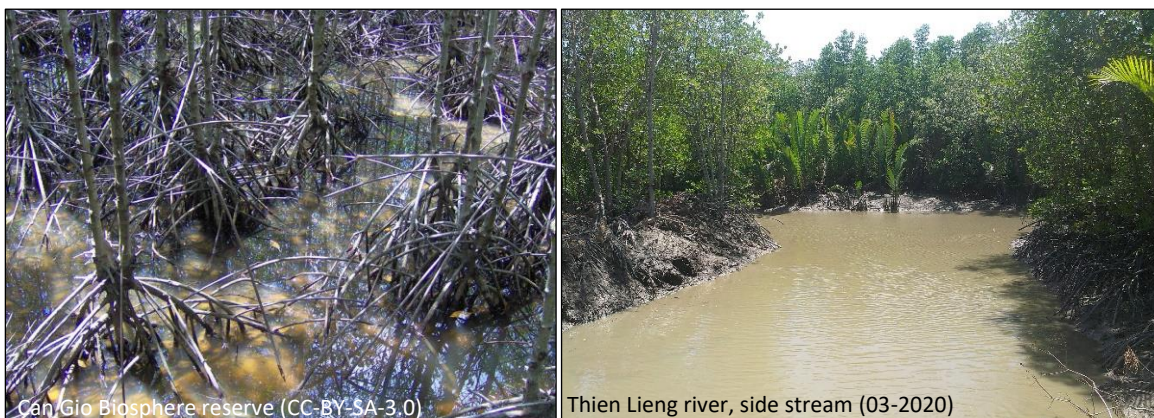
Figure 4.3-1 Mangrove estuary in Thien Lieng, Can Gio.

In addition, the results showed an increase in the Fe^{2+} and Mn^{2+} concentrations in the sample at 2 m depth, caused most likely by the higher TSS content.

Table 4.3-1 River water quality at pilot site location for LRO+MCDI pilot plant

Parameter		Sample 0 m[a]	Sample 2 m[b]	Concentration range[c]			Avg.[c]	Std. dev.
Temp.	°C	30.2	30.1	N/A[d]			N/A[d]	-
pH	-	7.4	7.4	N/A[d]			N/A[d]	-
LF	mS/cm	35.9	35.7	33	-	42	38	±3
Turbidity	NTU	N/A[d]	N/A[d]	81	-	256	169	±70
TSS	mg/L	62.5	140	145	-	345	229	±57
Fe^{2+}	mg/L	0.26	0.53	N/A[d]			N/A[d]	-
Mn^{2+}	mg/L	0.002	0.04	N/A[d]			N/A[d]	-
Na^+	mg/L	6956	6998	4048	-	7968	5704	±1204
K^+	mg/L	239	134	203	-	316	256	±37
Ca^{2+}	mg/L	242	267	158	-	738	417	±232
Mg^{2+}	mg/L	821	502	331	-	1082	662	±272
Cl^-	mg/L	14157	14215	16590	-	21894	19783	±1535
SO_4^{2-}	mg/L	1720	1728	1873	-	2144	1988	±89
TC	mg/L	32.7	33.4	24.3	-	162	81	±59
TOC [d]	mg/L	9.6	11.4	6.5	-	N/A[d]	21	±30
TIC	mg/L	23.1	22.1	17.7	-	152	60	±56
HCO_3^- [e]	mg/L	117	112	89.8	-	774	306	-
TN	mg/L	N/A[d]	N/A[d]	0.24	-	0.31	0.27	±0.03

[a] Sample from river surface (26.03.2019)
[b] Sample from 2 m depth (26.03.2019)
[c] Samples taken between March and September 2020
[d] Dissolved TOC, after filtration (0.45 μm)
[e] Calculated from TIC

Figure 4.3-2 also shows the changes in conductivity measured over one day, which correlated well with the daily fluctuations in the water level (Cau-ca.com, 2020). During high tide, the effect of seawater intrusion on the river basin is higher. The large fluctuations in conductivity (33-42 mS/cm) were an indication for the influence of **seawater intrusion** on the salinity (TDS) of the river due to the **maritime tidal effects**. At high tide, seawater intrusion is higher. At low tide, the hydraulic currents of the seawater are lower than the inflow of fresh water by the riverine tide and the saltwater intrusion is reduced.

In addition to the daily tidal fluctuations, **seasonal variations** in TDS and TSS were also taken into account to assess the modularity and adaptability of the concept defined in Section 4.1. The large fluctuation ranges measured in the analyses between March and September were an indication of the differences between the dry and rainy seasons. These results were compared with TDS and TSS values from the literature at four different locations in Can Gio near the pilot site (Thanh-Nho et al., 2018). These are summarized in Table 4.3-2. Measurements revealed that the fluctuation in TDS during wet season is lower and that the highest salinity are both similar at ca. 29 mS/cm during high tide. However, a larger difference in salinity was identified at low tide, with a min. TDS value of 7.4 g/L and as low as 0.2 g/L for dry and wet season, respectively. The max. TSS was measured to 207 and 283 mg/L.
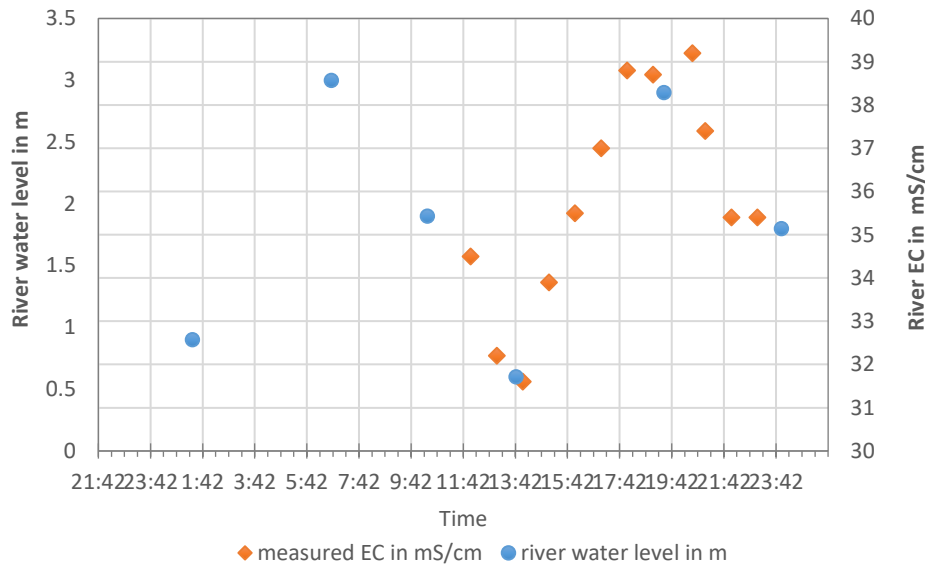
Figure 4.3-2 Hourly fluctuations in river water level (Cau-ca.com, 2020) and measured salinity during wet season (September) at pilot site.

Table 4.3-2 Literature TDS and TSS values at Can Gio (Thanh-Nho et al., 2018)

	Dry season					Wet season				
	Average	Std. dev.	Min.		Max.	Average	Std. dev.	Min.		Max.
TDS (g/L)	18.2	±6.5	7.4	-	26.1	13.1	±7.9	0.2	-	25.6
TSS (mg/L)	70.5	±49	16	-	207	73.9	±63	22.8	-	283

4.3.2 UF pre-treatment

For the reduction of TSS a UF-membrane ($8\,\mathrm{m}^2$) was installed as pre-treatment (See Section 3: Materials and Methods). Water samples and measurements on site showed a **reduction in TSS and turbidity of 99.1% and 99.7%** respectively after commissioning.

The suction pressure was kept constant at p = 50.1±2.8 mbar for a low-flux operation. The maximum water flow achieved at the beginning of the trials was around 180 L/h, which corresponded to a water flux of $J = 22.5\,\mathrm{L/(m^2\,h)}$ and a maximum permeability of $443\,\mathrm{L/(m^2\,h\,bar)}$ with respect to the $8\,\mathrm{m}^2$ membrane surface.

The time course of the flux and the permeability for 146 days of operation is shown in Figure 4.3-3 showing the decrease of the filtration performance over time. After approx. 70 days of operation, the water flux and permeability dropped to around 200 L/h and $11\,\mathrm{L/(m^2\,h)}$, respectively. Measurements were taken again on operation day 146 showing values of 129 L/h and $8.8\,\mathrm{L/(m^2\,h)}$.
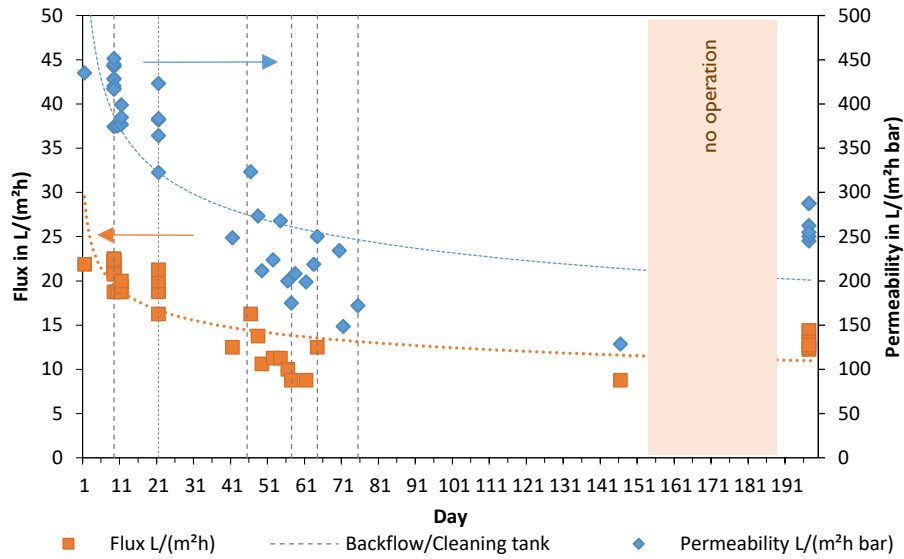
Figure 4.3-3 Flux *J* and permeability over time of the UF pre-treatment at pilot site.

The **decrease in permeability** is a normal effect following the organic/inorganic matter deposit on the membrane surface and membrane fouling/scaling that cannot be fixed by regular backwashing alone. In order to effectively mitigate fouling, chemical cleaning of the membranes is normally needed. However, studies have shown that operating the UF system at stable, low flux conditions allows a robust, maintenance-free, low-cost and user-friendly treatment with a great potential for implementation (Peter-Varbanets et al., 2011).

The use of novel UF membranes for the pilot trials allowed the **sustainable approach without chemical cleaning** and only frequent backflush and mechanical cleaning. This was done by regularly backflushing the membranes (p = 120 bar) with UF permeate every 9 minutes for periods of 60 seconds. That was possible because the special fitting and characteristic of the membrane units in module frames that support the flat membrane sheets and allow mechanical resistance to higher backflush.

TSS measurements on the UF-tank surface and bottom revealed the **accumulation of sludge** and increase in solids in the tank from ca. 250 mg/L to >600 mg/L TSS, respectively. Accumulated sludge was, therefore, discharged regularly from the tank which was refilled with fresh river water. The increase of TSS was also observed in consecutive days, for example from 212 mg/L on day 10 to 305 mg/L on day 11. Additionally, the effect of longer backflush with permeate (up to 60 min) was also investigated during the first 2 months of operation. The *J* and permeability values Figure 4.3-4 shows over the course of 1 day to show the performance of the UF and the intense backflushing. Results show the slow decrease for the first hours of the initial $J = 16.5$ L/(m² h) and 330 L/(m² h bar) and the immediate increase after the 1 h backflush (12:17) to values of $J = 22.5$ L/(m² h) and 452 L/(m² h bar).
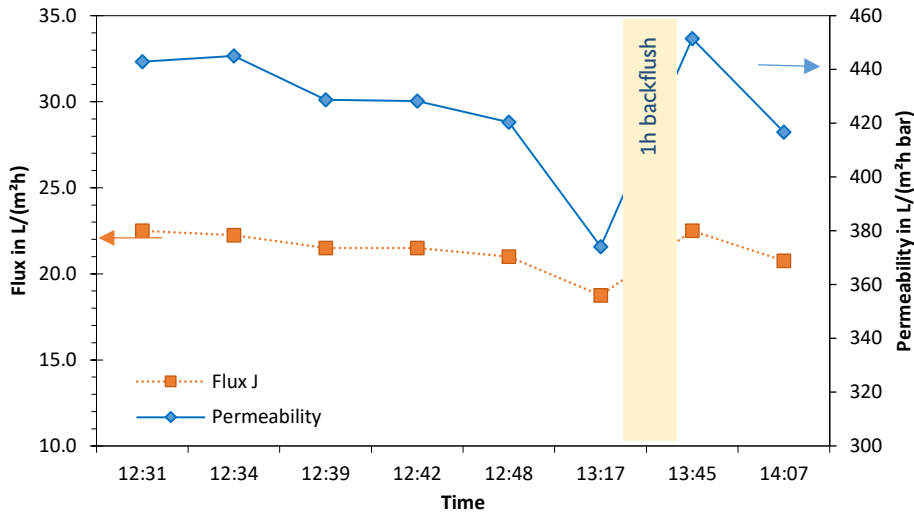
Figure 4.3-4 Hourly fluctuations of flux *J* and permeability of UF at pilot site (day 9).

However, results also showed that the permeability and *J* decreased again to similar values in the following days or even hours, so that no long-term effect of the long backflushing could be condirmed. Additionally, the longer backflush accounted for permeate loss and increased membrane stress so that **sludge discharge** was identified as the most efficient non-chemical cleaning method. Therefore, the relationship between TSS of the raw water, the accumulation of solids in the tank (surface and bottom) and its effect on permeability still needs be studied further. For this reason, a **chemical cleaning** was carried out after ca. 200 days of operation to evaluate the effect of fouling mitigation on the performance of the membranes. The cleaning of bio- and organic fouling was carried out by soaking the membranes in 0.5%-peroxide (H_2O_2) solution over the course of 24 h. The results of the *J* and permeability are shown in Figure 4.3-5.
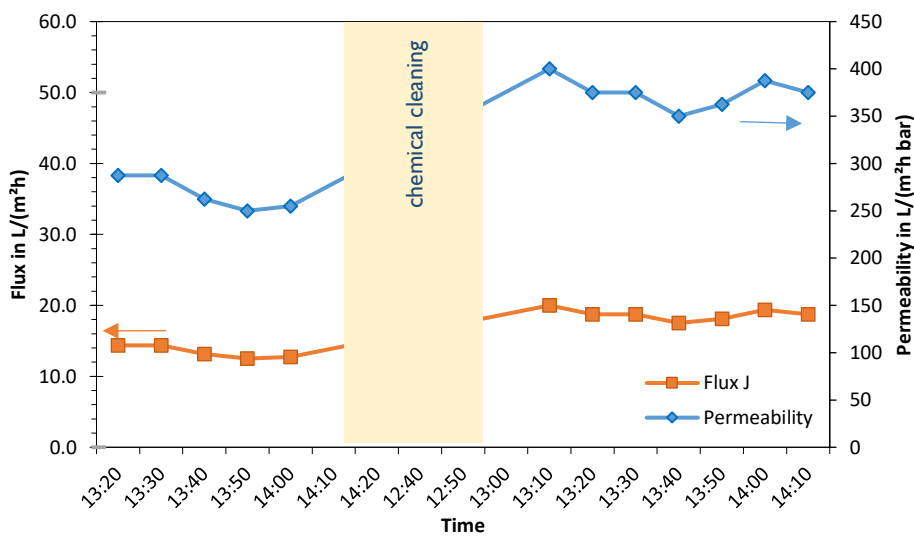
Figure 4.3-5 Flux *J* and permeability before and after chemical cleaning (day 204-206).

For the cleaning, the UF-Tank was emptied and filled with 700 L of 0.5%-H_2O_2 solution and left over night. The soaking of the membranes was the easiest method to carry out by the local supervisor on-site since backflush via gravity was not possible/would have taken too long.

Results showed that after chemical cleaning, J and permeability increased by 28% from 13.4 L/(m^{2}h) and 269 L/(m^{2}h bar) to 18.8 L/(m^{2}h) and 375 L/(m^{2}h bar), respectively. Since H_2O_2 is an **environmental-friendly chemical**, its use as cleaning agent was a sustainable method that proved useful for mitigating organic and bio-fouling. In contrast to mechanical cleaning, J and permeability did not dropped within the first hours of operation after the cleaning. However, no long-term effect of the chemical cleaning was possible in this study.

The overall performance of the **membranes improved to 86%** of the initial J and permeability values of 21.7 L/(m^{2}h) and 433 L/(m^{2}h bar) measured on day 1. The drop in the performance (14%) can be attributed to different factors which included the influence of a possible irreversible fouling build-up on the membranes surface or the effect of scaling, which needs to be further studied. Additionally, backflush of the membranes with cleaning solution instead of soaking might also have better result against persistent fouling.

Furthermore, the influence of the accumulation of solids in the filtration tank (TSS) on the J and permeability was an indication that the membrane performance was affected directly by river water quality and the frequency of tank cleanings that was done by filling fresh river water after sludge discharge. Since sample taking for TSS measurements was not always possible, measurements of both TSS and turbidity were carried out at the beginning of the trials and their relationship was used for the determination of TSS in further experiments. The correlation (R^2=0.80) between TSS and turbidity is shown in Figure 4.3-6.
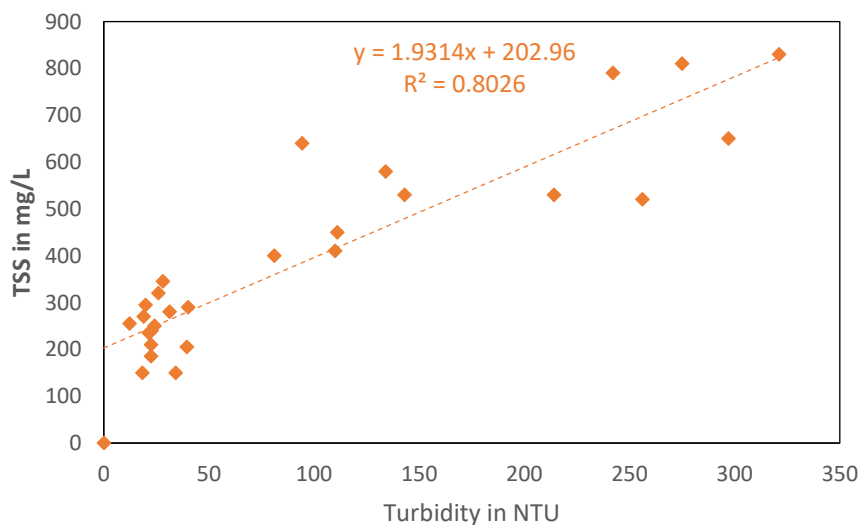
Figure 4.3-6 Correlation between TSS and turbidity of measured river and UF-tank samples.

4.3.3 MCDI desalination

The MCDI system was tested at three different salt concentrations $c_{feed,CDI,1}$ = 1250 mg/L, $c_{feed,CDI,2}$ = 1800 mg/L and $c_{feed,CDI,3}$ = 2400 mg/L in order to determine the optimal operating parameters for the desalination after the LPRO. The results of the pilot trials in Figure 4.3-7 and Figure 4.3-8 show the **relationship of SEC and feed concentration, RE and WR.**
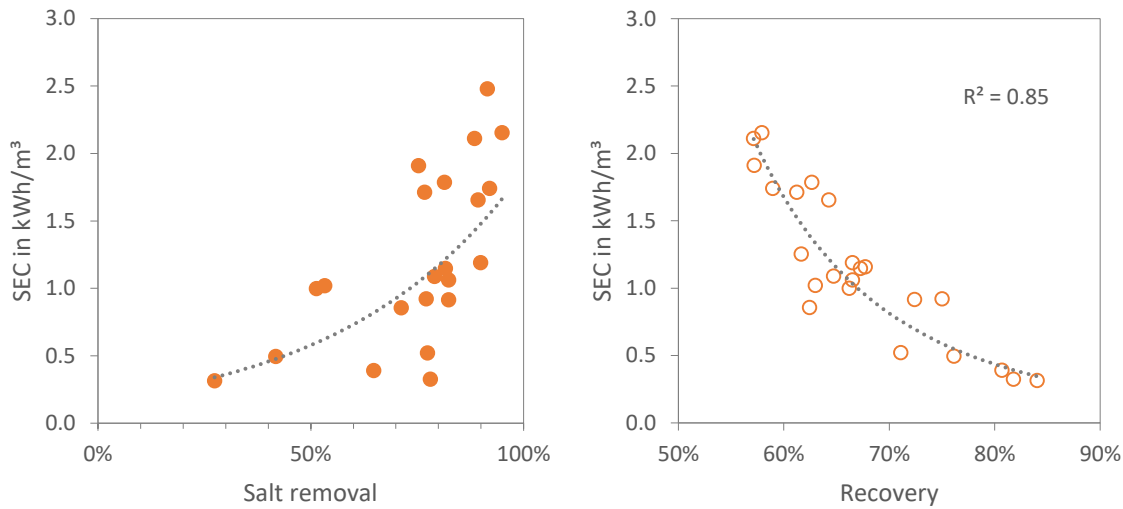
Figure 4.3-7 Relationship between SEC of MCDI pilot-scale plant and removal RE (left) and recovery WR (right).
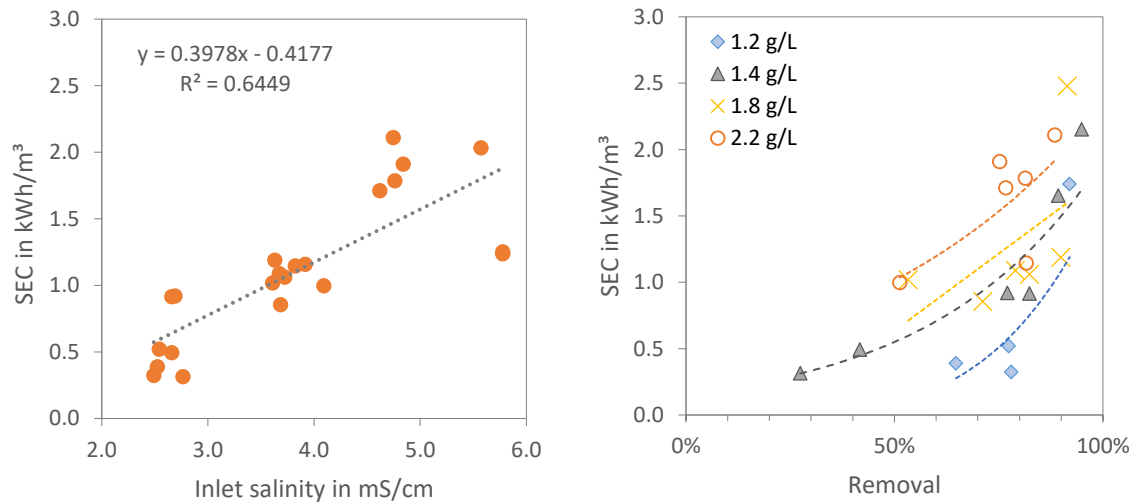
Figure 4.3-8 SEC of MCDI pilot-scale plant at increasing (a) inlet salinity and (b) removal RE at different feed salinities (1.2-2.2 g/L).

With higher RE and increasing feed concentration, higher consumption SEC was necessary to reach drinking water quality (TDS<450 mg/L). The increase from 25% to 75% removal tripled the energy requirements from $SEC_{25\%}$ = 0.3 kWh/m³ to $SEC_{75\%}$ = 1 kWh/m³.

Similar to the RO, results also showed that the SEC of the MCDI decreased with higher WR (Figure 4.3-7b). The optimization tests in Figure 4.3-8b at three inlet concentrations showed that the desalination to TDS < 450 mg/L for the production of drinking water quality was achieved with energy requirements of $SEC_{MCDI,1}$ = 0.39 kWh/m^3, $SEC_{CDI,2}$ = 1.1 kWh/m^3 and $SEC_{CDI,3}$ = 2.1 kWh/m^3. Here, only the energy consumption for desalination was considered and not that for the feed pump and the efficiency loss in the power supply.

The relationship between increasing RE and SEC at different inlet salinities in Figure 4.3-8b also revealed the direct effect of feed water quality on the process efficiency. While a RE of 75% for an inlet salinity of 1.2 g/L required only a SEC<0.4 kWh/m^3, the SEC for the desalination of inlet TDS = 2.2 g/L quadrupled to a SEC>1.7 kWh/m^3. The exponential increase in SEC shown by the pilot trials was in line with the experimental investigation in lab-scale with the MCDI and the behaviour seen in literature (Zhao et al., 2013a), however slightly higher values. The lab-scale MCDI showed SEC values (without pump) of 0.2-0.6 kWh/m^3 and 0.4-1 kWh/m^3 for the desalination of 1 and 2 g/L, respectively while literature calculation indicate SEC<1 kWh/m^3. In comparison with the results of the pilot-scale plant SAR+MCDI (Concept A), which showed a higher SEC of 2.2 kWh/m^3 (incl. pump) for 1.65 g/L, indicate that the obtained values are good within a tolerance range.

4.3.4 RO vs. LPRO

A key objective of the pilot trials was to compare the performance of the LPRO+MCDI combination system with a single-stage SWRO. For this, XLE (LPRO) and SW30 (RO) membranes (DuPont, 2020) were tested individually at different pressures in order to evaluate the WR and the salt rejection RE as a function of the SEC (see Figure 4.3-9 and Figure 4.3-10). The results of the **SW30 membranes** showed a maximum TDS removal from 22.4 g/L to 0.16 g/L at an operating pressure of 65 bar, which corresponded to a desalination of >99.2% and a WR of approx. 55%. The energy demand of the RO at this operating pressure was around SEC_{SW30} = 4.90 kWh/m^3. Results showed that higher operating pressures, yielded greater WR and, thus, lower SEC.

The tested **low-pressure membranes (XLE)** achieved a salt removal of 91.7% from TDS = 22.4 g/L to 1.86 g/L with an SEC_{XLE} = 4.73 kWh/m^3. The membranes were tested up to an operating pressure of 40 bar achieving a maximum WR of 46%. In contrast to the SW30 membranes, different salt retention levels (12<RE<56%) were achieved depending on the operating pressure. With increasing operating pressures, the LPRO membrane achieved larger WR, which had a positive impact on the SEC.
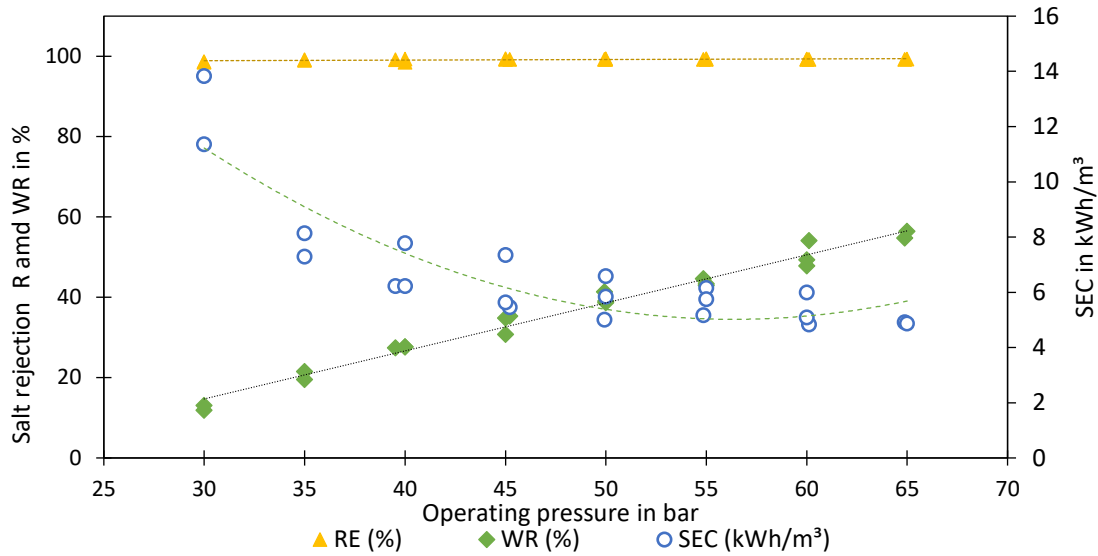
Figure 4.3-9 R, WR and SEC for SW30 membrane with increasing operating pressure at pilot-scale plant.
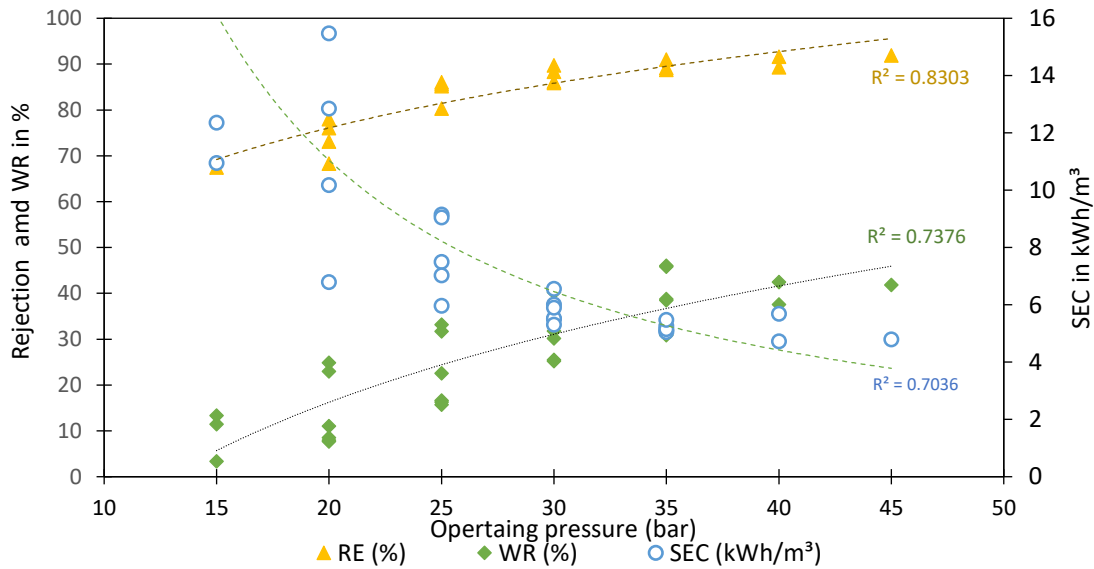
Figure 4.3-10 R, WR and SEC for XLE membrane with increasing operating pressure at pilot-scale plant.

Both membranes showed a decrease in SEC with increasing permeate flows (e.g. WR). However, the long-term operation at high pressures and fluxes can significantly reduce the lifespan of the RO unit including increase in fouling and scaling. In comparison to the RO, running the LPRO at the standard operating pressure enabled an enhanced permeate flux. Additional energy saving can be achieved by use of smaller pressure pumps. This was important for designing a **modular process LPRO+MCDI** which could be operated with a smaller pump depending on the target product water quality.

4.3.5 MCDI+LPRO

The results of the modular desalination system MCDI+LPRO as a combination process including UF pre-treatment are summarized in Figure 4.3-11. Results show the continuous desalination performance of the pilot-scale plant as an example on operation day 21 (27.09.2020).
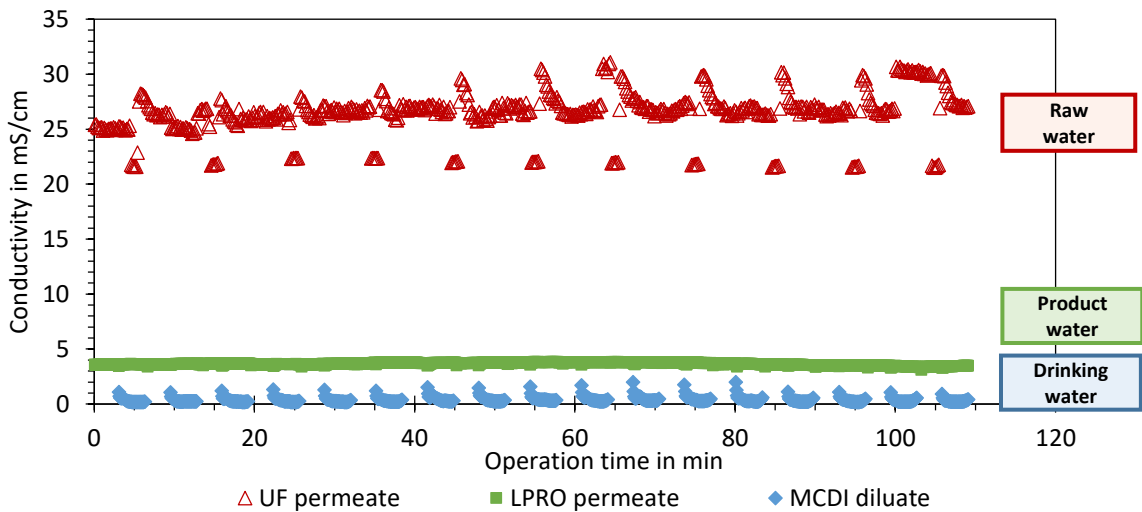
Figure 4.3-11 Salinity over time at pilot-scale plant in Can Gio for all three stages: UF-pre-treatment (red), LPRO (green) and MCDI (blue) on day 21.

River water with an average concentration of 26.5±2 mS/cm (TDS = 17.0±1.3 g/L) was desalinated for the production of product water using the LPRO (EC = 3.6±0.1 mS/cm) and drinking water (EC = 342±158 μS/cm) by use of MCDI.

The fluctuations in the conductivity measurements of the raw water show the tank refilling during the backwash processes every 10 min. The intermittent production of drinking water corresponded to the discontinuous MCDI desalination and the alternating between CP and DP.

The desalination of the product water (EC$_{input}$ = 3.6 mS/cm) by means of the MCDI resulted in an average SEC of 1.1 kWh/m^3 with a WR of 65% (Table 4.3-4). The charge efficiency of 97% showed that the parameters were properly chosen.

Table 4.3-3 Averaged results of the MCDI at pilot-site location.

Average EC input	Average EC pure	Average removal	SEC	WR	Charge efficiency
3.67 mS/cm	0.78 mS/cm	0.79%	1.0 kWh/m³	0.65%	97%
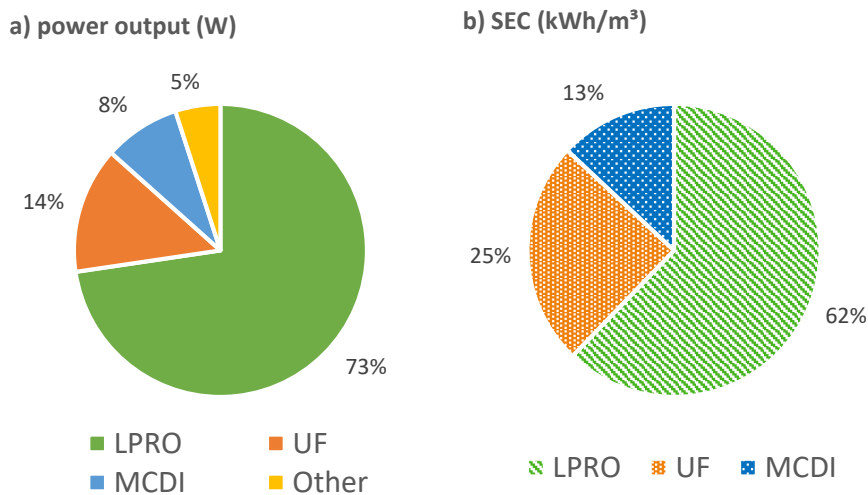
Figure 4.3-12 LPRO+MCDI pilot-scale plant: a) Comparison of power requirements (total = 1520 W) and b) averaged SEC distribution (SEC$_{total}$ = 7.8 kWh/m³).

An analysis of the power requirements and the SEC of the three stages (UF, LPRO, MCDI) is shown in Figure 4.3-12, which shows that the LPRO has highest power demand (P_{LPRO} = 1.2 kW) followed by the UF (P_{blower} + $P_{UF,pump}$ = 200 W) and the MCDI with around $P_{MCDI,PS}$ = 95 W and $P_{MCDI,pump}$ =35 W.

The SEC of the three technologies is divided in Figure 4.3-12b showing a slight different energy usage for the production of 1 m^3, which was calculated depending on the different capacity of each plant. With an average of 1.0 kWh/m^3 the MCDI had the lowest specific energy consumption, followed by the UF with 1.9 kWh/m^3 and the with LPRO4.8 kWh/m^3. In general, results showed that the three stage process could be operated continuously with an SEC of 7.8 kWh/m^3 including intake and UF pre-treatment.

A long-term operation of the pilot trials was not possible due to the remote location and lack of local contact person to continue the operation of the system. Further tests with optimized parameters are recommended for the evaluation of the long-term performance and to evaluate the feasibility of operating with feed water with high fouling potential. The use of upfront UF-treatment was an important fouling prevention for the membranes.

4.3.6 LPRO+MCDI vs single-stage RO

A comparison of the combined LPRO+MCDI and the single-stage SWRO is shown in Table 4.3-4. Here, the results of different operational days were summarized and averaged for the three separate processes LPRO, SWRO and MCDI. The UF was excluded since the pre-treatment was the same for all processes.

The average SEC achieved for the production of permeate with a conductivity of 2.3 mS/cm with the LPRO was SEC_{XLE} = 5.2 kWh/m^3. Experiments with the MCDI (see 4.3.3) showed an average SEC_{MCDI} = 0.6 kWh/m^3 for the desalination of 2.6 g/L including the MCDI pump. This resulted in a total energy consumption of $SEC_{XLE+MCDI}$ = 5.8 kWh/m^3 for the production of drinking water. Compared to the SEC_{SW30} = 5.5 kWh/m^3, the SEC of the combined system was slightly higher than for the SWRO process. ($\Delta SEC = SEC_{XL+MCDI} - SEC_{SW30}$ = 0.30 kWh/m^3).

Results showed therefore, that an **optimization of the combined processes** is still required to make it compete with traditional SWRO, in particular the desalination step with the MCDI. This could be achieved e.g. by the recirculation of the concentrate flow from the MCDI to the inlet of the LPRO what can improve the yield and lower the SEC.

Table 4.3-4 Comparison of pilot-scale LPRO+MCDI and single-pass RO

	LPRO (XLE)	MCDI	LPRO+MCDI[a]	RO (SW30)
Feed flow (L/h)	575	150 [b]	575	615
Cond. feed (mS/cm)	28-34	2.6	28-34	28-34
Cond. Permeate (mS/cm)	2.3	0.60	2.3 | 0.60	0.25
Pressure (bar)	40	<0.3	40 | 0.3	55-65
Permeate Flow (L/h)	230	180[b]	230 |180	305
Concentrate Flow (L/h)	345	30 [b]	375	310
R (%)	>90	>75	>97.5	>99
WR (%)	40	75	30	50
SEC (kWh/m³)	5.2	0.6	5.8	5.5
SEC_{rem} (Wh/g)	-	0.44	-	-

All values rounded for simplification
[a]Resulting values from both processes
[b]Averaged from DP, PP and/or CP

Additionally, the operating parameters of the MCDI can generally still be optimized to achieve the **highest efficiency** possible. Here, tests should target lower the SEC_{MCDI} with higher water volume flows by optimizing the parameters in the regeneration phase. This should also allow the optimization of the SEC_{rem} to values lower than 0.44 Wh/g as seen in the pilot trials with low saline BW of $SR_{SAR+MCDI}$ = 0.39 Wh/g (see Section 4.2.3).

4.3.7 Performance evaluation LPRO+MCDI system

Due to the high salt content in Can Gio (high saline BW), only the **combined LPRO+MCDI** system was suitable for the production of drinking water during the rainy and dry seasons using the LPRO membrane (XLE, DuPont, 2020). The seasonal fluctuations in salinity enabled

the modular concept to produce two water qualities for various purposes: LPRO in the dry season or during low-tide can be used for product water for the household (washing, flushing toilets, watering, etc.) or for animal feeding, while only a smaller part is used for the production of drinking water with the MCDI.

The use of the LPRO for **producing drinking water** may be sufficient during the rainy season, or high-tide, or all-year round **at locations with lower salinity** than at the pilot plant, for example on river banks that are closer inland. This was tested by Jeong et al. (2020) at a salt concentration of 10 g/L and lower, showing that a NF-MCDI system was able to achieve drinking water with lower SEC than conventional BWRO. The hybrid NF system (NE90-2540, Toray, Japan) was operated at pressures ranging between 20 and 38 bar and recovery rates of 30-50%. The MCDI (E-100, Siontech, South-Korea) achieved a SEC of 0.52 kWh/m^3 for the desalination of 2.8 g/L, which was in line with the SEC_{MCDI} value obtained with the LPRO+MCDI pilot-scale plant of 0.6 kWh/m^3. Computer-based calculations also showed that LPRO membranes of the LC series (DuPont, 2020) could be used for obtaining drinking water at the Can Gio site, but only with a higher resulting SEC.

The use of a **single-stage SWRO** would be advantageous with regard to SEC in the actual setting. However, it must be taken into account that the necessary pump pressure is significantly higher and is therefore linked with higher investment costs (pump, piping). Additionally, remineralisation may be needed to replace minerals removed from the water by desalination, which is an additional costly process intended to meet mineral demand by humans and plants.

To evaluate the data from the **UF pre-treatment**, further long-term tests of several months (6-12 months) are necessary in order to be able to make a well-founded statement about the performance of the UF membranes from Weise Water GmbH. These examinations are carried out with the support of a local contact person in Thien Lieng in order to regularly check the data (pressure and water flow) and to switch the system back on manually in the event of a power failure.

5 CONCEPT EVALUATION

As a final chapter, the two concepts for BW desalination (Concept A for low saline BW, and Concept B for high saline BW) are evaluated using a comparative multi-criteria approach. The main objective was to assess the concepts not only through the pilot results, but also including social, economic and environmental aspects, as well as evaluating the technology as whole.

5.1 Evaluation criteria

A holistic evaluation of desalination technologies considers several different indicators which can be divided in four principal categories: **economic, social, environmental** and **technical** (Fritz et al., 2020; Gude et al., 2010; Wencki et al., 2020). Each category includes a wide range of different assessment criteria (specific or universal) to evaluate the overall advantages and disadvantages of a technology or process. These include:

- **Social:** water availability, political legitimacy and social acceptance are three important aspects within the social criteria.

- **Economic:** this category considers economic-profitability, operating and capital costs as well as income and risk management. While a monetary evaluation fits well into traditional economic decision-making processes, monetization can be ambiguous and a controversial issue, especially in relation to social aspects (Wencki et al., 2020).

- **Environmental:** use of resources, emissions and land use, including brine disposal, are important sustainability criteria that consider technical-related aspects like water recovery rate, energy consumption including energy and productivity losses.

- **Technical:** universal criteria include plant capacity, water quality, reliability (robustness) and safety of the systems including fouling and breakdowns. Also important is the consideration of its ease-of-use, the minimum level of training required to operate the plant, operational flexibility and level of automation.

 * underlined are the 10 criteria selected for this evaluation

The relation between all these factors is very complex and, most importantly, site specific. By weighting each chosen criteria, the overall outcome of a multi-criteria analysis is defined. For this study, **10 different criteria** with equal weight were selected based on literature reviews (Fritz et al., 2020; Gude et al., 2010; Wencki et al., 2020) for a qualitative and **semi-quantitative analysis** using three marks for evaluation: more positive impacts (+), some advantages and disadvantages (+/-) and more negative impacts (-).

5.2 Concept A – Low salinity TDS < 5 g/L

Social criteria

Water availability (+). Access to fresh water is available at the pilot-site location through the municipal water supply. However, the water supply services have the main disadvantages of: dependency on water cuts, low supply pressure, and in this particular case, high iron contents. Water cuts are bypassed by use of a reservoir or cistern. Since the water supply pressure is too low, an additional pump is used to pump to the rooftop, which allows independent supply from electrical energy due to power cuts. Additionally, a filter system is used for deironing the water.

By use of desalinated groundwater coupled with renewable energy, water supply would be completely autonomous and independent from the local water and power supply.

Political legitimacy and social acceptance (+/-). The presence of As in the groundwater was an issue that affected social acceptance for the use of groundwater as drinking water source. However, by use of SAR, arsenic removal takes place underground so that the risk of As exposure to the user is completely minimized. With regards to groundwater usage in the region, actual policies restrict groundwater usage due to over-extraction for agriculture and other water intensive applications. The use of groundwater for household through saline wells can increase the potential for groundwater usage and at the same time reduce pressure on the existing water supply system. However, the increased pumping even at saline wells should be always monitored and controlled by local institutions to evaluate the long-term sustainable extraction.

Economic criteria

CAPEX and OPEX (-). A cost estimation for the SAR+MCDI desalination plant for the pilot-scale plant in Tra Vinh is presented in Table 5.2-1. This includes the pumping of the water to the rooftop ("Intake") due to low pressure of local water supply (see criteria "Water availability").

Table 5.2-1 Cost estimation of the SAR+MCDI pilot-scale plant

	Intake[#] Cost[*] (USD/year)	MCDI Cost[*] (USD/year)	SAR Cost[*] (USD/year)
Pump	150	35	44
Electrodes[a]	-	2354	-
Power supply	-	1417	-
System, piping, etc.	63	25	45
Pre-treatment[b]	340	135	-
Maintenance[c]	50	150	25
Electricity costs[d]	266	658	263
Yearly costs[*]	**869**	**4774**	**527**
Flow (L/h)[e]	500	60	-
Infiltration rate (m³/m³)[f]	-	-	0.22
Plant capacity (m³/d)[g]	10x2	10	10
SEC (kWh/m³)	0.89	2.2[h]	0.88
Water unit cost USD/m³	**0.24**	**1.31**	**0.14**

[*]Based on actual costs of pilot-plant or from standard market prices and a 10 year life time.
Individual prices were upscaled <u>linearly</u> to meet plant capacity based on permeate flows (see [e])
[#]Intake refers to the actual water installation on the house incl. pumping of water from local supplier to the rooftop
[a] Electrode life time: 5 years
[b] Pre-treatment for all processes: Sand filter
[c] Estimated value incl. chemicals and labour costs
[d] Based on electricity prices of 0.082 USD/kWh and SEC
[e] From pump data sheets. MCDI permeate flow from experimental results: WR = 33%
[f] $Q_E = 0.22$ m³/m³; $V_I = 1.1$ m³
[g] Based on 16 hrs/day. For target 10 m³/day: Feed pump WR = 50% (= 20 m³/d); from permeate flow: MCDI factor = 10.4; SAR = 1.1
[h] SEC_{MCDI}= 1.75 kWh/m³; SEC_{pump} = 0.45 kWh/m³

Since the production of drinking water is more energy intensive than the water supply (intake) and pre-treatment (SAR), the MCDI shows the highest specific cost with 1.27 USD/m^3. The MCDI also showcases the lowest WR and the higher investment costs for electrode and power supply. Therefore, future optimization focusing on WR and SEC can significantly reduce the costs. On the other hand, the arsenic removal was achieved with very low economic efforts, with a specific cost of 0.11 USD/m^3, which highlights the economic advantages of the process.

<u>Economic profitability/ Income (-).</u> The city of Tra Vinh is characterized by a mixture of socio-economic classes in a relatively dense urban area. Average family/household incomes are quite divers and the capability of acquirement of an autonomous water treatment system at a household level is very limited for the great majority. At current electricity prices (approx. US$0.08), the use of solar is not profitable at the moment. With a capacity of 11.2 kWh/d and an annual yield of 1435 kWh/kWp, the return of investment of the PV system installed in Tra Vinh (CAPEX = US$15.000) is well over 25 years with a fixed tariff for feeding onto the grid

of US$0.0832. However, the decreasing PV prices and increasing environmental pressure from the Government is pushing towards the use of non-conventional energy sources.

Environmental criteria

Emissions (+). For the SAR process, there are no literature studies on LCA. However, the very low SEC values of < 0.9 kWh/m^3 and its easy design (pump, tank, injector) suggest that the SAR process has a very **low environmental impact**. The MCDI can also be considered as an environmentally friendly desalination technology based on the results from impact assessment and cumulative energy demand (Yu et al., 2016). However, previous studies on LCA have indicated that electricity consumption in the MCDI has a relatively lower impact (10%) compared **to material utilization** (e.g. Ti current collector on the electrode) and **chemical use** (e.g. DMAC solvent) (52%-90%) which suggests that additional efforts to substitute or reduce these can enhance the overall environmental performance of CDI systems (Shiu et al., 2019; Yu et al., 2016).

Utilizing RES such as solar and wind energy (for larger plants) can be one of the most effective measures to improve the overall sustainability of the desalination process, reducing impacts in most major impact categories (Al-Kaabi et al., 2021). However, the low electricity prices in Vietnam and lack of regulatory framework to support the installations of PV modules or wind turbines at household level makes the use of RES less affordable. Additionally, noise pollution of the wind turbine seemed to be a major factor against the acceptability of wind energy use.

Energy/ productivity losses (+/-). Although the SEC for the holistic process (pumping, pre-treatment, desalination, and supply) was below 4 kWh/m^3, the power supply unit used for the MCDI showed an **efficiency of only η ≈ 20%** for the conversion of alternating voltage (AC) to direct voltage (DC). The major problem occurs in the conversion to low DC voltage (<2 V) to very high currents (up to 120 A), which is outside the optimal operating limits of most commercially available power supply units. The development of new power supply system to increase this efficiency to η>80% is an important improvement for the CDI-technology.

Brine disposal (+). The use of SAR for the subsurface removal of As allowed the safe production and discharge of concentrated brine from the desalination process as a **non-toxic, arsenic-free waste stream**. Therefore, the disposal of brine though the canalisation was considered non-critical to the environment. However, the risk of accumulation of toxic substances even in the smallest quantity should be monitored and the need of a proper disposal method should be considered, especially for larger plants.

Technology criteria

<u>Technical reliability (+/-).</u> Both SAR and MCDI technologies are missing safety mechanisms for continuous safe water supply (e.g. pump, filter, water meters). For the SAR process, if no infiltration cycle is carried out, the risk of prolonged over-extraction may result in water quality changes and even blocking of well. In several occasions, more water was extracted than the capacity of the plant, mainly due to consumer's behaviour. However, additional reasons for over-extraction included the obstruction of the water meter due to particles (unsealed well), as well as incomplete infiltration cycles due to a leakage between pump and pressure vessel caused by corrosion, affecting the daily automatic infiltrations. Nevertheless, all technical problems were successfully solved and were mostly due to the materials that are not related to the process itself. Most importantly, even when technical failure occurred, **no As breakthrough** was observed showing that the SAR+MCDI process has high technical reliability.

<u>Safety (incl. fouling) (+).</u> The pre-treatment via SAR for Fe^{2+} and Mn^{2+} removal and the sand filter installed for particulate matter and NOM removal worked actively as **fouling prevention** minimizing the fouling potential of the SAR+MCDI system. Particles and iron deposition have been proven to affect both the adsorption capacity and the charge efficiency of the MCDI, the latter causing sometimes irreversible effects on the electrode micropores. However, the propensity of fouling increased due to higher temperatures of up to 30°C. Regarding the process safety in general, drinking water standard was achieved and long-term results proved that SAR+MCDI was a suitable mitigation technique with the salient advantage of **no toxic waste production** with no As breakthrough.

<u>Ease-of-use (+/-).</u> The MCDI system operation is much unknown and complex, and would require **professional support** in any case of failure. The SAR system is more robust, and it only requires a pump for its operation. Maintenance in regular operation encompasses only the mechanical cleaning of a strainer on top of the SAR tank and the standard pump work. Fully automatized processes are generally easy to run but require a local contact support that can operate the system for maintenance and in case of reparations. The main drawbacks of the SAR+MCDI operation was that, besides pump repairs, no other component could be operated or repaired by the local users. However, this is the case also for simpler technologies that require a minimum technical knowledge for operation.

5.3 Concept B – Mid-salinity range 5 < TDS < 20 g/L

Social criteria

Water availability (+). In Thien Lieng, similar to other municipalities in Can Gio, access to clean or potable **water is currently very limited** due to its remote location. Although it is completely surrounded by water, saline intrusion affects the quality of both surface and groundwater. There are around 125 households with around 800-1000 inhabitants and a daily water requirement of around 100-120 m^3 on the island. Since there are no water pipes from the nearest central water supply to the community, up to 80 m^3 of fresh water are transported from the mainland by boat every 1-2 days (Figure 5.3-1). Therefore, there is a great potential and positive response towards the concept from the local people.

Figure 5.3-1 Water supply by boat in Thien Lieng subsidized by the local government.

Political legitimacy and social acceptance (+). The users on the island pay a fixed water price of 5,000 VND/m^3 (approx. 0.22 USD/m^3). However, the maximum supply per person is limited to 3 m^3 per month. The households are supplied by a central pumping station on the island with storage tanks with a capacity of 170 m^3. The external water supply is subsidized by the government by providing approx. 24,000 VND/m^3 for the transport in addition to the water price of 2,000-4,000 VND/m^3 for a total price of approx. 1.10-1.30 USD per m^3.

As a result, the economic advantages for a decentralized drinking water system are promising at this point which increased the prospects of success for political acceptance. For this reason, the work with the WaKap pilot plant was also supported by the local government (permits, transport, security, etc.).

Economic criteria

Investment and operational costs (-). Some recent developments, such as the increase of unit capacity, improvements in process design and materials, and the use of hybrid systems have contributed to cost reduction as well as reduction in energy consumption. The development of

new and emerging low-energy desalination technologies, such as adsorption desalination, will have an impact on cost variation estimation in the future (Ghaffour et al., 2013).

An estimation of the costs including CAPEX and OPEX of the pilot plant for 10 m³ capacity are summarized in Table 5.3-1 showing the yearly costs for a 10 year life-span of the plant (amortization).

The specific water costs were calculated to 0.97 USD/m³ for the combined treatment plant which is lower than the actual costs of 1.10-1.30 USD/m³ for the supply by boat. However, the lower investment costs of the SWRO and slightly lower electricity expenses, showed that the single pass SWRO is currently more economic than the combined process. By separating the costs of for the production of the two different water qualities and assuming a pre-treatment cost of US$0.20, the specific costs of the LPRO and the MCDI were estimated to 0.26 USD/m³ and MCDI 0.51 USD/m³ for drinking water.

Table 5.3-1 Cost estimation of the LPRO+MCDI pilot-scale plant vs. SWRO

	SWRO		LPRO+MCDI	
	Cost* (USD/year)	% of total cost	Cost* (USD/year)	% of total cost
Membrane modules 2540[a,b]	344	11.8	256	7.2
Membranne housing	295	10.1	220	6.2
High pressure pump	91	3.1	53	1.5
Electrodes[b]	-	-	366	-
Power supply	-	-	450	-
System, piping, etc.	154	5.3	137	3.9
Pre-treatment (UF)	238	8.2	177	5.0
Maintenance[c]	102	3.5	114	3.2
Electricity costs[d]	1646	57	1736	49
Intake (incl. feed pump)	41	1.4	30	0.9
Yearly costs*	**2912**	100	**3539**	100
Permeate flow (L/h)[e]	305		410	
Plant capacity (m³/d)[f]	10		10	
SEC (kWh/m³)	5.5		5.8	
Water cost USD/m³	**0.80**		**0.97**[g]	

*Based on actual costs of pilot-plant or from standard market prices and 10 year life time
Individual prices were upscaled <u>linearly</u> to meet plant capacity based on permeate flows (see [e]). No influence of upscaling on price were included.
[a] Spiral wound modules 2540-SW30 or XLE
[b] Life time: 5 years
[c] Estimated value incl. chemicals and labor costs
[d] Based on electricity prices of 0.082 USD/kWh and SEC
[e] Flow from experimental results; water recovery: RO = 49%; LPRO = 40%; MCDI = 75%
[f] From permeate flow and 16 hrs/day operation: Factor SWRO = 2; LPRO+MCDI = 1.5
[g] specific costs: Pre-treatment = US$0.20; LPRO = US$0.26; MCDI = US$0.51

<u>Economic profitability/ Income (+/-).</u> Low income is a major challenge for the affordability of decentralized plants at household level in general. In this pilot-concept, the autonomous production of both drinking water and additional process water allowed the sustainable use of

desalinated water as an independent source of water supply with specific prices for each water-use. However, the already **low water prices** make a private investment less attractive. On the contrary, an investment from the institutional or governmental side is more lucrative since the subsidy of the external water supply is very costly (1.10-1.30 USD per m^3).

Additional socio-economic advantages of this pilot plant is the creation of jobs through the production of salt from brine as usable by-product from "waste-stream". In comparison to current salt mining practices in evaporation ponds in the region, an additional gained-value by use of the LPRO+MCDI system is the high quality of the salt, since influent stream is pre-treated by UF.

Environmental criteria

Emissions (+/-). Enhancing the overall environmental impact of water desalination systems is still an ongoing field of research. This includes the use of green membranes and solvents for the LPRO-modules and environmental friendly alternatives to the current collector and solvents for the MCDI electrodes (Shiu et al., 2019; Yu et al., 2016). While the overall environmental impacts of RO manufacturing have been improved and can be estimated lower than of MCDI, desalination still remains an energy intensive process.

Brine disposal (+). The modular concept of the LPRO+MCDI allowed the sustainable brine disposal through recirculation (1) and re-concentration (2).

1. Recirculation of the MCDI concentrate to the LPRO feed could increase the water recovery rate and lower the SEC by sinking feed salinity for the RO process. Higher WR also provide less brine production (in m^3).
2. In order to follow zero-liquid-discharge (ZLD), the produced brine could be treated in evaporation ponds that are located next to the pilot site. Salt production through evaporation ponds is already practiced in the region. However, salt production can be limited seasonally due to changes in feed salinity, evapo-transpiration rates and temperatures.

Figure 5.3-2 Salt mines (left) and fishing (right) as sources of income in Thien Lieng.

Due to practical reasons during the course of pilot trials, either method was employed. The brine from the LPRO+MCDI pilot-scale plant was discharged directly into the river. The possibility of recirculation and ZLD using evaporation ponds must be further investigated.

Energy/ productivity losses (+/-). The power supply unit used for the MCDI showed an efficiency of only $\eta \approx 20\%$ for the conversion of 230 V AC to <2 V DC at very high currents, which is outside the optimal operating limits of most commercially available power supply units. The development of new power supply system to increase this efficiency to $\eta > 80\%$ is an important improvement

Technology criteria

Technical reliability (+/-). For lower salt concentration (e.g. rainy season or high tide), LPRO was used to produce drinking water. If the salt concentration was higher (e.g. dry season or low tide), the combination of both technologies LPRO+MCDI was used. The main advantage hereby is the production of water according to the consumer's need and increasing the sustainability of the process.

Safety (fouling or break downs) (+/-). In order to keep the water flux as high as possible, sludge discharge from filtration tank at regular intervals showed the best results.

Ease-of-use (-). Fully automatized processes are generally easy to run but require a local contact support that can operate the system for maintenance and reparations. The main drawbacks of the combined LPRO+MCDI system were programming involved for the autonomous operation and the reliability on local support when a problem was encountered.

5.4 Evaluation comparison

A summary of the grading results of each evaluation criteria is given in Table 5.4-1. The evaluation shows that both Concept A and Concept B are characterized by positive and negative impacts amongst the four categories. Both concepts have a better effect on social and environmental criteria while the economic issues are the most critical aspects.

Table 5.4-1 Results of semi-quantitative evaluation for Concept A and Concept B

Evaluation criteria	Concept A SAR+MCDI	Concept B LPRO+MCDI
Social criteria		
water availability	+	++
political legitimacy and social acceptance	+/-	+
Economic criteria		
investment & operational costs	-	+/-
profitability & income	+/-	+/-
Environmental criteria		
emissions	+/-	+/-
brine disposal	+	+
energy / productivity losses	+/-	+/-
Technology Criteria		
technical reliability	+/-	+/-
safety	+	+/-
ease-of-use	+/-	-

+ more positive impacts
+/- some advantages and disadvantages
- more negative impacts

For both concepts, the increase in water availability was the most evident advantage, while the most important benefit regarding environmental aspects was found in the brine disposal strategies. In concept A, most advantages were given through the implementation of the SAR system, which showed the most sustainability gain and the most affordability. However, economic profitability in general was the most critical issue given by the high investment cost and the low income of the consumers.

6 CONCLUSIONS AND OUTLOOK

6.1 Conclusion

The use of membrane capacitive deionisation (MCDI) as an integrated solution for low (TDS = 1.65 g/L) and high (TDS = 24 g/L) saline BW desalination seems as a feasible solution for the production of drinking water, also in remote areas. MCDI was successfully tested in combination with subsurface arsenic removal (SAR) and low-pressure reverse osmosis (LPRO) in two pilot-scale plants under real environments in South Vietnam showing the advantages of upscaling to achieve lower SEC and improve the overall efficiency in comparison to the results seen under laboratory conditions.

High water recovery rates and low energy consumption were the main advantages of the MCDI, while the efficiency of the power supply showed the highest deficit. Operational parameters must be adjusted individually to obtain optimum efficiency, which can be sometimes difficult to determine. An increase of WR can yield lower SEC only when the parameters are chosen properly. In general, optimized operation included lower volume flows during electrode regeneration (discharge phase, DP) and longer times for the desalination (charge phase, CP) for high WR and lower SEC.

Long-term results proved that SAR is a feasible mitigation technique and confirmed its salient advantages: non-toxic waste production, little maintenance and low costs. Although several technical problems were encountered, all problems were successfully eased and drinking water standard was achieved without As breakthrough or well blocking. The success of the As removal was attributed to the reliability in water quality through the fixed infiltration-to-abstraction ratio (Q_E) and the controlled water demand, its ease-of-use

provided by the fully automated infiltration cycles, and the robust components (stainless steel when needed) for technical safety.

The advantages of the modular concept LPRO+MCDI were the selective production of two water qualities, increasing the plant flexibility and reducing the specific environmental footprint for both products. UF pre-treatment at low-flux operation and with less chemical cleaning allowed an improved environmental efficiency while lowering the operational costs. However, investment costs and SEC of LPRO+MCDI are still higher than conventional SWRO. In order to make the combined process affordable and compete with SWRO, an optimization of the MCDI efficiency and lowering of the costs is needed.

The use of RES for energy supply using solar and wind allowed an autonomous operation of the desalination system (autonomy degree <97%). However, the low energy prices and the lack of subsidization are still the major drawback for full implementation of RES in Vietnam.

While the capital costs of the pilot-scale plants remain too high for an application at household level in Vietnam, the possibility of up-scaling for community use seems feasible. In order to enable a full deployment of decentralized technologies for drinking water production in remote areas, tools for facilitating ease-of-use and increasing the social acceptance and raising awareness of the environmental responsibility of the consumers is necessary. This can be achieved through political support and initiatives to provide technological support at local level.

6.2 Future work

Further investigation for evaluating the concept practicability should include the optimization of the MCDI, especially with regards to the energetic efficiency of the power supply and its evaluation in long-term operation regarding electrode module wear. Additional improvement of the LPRO+MCDI can be achieved by optimizing the energy usage of RO pumps, the MCDI parameters and including concentrate recirculation to increase WR.

Additionally, new technological insight for the combination process LPRO+MCDI could be obtained by testing the concept at lower feed salinities (e.g. Jeong et al. (2020)). This should also consider an evaluation of advantages besides only SEC and economic feasibility of the concept and technologies.

This is illustrated in Figure 6.2-1 which shows a new proposed concept scheme for BW desalination shifting the salinity range from high saline concentration (<20 g/L) to a medium- or low saline range (5<TDS<10 g/L) (green area).
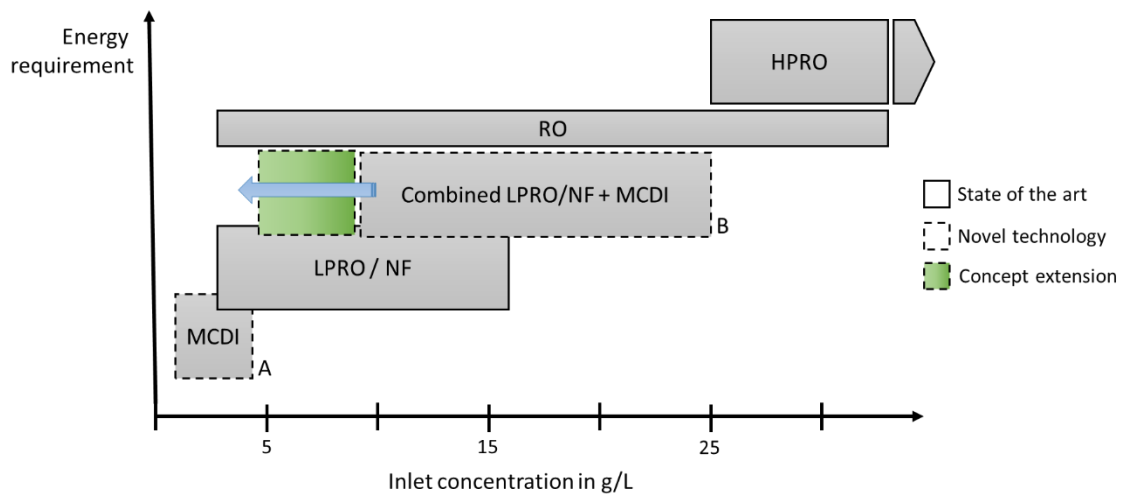

Figure 6.2-1 Outlook: updated concept scheme for BW desalination

7 REFERENCES

Acharyya, A., 2014. Groundwater, Climate Change and Sustainable Well Being of the Poor: Policy Options for South Asia, China and Africa. Procedia - Soc. Behav. Sci. 157, 226–235. https://doi.org/10.1016/J.SBSPRO.2014.11.025

Agusa, T., Trang, P.T.K., Lan, V.M., Anh, D.H., Tanabe, S., Viet, P.H., Berg, M., 2014. Human exposure to arsenic from drinking water in Vietnam. Sci. Total Environ. 488–489, 562–569. https://doi.org/10.1016/J.SCITOTENV.2013.10.039

AHK Vietnam, 2019. VIETNAM Photovoltaik & Smart Grids Zielmarktanalyse 2019 mit Profilen der Marktakteure. Ho Chi Minh City.

Ahmad, M., 2012. Iron and Manganese removal from groundwater Geochemical modeling of the Vyredox method. DUO – Res. Arch.

Ahmed, M., Shayya, W.H., Hoey, D., Al-Handaly, J., 2001. Brine disposal from reverse osmosis desalination plants in Oman and the United Arab Emirates. Desalination 133, 135–147. https://doi.org/10.1016/S0011-9164(01)80004-7

Ahmed, M., Shayya, W.H., Hoey, D., Mahendran, A., Morris, R., Al-Handaly, J., 2000. Use of evaporation ponds for brine disposal in desalination plants. Desalination 130, 155–168. https://doi.org/10.1016/S0011-9164(00)00083-7

Al-Amoudi, A., Lovitt, R.W., 2007. Fouling strategies and the cleaning system of NF membranes and factors affecting cleaning efficiency. J. Memb. Sci. https://doi.org/10.1016/j.memsci.2007.06.002

Al-Kaabi, A., Al-Sulaiti, H., Al-Ansari, T., Mackey, H.R., 2021. Assessment of water quality variations on pretreatment and environmental impacts of SWRO desalination. Desalination 500, 114831. https://doi.org/10.1016/j.desal.2020.114831

Ali, A., Tufa, R.A., Macedonio, F., Curcio, E., Drioli, E., 2018. Membrane technology in renewable-energy-driven desalination. Renew. Sustain. Energy Rev. 81, 1–21. https://doi.org/10.1016/j.rser.2017.07.047

Alkaisi, A., Mossad, R., Sharifian-Barforoush, A., 2017. A Review of the Water Desalination Systems Integrated with Renewable Energy. Energy Procedia 110, 268–274. https://doi.org/10.1016/j.egypro.2017.03.138

AlMarzooqi, F.A., Al Ghaferi, A.A., Saadat, I., Hilal, N., 2014. Application of Capacitive Deionisation in water desalination: A review. Desalination 342, 3–15. https://doi.org/10.1016/j.desal.2014.02.031

AlTaee, A., Sharif, A.O., 2011. Alternative design to dual stage NF seawater desalination using high rejection brackish water membranes. Desalination 273, 391–397. https://doi.org/10.1016/j.desal.2011.01.056

Aminfard, S., Davidson, F.T., Webber, M.E., 2019. Multi-layered spatial methodology for assessing the technical and economic viability of using renewable energy to power brackish groundwater desalination. Desalination 450, 12–20. https://doi.org/10.1016/j.desal.2018.10.014

Atlas, R., 2018. Purification of Brackish Water using Hybrid CDI-EDI Technology. San Antonio.

Avlonitis, S.A., 2002. Operational water cost and productivity improvements for small-size RO desalination plants. Desalination 142, 295–304. https://doi.org/10.1016/S0011-9164(02)00210-2

Ayers, J.C., Goodbred, S., George, G., Fry, D., Benneyworth, L., Hornberger, G., Roy, K., Karim, M.R., Akter, F., 2016. Sources of salinity and arsenic in groundwater in southwest Bangladesh. Geochem. Trans. 17, 1–22. https://doi.org/10.1186/s12932-016-0036-6

Azhar, F. El, Harrak, N. El, Azhar, M. El, Hafsi, M., Elmidaoui, A., 2013. Feasibility of Nanofiltration process in dual stage in desalination \nof the seawater. IOSR J. Appl. Chem. 5, 35–42.

Basile, A. (Angelo B., Cassano, A., Figoli, A., 2018. Current Trends and Future Developments on (Bio-) Membranes : Renewable Energy Integrated with Membrane Operations. Elsevier.

Berg, M., Stengel, C., Trang, P.T.K., Hung Viet, P., Sampson, M.L., Leng, M., Samreth, S., Fredericks, D., 2007. Magnitude of arsenic pollution in the Mekong and Red River Deltas - Cambodia and Vietnam. Sci. Total Environ. 372, 413–425. https://doi.org/10.1016/j.scitotenv.2006.09.010

Biesheuvel, P.M., Bazant, M.Z., Cusick, R.D., Hatton, T.A., Hatzell, K.B., Hatzell, M.C., Liang, P., Lin, S., Porada, S., Santiago, J.G., Smith, K.C., Stadermann, M., Su, X., Sun, X., Waite, T.D., van der Wal, A., Yoon, J., Zhao, R., Zou, L., Suss, M.E., 2017a. Capacitive Deionization -- defining a class of desalination technologies. arXiv.

Biesheuvel, P.M., Bazant, M.Z., Cusick, R.D., Hatton, T.A., Hatzell, K.B., Hatzell, M.C., Liang, P., Lin, S., Porada, S., Santiago, J.G., Smith, K.C., Stadermann, M., Su, X., Sun, X., Waite, T.D., van der Wal, A., Yoon, J., Zhao, R., Zou, L., Suss, M.E., 2017b. Capacitive Deionization -- defining a class of desalination technologies.

Biesheuvel, P.M., Dykstra, J.E., 2020. Physics of electrochemical processes, June 2, 20. ed. phisicsofeletrochemicalproces.com.

Biesheuvel, P.M., Porada, S., Levi, M., Bazant, M.Z., 2014. Attractive forces in microporous carbon electrodes for capacitive deionization. J. Solid State Electrochem. 18, 1365–1376. https://doi.org/10.1007/s10008-014-2383-5

Binh, N.T., 2015. Vulnerability and adaptation to salinity intrusion in the Mekong delta of Vietnam. Rheinischen Friedrich-Wilhelms-Universität.

Brecht, H., Dasgupta, S., Laplante, B., Murray, S., Wheeler, D., 2012. Sea-Level Rise and Storm Surges. J. Environ. Dev. 21, 120–138. https://doi.org/10.1177/1070496511433601

Brunsting, J.H., McBean, E.A., 2014. In situ treatment of arsenic-contaminated groundwater by air sparging. J. Contam. Hydrol. 159, 20–35. https://doi.org/10.1016/j.jconhyd.2014.01.003

Bundschuh, J., Litter, M.I., Parvez, F., Román-Ross, G., Nicolli, H.B., Jean, J.S., Liu, C.W., López, D., Armienta, M.A., Guilherme, L.R.G., Cuevas, A.G., Cornejo, L., Cumbal, L., Toujaguez, R., 2012. One century of arsenic exposure in Latin America: A review of history and occurrence from 14 countries. Sci. Total Environ. https://doi.org/10.1016/j.scitotenv.2011.06.024

Bundschuh, J., M. Holländer, H., Ma, L.Q., 2014. In-Situ Remediation of Arsenic-Contaminated Sites, Arsenic in the Environment. CRC Press. https://doi.org/10.1201/b17619

Buschmann, J., Berg, M., Stengel, C., Winkel, L., Sampson, M.L., Trang, P.T.K., Viet, P.H., 2008. Contamination of drinking water resources in the Mekong delta floodplains: Arsenic and other trace metals pose serious health risks to population. Environ. Int. 34, 756–764. https://doi.org/10.1016/j.envint.2007.12.025

Caldera, U., Bogdanov, D., Breyer, C., 2016. Local cost of seawater RO desalination based on solar PV and wind energy: A global estimate. Desalination 385, 207–216. https://doi.org/10.1016/j.desal.2016.02.004

Calì, G., Fois, E., Lallai, A., Mura, G., 2008. Optimal design of a hybrid RO/MSF desalination system in a non-OPEC country. Desalination 228, 114–127. https://doi.org/10.1016/j.desal.2007.08.012

Cañas Kurz, E.E., Luong, V.T., Hellriegel, U., Leidinger, F., Luu, T.L., Bundschuh, J., Hoinkis, J., 2020. Iron-based subsurface arsenic removal (SAR): Results of a long-term pilot-scale test in Vietnam. Water Res. 181, 115929. https://doi.org/10.1016/j.watres.2020.115929

Cau-ca.com, 2020. Tide tables: tides for fishing [WWW Document]. URL https://cau-ca.com/ (accessed 7.1.20).

Cerci, Y., Cengel, Y., Wood, B., Kahraman, N., Karkas, E.S., 2003. Improving the thermodynamic and economic efficiencies of desalination plants: minimum work required for desalination and case studies of four working plants. Springfiled.

Chakrabarti, D., Singh, S.K., Rashid, M.H., Rahman, M.M., 2019. Arsenic: Occurrence in Groundwater, in: Encyclopedia of Environmental Health. Elsevier, pp. 153–168. https://doi.org/10.1016/B978-0-12-409548-9.10634-7

Chakraborti, D., Rahman, M.M., Mukherjee, A., Alauddin, M., Hassan, M., Dutta, R.N., Pati, S., Mukherjee, S.C., Roy, S., Quamruzzman, Q., Rahman, M., Morshed, S., Islam, T., Sorif, S., Selim, M., Islam, M.R., Hossain, M.M., 2015. Groundwater arsenic contamination in Bangladesh—21 Years of research. J. Trace Elem. Med. Biol. 31, 237–248. https://doi.org/10.1016/j.jtemb.2015.01.003

Chung, T.C., 2018. Evaluating the desalination performance and efficiency of capacitice deionization with activated carbon electrodes.

Clancy, T.M., Hayes, K.F., Raskin, L., 2013. Arsenic waste management: A critical review of testing and disposal of arsenic-bearing solid wastes generated during arsenic removal from drinking water. Environ. Sci. Technol. 47, 10799–10812. https://doi.org/10.1021/es401749b

Colombani, N., Osti, A., Volta, G., Mastrocicco, M., 2016. Impact of Climate Change on Salinization of Coastal Water Resources. Water Resour. Manag. 30, 2483–2496. https://doi.org/10.1007/s11269-016-1292-z

Dasgupta, S., Akhter, F., Zahirul, K., Khan, Z., Choudhury, S., Nishat, A., 2014a. River Salinity and Climate Change Evidence from Coastal Bangladesh (No. 6817).

Dasgupta, S., Hossain, M.M., Huq, M., Wheeler, D., 2014b. Climate Change, Groundwater Salinization and Road Maintenance Costs in Coastal Bangladesh (No. 7147).

Dash, R., Weinstein, L., 2013. Capacitive deionization may help solve water problems in India. World Water 09/10, 16–17.

Delgado-Torres, A.M., García-Rodríguez, L., del Moral, M.J., 2020. Preliminary assessment of innovative seawater reverse osmosis (SWRO) desalination powered by a hybrid solar photovoltaic (PV) - Tidal range energy system. Desalination 477, 114247. https://doi.org/10.1016/j.desal.2019.114247

DESWARE, 2018. Energy Requirements Of Desalination Processes. Encycl. Desalin. Water Resour. Energy Requir. Desalin. Process.

Dorji, P., Kim, D.I., Hong, S., Phuntsho, S., Shon, H.K., 2020. Pilot-scale membrane capacitive deionisation for effective bromide removal and high water recovery in seawater desalination. Desalination 479, 114309. https://doi.org/10.1016/j.desal.2020.114309

Dow, 2018. FILMTEC NF90 1–2.

Dow Chemical, 2018. Water Application Value Engine [WWW Document].

Dow Chemical, 2017. WAVE RONF System Design.

DuPont, 2020. FILMTEC ™ Reverse Osmosis Membranes Technical Manual.

Dykstra, J.E., Keesman, K.J., Biesheuvel, P.M., van der Wal, A., 2017. Theory of pH changes in water desalination by capacitive deionization. Water Res. 119, 178–186. https://doi.org/10.1016/j.watres.2017.04.039

Ettouney, H., Rizzuti, L., 2007. Solar desalination: A challenge for sustainable fresh water in the 21stcentury, in: NATO Security through Science Series C: Environmental Security. Springer Netherlands, Dordrecht, pp. 1–18. https://doi.org/10.1007/978-1-4020-5508-9_1

Fan, C.-S., Liou, S.Y.H., Hou, C.-H., 2017. Capacitive deionization of arsenic-contaminated groundwater in a single-pass mode. Chemosphere 184, 924–931. https://doi.org/10.1016/j.chemosphere.2017.06.068

Fan, C.S., Tseng, S.C., Li, K.C., Hou, C.H., 2016. Electro-removal of arsenic(III) and arsenic(V) from aqueous solutions by capacitive deionization. J. Hazard. Mater. 312, 208–215. https://doi.org/10.1016/j.jhazmat.2016.03.055

Farrell, J., Chaudhary, B.K., 2013. Understanding Arsenate Reaction Kinetics with Ferric Hydroxides. Environ. Sci. Technol. 47, 8342–8347. https://doi.org/10.1021/es4013382

FERMANOX, 2017. Info-Blatt: Höhere Lebensdauer der Brunnen mit FERMANOX [WWW Document]. URL https://www.fermanox-wasseraufbereitung.de/downloads

Figoli, A., Fuoco, I., Apollaro, C., Chabane, M., Mancuso, R., Gabriele, B., De Rosa, R., Vespasiano, G., Barca, D., Criscuoli, A., 2020. Arsenic-contaminated groundwaters remediation by nanofiltration. Sep. Purif. Technol. 238. https://doi.org/10.1016/j.seppur.2019.116461

Figoli, A., Hoinkis, J., Bundschuh, J., 2016. Membrane Technologies for Water Treatment: Removal of Toxic Trace Elements with Emphasis on Arsenic, Fluoride and Uranium, Sustainable Water Developments. CRC Press.

Flora, S.J.S., 2015. Arsenic: Chemistry, Occurrence, and Exposure, in: Handbook of Arsenic Toxicology. Elsevier, pp. 1–49. https://doi.org/10.1016/B978-0-12-418688-0.00001-0

Fritz, M., Hohmann, C., Tettenborn, F., 2020. Framework conditions to design sustainable business models for decentralised water treatment technologies in Viet Nam for international technology providers. J. Water Reuse Desalin. 10, 317–331. https://doi.org/10.2166/wrd.2020.016

Gaikwad, M.S., Balomajumder, C., 2017. Simultaneous electrosorptive removal of chromium(VI) and fluoride ions by capacitive deionization (CDI): Multicomponent isotherm modeling and kinetic study. Sep. Purif. Technol. 186, 272–281. https://doi.org/10.1016/j.seppur.2017.06.017

Galliari, J., Santucci, L., Misseri, L., Carol, E., Alvarez, M. del P., 2021. Processes controlling groundwater salinity in coastal wetlands of the southern edge of South America. Sci. Total Environ. 754, 141951. https://doi.org/10.1016/j.scitotenv.2020.141951

Garg, M.C., 2019. Renewable Energy-Powered Membrane Technology: Cost Analysis and Energy Consumption, in: Current Trends and Future Developments on (Bio-) Membranes. Elsevier, pp. 85–110. https://doi.org/10.1016/B978-0-12-813545-7.00004-0

Garg, M.C., Joshi, H., 2014. Optimization and economic analysis of small scale nanofiltration and reverse osmosis brackish water system powered by photovoltaics. Desalination 353, 57–74. https://doi.org/10.1016/j.desal.2014.09.005

Garrido Hoyos, S.E., Avilés Flores, M., Ramírez González, A., Calderón Mólgora, C., Potabilización Alberto Nieto Rodríguez, D., Nieto Rodríguez, A., 2007. Removal arsenic in drinking water by capacitive deionisation. Rev. AIDIS Ing. y Ciencias Ambient. Investig. desarollo y Pract. 1.

Garrido, S.E., Aviles, M., Ramirez, A., Calderon, C., Ramirez-Orozco, A., Nieto, A., Shelp, G., Seed, L., Cebrian, M., Vera, E., 2008. Arsenic removal from water of Huautla, Morelos, Mexico using capacitive deionization. pp. 665–676. https://doi.org/10.1201/b11334-87

Gaublomme, D., Strubbe, L., Vanoppen, M., Torfs, E., Mortier, S., Cornelissen, E., De Gusseme, B., Verliefde, A., Nopens, I., 2020. A generic reverse osmosis model for full-scale operation. Desalination 490, 114509. https://doi.org/10.1016/j.desal.2020.114509

Ghaffour, N., Missimer, T.M., Amy, G.L., 2013. Technical review and evaluation of the economics of water desalination: Current and future challenges for better water supply sustainability. Desalination 309, 197–207. https://doi.org/10.1016/j.desal.2012.10.015

Giang, P.Q., Toshiki, K., Sakata, M., Kunikane, S., Vinh, T.Q., 2014. Modelling Climate Change Impacts on the Seasonality of Water Resources in the Upper Ca River Watershed in Southeast Asia. Sci. World J. 2014, 1–14. https://doi.org/10.1155/2014/279135

Goh, P.S., Lau, W.J., Othman, M.H.D., Ismail, A.F., 2018. Membrane fouling in desalination and its mitigation strategies. Desalination 425, 130–155. https://doi.org/10.1016/j.desal.2017.10.018

Goh, P.S., Matsuura, T., Ismail, A.F., Hilal, N., 2016. Recent trends in membranes and membrane processes for desalination. Desalination 391, 43–60. https://doi.org/10.1016/j.desal.2015.12.016

Golubenko, D.V., Karavanova, Y.A., Melnikov, S.S., Achoh, A.R., Pourcelly, G., Yaroslavtsev, A.B., 2018. An approach to increase the permselectivity and mono-valent ion selectivity of cation-exchange membranes by introduction of amorphous zirconium phosphate nanoparticles. J. Memb. Sci. 563, 777–784. https://doi.org/10.1016/J.MEMSCI.2018.06.024

Gonzalez, B., Heijman, S.G.J., Rietveld, L.C., van Halem, D., 2019. Arsenic removal from geothermal influenced groundwater with low pressure NF pilot plant for drinking water production in Nicaraguan rural communities. Sci. Total Environ. 667, 297–305. https://doi.org/10.1016/j.scitotenv.2019.02.222

Gouzinis, A., Kosmidis, N., Vayenas, D.., Lyberatos, G., 1998. Removal of Mn and simultaneous removal of NH3, Fe and Mn from potable water using a trickling filter. Water Res. 32, 2442–2450. https://doi.org/10.1016/S0043-1354(97)00471-5

Green, T.R., Taniguchi, M., Kooi, H., Gurdak, J.J., Allen, D.M., Green, T.R.;, Gurdak, J.J.;, Allen, D.M.;, Hiscock, K.M.;, Treidel, H., Aureli, A., 2011. Beneath the surface of global change: Impacts of climate change on groundwater. J. Hydrol. 405, 532–560.

Greene, R., Timms, W., Rengasamy, P., Arshad, M., Cresswell, R., 2016. Soil and aquifer salinization: Toward an integrated approach for salinity management of groundwater, in: Integrated Groundwater Management: Concepts, Approaches and Challenges. Springer International Publishing, pp. 377–412. https://doi.org/10.1007/978-3-319-23576-9_15

Greenlee, L.F., Lawler, D.F., Freeman, B.D., Marrot, B., Moulin, P., 2009. Reverse osmosis desalination: Water sources, technology, and today's challenges. Water Res. 43, 2317–2348. https://doi.org/10.1016/j.watres.2009.03.010

Grischek, T., Feistel, U., Ebermann, J., Musche, F., Bruntsch, S., Uhlmann, W., 2016. Field experiments on subsurface iron removal in the Lusatian mining region, in: Drebenstedt, C., Michael, P. (Eds.), Mining Meets Water - Conflicts and Solutions. IMWA 2016, Freiberg, pp. 292–297.

Grischek, T., Winkelnkemper, T., Ebermann, J., Herlitzius, J., 2015. Small scale subsurface iron removal in Germany. Khon Kaen.

Gude, V.G., Nirmalakhandan, N., Deng, S., 2010. Renewable and sustainable approaches for desalination. Renew. Sustain. Energy Rev. 14, 2641–2654. https://doi.org/10.1016/j.rser.2010.06.008

Hallberg, R.O., Martinell, R., 1976. Vyredox - In Situ Purification of Ground Water. Ground Water 14, 88–93. https://doi.org/10.1111/j.1745-6584.1976.tb03638.x

Hamed, O.A., 2005. Overview of hybrid desalination systems — current status and future prospects. Desalination 186, 207–214. https://doi.org/10.1016/j.desal.2005.03.095

Hassanvand, A., Wei, K., Talebi, S., Chen, G.Q., Kentish, S.E., 2017. The Role of Ion Exchange Membranes in Membrane Capacitive Deionisation. Membranes (Basel). 7, 54. https://doi.org/10.3390/membranes7030054

Hawks, S.A., Ramachandran, A., Porada, S., Campbell, P.G., Suss, M.E., Biesheuvel, P.M., Santiago, J.G., Stadermann, M., 2019. Performance metrics for the objective assessment of capacitive deionization systems. Water Res. 152, 126–137. https://doi.org/10.1016/j.watres.2018.10.074

Hellriegel, U., Cañas Kurz, E.E., Luong, T.V., Bundschuh, J., Hoinkis, J., 2020. Modular treatment of arsenic-laden brackish groundwater using solar-powered subsurface arsenic removal (SAR) and membrane capacitive deionization (MCDI) in Vietnam. Water Reuse Desalin. X.X., Manuscript submitted 03.2020.

Henning, A.-K.K., Rott, U., 2003. Untersuchungen zur Manganoxidation bei der In-situ-Aufbereitung von reduzierten Grundwässern. Grundwasser 8, 238–247. https://doi.org/10.1007/s00767-003-0005-8

Hien, L.T., Quy, P.N., Viet, N.T., 2009. Assessment of salinity intrusion in the Red River under effect of climate change, in: ICEC.

Hou, Q., Sun, J., Jing, J., Liu, C., Zhang, Y., Liu, J., Hua, M., 2018. A Regional Scale Investigation on Groundwater Arsenic in Different Types of Aquifers in the Pearl River Delta, China. Geofluids 2018, 1–9. https://doi.org/10.1155/2018/3471295

Hssaisoune, M., Bouchaou, L., Sifeddine, A., Bouimetarhan, I., Chehbouni, A., 2020. Moroccan Groundwater Resources and Evolution with Global Climate Changes. Geosciences 10, 81. https://doi.org/10.3390/geosciences10020081

Huang, K.Z., Tang, H.L., 2020. Temperature and desorption mode matter in capacitive deionization process for water desalination. Environ. Technol. 41, 3456–3463. https://doi.org/10.1080/09593330.2019.1611941

Hummer, 2020. Hummer 2kW wind turbine power generation curve [WWW Document]. Front Gener. Wind turbine. URL http://www.allwindturbine.com/products_info/Hummer-2KW-Wind-Turbine-Price-227775.html (accessed 12.1.20).

Huq, M.E., Fahad, S., Shao, Z., Sarven, M.S., Khan, I.A., Alam, M., Saeed, M., Ullah, H., Adnan, M., Saud, S., Cheng, Q., Ali, S., Wahid, F., Zamin, M., Raza, M.A., Saeed, B., Riaz, M., Khan, W.U., 2020. Arsenic in a groundwater environment in Bangladesh: Occurrence and mobilization. J. Environ. Manage. 262, 110318. https://doi.org/10.1016/j.jenvman.2020.110318

Idropan, 2018. Plimmer – CDI (Capacitive Deionization) [WWW Document]. URL http://www.idropan.com/en/portfolio-view/plimmer-cdi/ (accessed 8.13.18).

IPCC, 2014. Climate Change 2014: Synthesis Report. Contribution of Working Groups I,II and III to the Fifth Assessment Report of the Intergovernmental Panel on Climate Change, IPCC. IPCC, Geneva, Switzerland.

Jande, Y.A.C., Minhas, M.B., Kim, W.S., 2013. Ultrapure water from seawater using integrated reverse osmosis-capacitive deionization system. Desalin. Water Treat. 53, 3482–3490. https://doi.org/10.1080/19443994.2013.873352

Jeon, B.-H., Dempsey, B.A., Burgos, W.D., 2003. Kinetics and Mechanisms for Reactions of Fe(II) with Iron(III) Oxides. Environ. Sci. Technol. 37, 3309–3315. https://doi.org/10.1021/es025900p

Jeon, S. Il, Park, H.R., Yeo, J.G., Yang, S., Cho, C.H., Han, M.H., Kim, D.K., 2013. Desalination via a new membrane capacitive deionization process utilizing flow-electrodes. Energy Environ. Sci. 6, 1471–1475. https://doi.org/10.1039/c3ee24443a

Jeong, K., Yoon, N., Park, S., Son, M., Lee, J., Park, J., Cho, K.H., 2020. Optimization of a nanofiltration and membrane capacitive deionization (NF-MCDI) hybrid system: Experimental and modeling studies. Desalination 493, 114658. https://doi.org/10.1016/j.desal.2020.114658

Jia, Y., Xi, B., Jiang, Y., Guo, H., Yang, Y., Lian, X., Han, S., 2018. Distribution, formation and human-induced evolution of geogenic contaminated groundwater in China: A review. Sci. Total Environ. 643, 967–993. https://doi.org/10.1016/j.scitotenv.2018.06.201

Jiang, S., Li, Y., Ladewig, B.P., 2017. A review of reverse osmosis membrane fouling and control strategies. Sci. Total Environ. 595, 567–583. https://doi.org/10.1016/j.scitotenv.2017.03.235

Jones, E., Qadir, M., van Vliet, M.T.H., Smakhtin, V., Kang, S., 2019. The state of desalination and brine production: A global outlook. Sci. Total Environ. 657, 1343–1356. https://doi.org/10.1016/j.scitotenv.2018.12.076

Kang, J., Kim, T., Jo, K., Yoon, J., 2014. Comparison of salt adsorption capacity and energy consumption between constant current and constant voltage operation in capacitive deionization. Desalination 352, 52–57. https://doi.org/10.1016/j.desal.2014.08.009

Karakish, A.A.K., 2005. Subsurface removal of iron and manganese from groundwater-case study, in: Ninth International Water Technology Conference, IWTC9. Cairo, pp. 415–429.

Kennish, M.J., 2018. Ecology of Estuaries: Volume 1: Physical and Chemical Aspects. CRC Press, Boca Raton, FL.

Khayet, M., 2016. Fouling and Scaling in Desalination. Desalination 393, 1. https://doi.org/10.1016/j.desal.2016.05.005

Khodabakhshi, A.R., Asgari, S., 2018. Fabrication and characterization of cation exchange nanocomposite membranes comprising ABS/PC polymer blend with NiFe2O4 nanoparticles. J. Environ. Chem. Eng. 6, 5434–5442. https://doi.org/10.1016/J.JECE.2018.08.031

Klingel, F., 2016. Potential of In-situ Groundwater Treatment for Iron , Manganese and Arsenic Removal in Vietnam. Artic. Submitt. to 4th Int. Symp. Vietnam Water Coop. Initia- tive Water Secur. a Chang. Era, 19.-20th Oct. 2015, Hanoi, Vietnam 10.

Koltuniewicz, A.B., 2017. Process Intensification: Definition and Application to Membrane Processes, in: Sustainable Membrane Technology for Water and Wastewater Treatment. Springer, Singapore, pp. 67–96. https://doi.org/10.1007/978-981-10-5623-9_3

Kurosawa, K., Egashira, K., Tani, M., 2013. Relationship of arsenic concentration with ammonium-nitrogen concentration, oxidation reduction potential and pH of groundwater in arsenic-contaminated areas in Asia. Phys. Chem. Earth 58–60, 85–88. https://doi.org/10.1016/j.pce.2013.04.016

Kurz, E.E.C., Hellriege, U., Figoli, A., Gabriele B, B., Bundschuh, J., Hoinkis, J., 2021. Small-scale membrane-based arsenic removal for decentralized applications – developing a conceptual approach for future utilization. Water Res. 116978. https://doi.org/10.1016/j.watres.2021.116978

Ky, N.V., 2018. EFFECTS OF THE SEA LEVEL RISE ON UNDERGROUND WATER RESOURCES IN HO CHI MINH AREA. Vietnam J. Sci. Technol. 54, 260. https://doi.org/10.15625/2525-2518/54/4B/12049

Landaburu-Aguirre, J., García-Pacheco, R., Molina, S., Rodríguez-Sáez, L., Rabadán, J., García-Calvo, E., 2016. Fouling prevention, preparing for re-use and membrane recycling. Towards circular economy in RO desalination. Desalination 393, 16–30. https://doi.org/10.1016/j.desal.2016.04.002

Le Luu, T., 2019. Remarks on the current quality of groundwater in Vietnam. Environ. Sci. Pollut. Res. 26, 1163–1169. https://doi.org/10.1007/s11356-017-9631-z

Li, S., Cai, Y.-H., Schäfer, A.I., Richards, B.S., 2019. Renewable energy powered membrane technology: A review of the reliability of photovoltaic-powered membrane system components for brackish water desalination. Appl. Energy 253, 113524. https://doi.org/10.1016/j.apenergy.2019.113524

Li, W., Krantz, W.B., Cornelissen, E.R., Post, J.W., Verliefde, A.R.D., Tang, C.Y., 2013. A novel hybrid process of reverse electrodialysis and reverse osmosis for low energy seawater desalination and brine management. Appl. Energy 104, 592–602. https://doi.org/10.1016/j.apenergy.2012.11.064

Li, Y., Zhang, C., Jiang, Y., Wang, T.J., Wang, H., 2016. Effects of the hydration ratio on the electrosorption selectivity of ions during capacitive deionization. Desalination 399, 171–177. https://doi.org/10.1016/j.desal.2016.09.011

Litter, M., Cortina, J., Fiúza, A., Futuro, A., Tsakiroglou, C., 2014. In-situ technologies for groundwater treatment. The case of arsenic., in: In-Situ Remediation of Arsenic-Contaminated Sites. CRC Press (arsenic in the Environment), pp. 1–33.

Litter, M.I., Morgada, M.E., Bundschuh, J., 2010. Possible treatments for arsenic removal in Latin American waters for human consumption. Environ. Pollut. 158, 1105–1118. https://doi.org/10.1016/j.envpol.2010.01.028

Luong, V.T., Cañas Kurz, E.E., Hellriegel, U., Luu, T.L., Hoinkis, J., Bundschuh, J., 2019. Iron-based subsurface arsenic removal by aeration (SAR) – Results of a pilot-scale plant in Vietnam, in: Bundschuh, J., Bhattacharya, P. (Eds.), Environmental Arsenic in a Changing World As2018. CRC Press/Balkema, pp. 418–419.

Luong, V.T., Cañas Kurz, E.E., Hellriegel, U., Luu, T.L., Hoinkis, J., Bundschuh, J., 2018. Iron-based subsurface arsenic removal technologies by aeration: A review of the current state and future prospects. Water Res. 133, 110–122. https://doi.org/10.1016/j.watres.2018.01.007

Maier, M. V., Isenbeck-Schröter, M., Klose, L.B., Ritter, S.M., Scholz, C., 2017. In Situ-mobilization of Arsenic in Groundwater – an Innovative Remediation Approach? Procedia Earth Planet. Sci. 17, 452–455. https://doi.org/10.1016/j.proeps.2016.12.114

Manju, S., Sagar, N., 2017. Renewable energy integrated desalination: A sustainable solution to overcome future fresh-water scarcity in India. Renew. Sustain. Energy Rev. 73, 594–609. https://doi.org/10.1016/j.rser.2017.01.164

Marcovecchio, M.G., Mussati, S.F., Aguirre, P.A., Nicolás J, Scenna, 2005. Optimization of hybrid desalination processes including multi stage flash and reverse osmosis systems. Desalination 182, 111–122. https://doi.org/10.1016/j.desal.2005.03.011

MARD, 2020. Vietnam - Drought and Saltwater Intrussion. Flash Update No. 1 about the Drought and Saltwater Intrusion in the Mekong Delta.

McLusky, D.S., Elliott, M., 2004. The Estuarine Ecosystem. Oxford University Press. https://doi.org/10.1093/acprof:oso/9780198525080.001.0001

Mikhailov, V.N., Isupova, M. V., 2008. Hypersalinization of river estuaries in West Africa. Water Resour. 35, 367–385. https://doi.org/10.1134/S0097807808040015

Minhas, M.B., Jande, Y.A.C., Kim, W.S., 2014. Combined reverse osmosis and constant-current operated capacitive deionization system for seawater desalination. Desalination 344, 299–305. https://doi.org/10.1016/j.desal.2014.03.043

Mito, M.T., Ma, X., Albuflasa, H., Davies, P.A., 2019. Reverse osmosis (RO) membrane desalination driven by wind and solar photovoltaic (PV) energy: State of the art and challenges for large-scale implementation. Renew. Sustain. Energy Rev. 112, 669–685. https://doi.org/10.1016/j.rser.2019.06.008

Mohan, D., Pittman, C.U., 2007. Arsenic removal from water/wastewater using adsorbents-A critical review. J. Hazard. Mater. 142, 1–53. https://doi.org/10.1016/j.jhazmat.2007.01.006

Mondal, P., Majumder, C.B., Mohanty, B., 2006. Laboratory based approaches for arsenic remediation from contaminated water: Recent developments. J. Hazard. Mater. 137, 464–479. https://doi.org/10.1016/j.jhazmat.2006.02.023

Mossad, M., Zou, L., 2013. Study of fouling and scaling in capacitive deionisation by using dissolved organic and inorganic salts. J. Hazard. Mater. 244–245, 387–393. https://doi.org/10.1016/j.jhazmat.2012.11.062

Mossad, M., Zou, L., 2012. A study of the capacitive deionisation performance under various operational conditions. J. Hazard. Mater. 213–214, 491–497. https://doi.org/10.1016/j.jhazmat.2012.02.036

Mukherjee, A.B., Bhattacharya, P., 2001. Arsenic in groundwater in the Bengal Delta Plain: slow poisoning in Bangladesh. Environ. Rev. 9, 189–220. https://doi.org/10.1139/er-9-3-189

Mulder, M., 1996a. Transport in Membranes, in: Basic Principles of Membrane Technology. Springer Netherlands, Dordrecht, pp. 210–279. https://doi.org/10.1007/978-94-009-1766-8_5

Mulder, M., 1996b. Basic Principles of Membrane Technology. Springer Netherlands, Dordrecht. https://doi.org/10.1007/978-94-009-1766-8

Natasha, Shahid, M., Imran, M., Khalid, S., Murtaza, B., Niazi, N.K., Zhang, Y., Hussain, I., 2020. Arsenic Environmental Contamination Status in South Asia, in: Arsenic in Drinking Water and Food. Springer Singapore, Singapore, pp. 13–39. https://doi.org/10.1007/978-981-13-8587-2_2

National Research Council, 2010. Management and Effects of Coalbed Methane Produced Water in the Western Uniterd States. The National Academies Press, Washington DC.

Ngo-Duc, T., 2014. Climate Change in the Coastal Regions of Vietnam, in: Coastal Disasters and Climate Change in Vietnam. Elsevier, pp. 175–198. https://doi.org/10.1016/B978-0-12-800007-6.00008-3

Ngo, M.T., Lee, J.M., Lee, H.A., Woo, N.C., 2015. The sustainability risk of Ho Chi Minh City, Vietnam, due to saltwater intrusion. Geosci. J. 19, 547–560. https://doi.org/10.1007/s12303-014-0052-4

Nicomel, N.R., Leus, K., Folens, K., Van Der Voort, P., Du Laing, G., 2015. Technologies for arsenic removal from water: Current status and future perspectives. Int. J. Environ. Res. Public Health. https://doi.org/10.3390/ijerph13010062

Norrman, J., Sparrenbom, C.J., Berg, M., Dang, D.N., Jacks, G., Harms-Ringdahl, P., Pham, Q.N., Rosqvist, H., 2015. Tracing sources of ammonium in reducing groundwater in a well field in Hanoi (Vietnam) by means of stable nitrogen isotope ($\delta15N$) values. Appl. Geochemistry 61, 248–258. https://doi.org/10.1016/j.apgeochem.2015.06.009

Palit, S., Misra, K., Mishra, J., 2019. Arsenic Contamination in South Asian Regions: The Difficulties, Challenges and Vision for the Future, in: Separation Science and Technology (New York). Elsevier Inc., pp. 113–123. https://doi.org/10.1016/B978-0-12-815730-5.00005-3

Parvaiz, A., Khattak, J.A., Hussain, I., Masood, N., Javed, T., Farooqi, A., 2021. Salinity enrichment, sources and its contribution to elevated groundwater arsenic and fluoride levels in Rachna Doab, Punjab Pakistan: Stable isotope ($\delta2H$ and $\delta18O$) approach as an evidence. Environ. Pollut. 268, 115710. https://doi.org/10.1016/j.envpol.2020.115710

Pazouki, P., Stewart, R.A., Bertone, E., Helfer, F., Ghaffour, N., 2020. Life cycle cost of dilution desalination in off-grid locations: A study of water reuse integrated with seawater desalination technology. Desalination 491, 114584. https://doi.org/10.1016/j.desal.2020.114584

Pellegrino, J., Gorman, C., Richards, L., 2007. A speculative hybrid reverse osmosis/electrodialysis unit operation. Desalination 214, 11–30. https://doi.org/10.1016/j.desal.2006.09.024

Pereira, L.S., Duarte, E., Fragoso, R., 2014. Water Use: Recycling and Desalination for Agriculture. Encycl. Agric. Food Syst. 5, 407–424. https://doi.org/10.1016/B978-0-444-52512-3.00084-X

Peter-Varbanets, M., Johnston, R., Meierhofer, R., Kage, F., Pronk, W., 2011. Gravity-driven membrane disinfection for household drinking water treatment. Futur. Water, Sanit. Hyg. Low-Income Ctries. Innov. Adapt. Engagem. a Chang. World - Proc. 35th WEDC Int. Conf.

Pimentel da Silva, G.D., Sharqawy, M.H., 2020. Techno-economic analysis of low impact solar brackish water desalination system in the Brazilian Semiarid region. J. Clean. Prod. 248, 119255. https://doi.org/10.1016/j.jclepro.2019.119255

Pokhrel, D., Bhandari, B.S., Viraraghavan, T., 2009. Arsenic contamination of groundwater in the Terai region of Nepal: An overview of health concerns and treatment options. Environ. Int. 35, 157–161. https://doi.org/10.1016/j.envint.2008.06.003

Porada, S., Zhang, L., Dykstra, J.E., 2020. Energy consumption in membrane capacitive deionization and comparison with reverse osmosis. Desalination 488, 114383. https://doi.org/10.1016/j.desal.2020.114383

Pritchard, D.W., 1967. What is an estuary: Physical Viewpoint, in: Estuaries. American Association for the Advancement of Science AAAS, Washington DC.

Prusty, P., Farooq, S.H., 2020. Seawater intrusion in the coastal aquifers of India - A review. HydroResearch 3, 61–74. https://doi.org/10.1016/j.hydres.2020.06.001

Qasim, M., Badrelzaman, M., Darwish, N.N., Darwish, N.A., Hilal, N., 2019. Reverse osmosis desalination: A state-of-the-art review. Desalination 459, 59–104. https://doi.org/10.1016/j.desal.2019.02.008

QCVN:01, 2009. Vietnamese National technical regulation on drinking water quality. CỘNG HÒA XÃ HỘI CHỦ NGHĨA VIỆT NAM.

Qu, Y., Campbell, P.G., Gu, L., Knipe, J.M., Dzenitis, E., Santiago, J.G., Stadermann, M., 2016. Energy consumption analysis of constant voltage and constant current operations in capacitive deionization. Desalination 400, 18–24. https://doi.org/10.1016/j.desal.2016.09.014

Rahman, M.M., Bakker, M., Freitas, S.C.B., van Halem, D., van Breukelen, B.M., Ahmed, K.M., Badruzzaman, A.B.M., 2014. Exploratory experiments to determine the effect of alternative operations on the efficiency of subsurface arsenic removal in rural Bangladesh | Expériences exploratoires pour déterminer l'effet des opérations alternatives sur l'efficacité de l'élimination. Hydrogeol. J. 23, 19–34. https://doi.org/10.1007/s10040-014-1179-0

Rahman, M.M.M., Bakker, M., Patty, C.H.L.H.L., Hassan, Z., Röling, W.F.M.F.M., Ahmed, K.M.M., van Breukelen, B.M.M., 2015. Reactive transport modeling of subsurface arsenic removal systems in rural Bangladesh. Sci. Total Environ., Arsenic in the Environment 537, 277–293. https://doi.org/10.1016/j.scitotenv.2015.07.140

Rajmohan, N., 2020. Groundwater Contamination Issues in the Shallow Aquifer, Ramganga Sub-basin, India, in: Kumar, M., Snow, D., Honda, R. (Eds.), Emerging Issues in the Water Environment during Anthropocene. Springer Singapore, Singapore, pp. 337–354. https://doi.org/10.1007/978-981-32-9771-5_18

Rajmohan, N., Masoud, M.H.Z., Niyazi, B.A.M., 2021. Impact of evaporation on groundwater salinity in the arid coastal aquifer, Western Saudi Arabia. CATENA 196, 104864. https://doi.org/10.1016/j.catena.2020.104864

Ramachandran, A., Oyarzun, D.I., Hawks, S.A., Stadermann, M., Santiago, J.G., 2019. High water recovery and improved thermodynamic efficiency for capacitive deionization using variable flowrate operation. Water Res. 155, 76–85. https://doi.org/10.1016/j.watres.2019.02.007

Rizzuti, L., Ettouney, H.M., Cipollina, A., 2007. Solar desalination for the 21st century : a review of modern technologies and researches on desalination coupled to renewable energies, in: NATO Advanced Research Workshop on Solar Desalination for the 21st Century. Springer, Hammamet, Tuni, p. 379.

Rott, U., Friedle, M., 2000. 25 Jahre unterirdische Wasseraufbereitung in Deutschland. Wasser Spec. 141, 99–107.

Rott, U., Kauffmann, H., 2008. A contribution to solve the arsenic problem in groundwater of Ganges Delta by in-situ treatment. Water Sci. Technol. 58, 2009–2015. https://doi.org/10.2166/wst.2008.751

Ruan, H., Zheng, Z., Pan, J., Gao, C., Van der Bruggen, B., Shen, J., 2018. Mussel-inspired sulfonated polydopamine coating on anion exchange membrane for improving permselectivity and anti-fouling property. J. Memb. Sci. 550, 427–435. https://doi.org/10.1016/J.MEMSCI.2018.01.005

Saadat, A.H.M., Islam, M.S., Parvin, F., Sultana, A., 2018. Desalination Technologies for Developing Countries: A Review. J. Sci. Res. 10, 77–97. https://doi.org/10.3329/jsr.v10i1.33179

Sankar, M.S., Vega, M.A., Defoe, P.P., Kibria, M.G., Ford, S., Telfeyan, K., Neal, A., Mohajerin, T.J., Hettiarachchi, G.M., Barua, S., Hobson, C., Johannesson, K., Datta, S., 2014. Elevated arsenic and manganese in groundwaters of Murshidabad, West Bengal, India. Sci. Total Environ. 488–489, 570–579. https://doi.org/10.1016/J.SCITOTENV.2014.02.077

Sarkar, A., Paul, B., 2017. Corrigendum to "The global menace of arsenic and its conventional remediation – A critical review" [Chemosphere 158 (September) (2016) 37–49](S004565351630683X)(10.1016/j.chemosphere.2016.05.043). Chemosphere 158, 630–631. https://doi.org/10.1016/j.chemosphere.2017.01.076

Sarkar, A., Paul, B., 2016. The global menace of arsenic and its conventional remediation - A critical review. Chemosphere 158, 37–49. https://doi.org/10.1016/J.CHEMOSPHERE.2016.05.043

Seed, L.P., Yetman, D.D., Pargaru, Y., Shelp, G.S., 2006. The desel system-capacitive deionization for the removal of ions from water, Water Environment Federation Technical Exhibition & Conference. Ontario.

Shan, H., Ma, T., Wang, Y., Zhao, J., Han, H., Deng, Y., He, X., Dong, Y., 2013. A cost-effective system for in-situ geological arsenic adsorption from groundwater. J. Contam. Hydrol. 154, 1–9. https://doi.org/10.1016/j.jconhyd.2013.08.002

Shemer, H., Semiat, R., 2017. Sustainable RO desalination – Energy demand and environmental impact. Desalination 424, 10–16. https://doi.org/10.1016/j.desal.2017.09.021

Shih, M.-C., 2005. An overview of arsenic removal by pressure-drivenmembrane processes. Desalination 172, 85–97. https://doi.org/10.1016/j.desal.2004.07.031

Shiu, H.-Y., Lee, M., Chao, Y., Chang, K.-C., Hou, C.-H., Chiueh, P.-T., 2019. Hotspot analysis and improvement schemes for capacitive deionization (CDI) using life cycle assessment. Desalination 468, 114087. https://doi.org/10.1016/j.desal.2019.114087

Singh, R., 2015a. Hybrid Membrane Systems – Applications and Case Studies, in: Membrane Technology and Engineering for Water Purification. Elsevier, pp. 179–281. https://doi.org/10.1016/B978-0-444-63362-0.00003-3

Singh, R., 2015b. Hybrid Membrane Plant Design and Operation, in: Membrane Technology and Engineering for Water Purification. Elsevier, pp. 283–337. https://doi.org/10.1016/B978-0-444-63362-0.00004-5

Singh, R., Singh, S., Parihar, P., Singh, V.P., Prasad, S.M., 2015. Arsenic contamination, consequences and remediation techniques: A review. Ecotoxicol. Environ. Saf. 112, 247–270. https://doi.org/10.1016/j.ecoenv.2014.10.009

Smedley, P.L., Nicolli, H.B., Macdonald, D.M.J., Barros, A.J., Tullio, J.O., 2002. Hydrogeochemistry of arsenic and other inorganic constituents in groundwaters from La Pampa, Argentina. Appl. Geochemistry 17, 259–284. https://doi.org/10.1016/S0883-2927(01)00082-8

Smith, M.J., Schreiber, E.S.G., Kohout, M., Ough, K., Lennie, R., Turnbull, D., Jin, C., Clancy, T., 2007. Wetlands as landscape units: spatial patterns in salinity and water chemistry. Wetl. Ecol. Manag. 15, 95–103. https://doi.org/10.1007/s11273-006-9015-5

Stein, S., Sivan, O., Yechieli, Y., Kasher, R., 2021. Redox condition of saline groundwater from coastal aquifers influences reverse osmosis desalination process. Water Res. 188, 116508. https://doi.org/10.1016/j.watres.2020.116508

Stollenwerk, K.G., Breit, G.N., Welch, A.H., Yount, J.C., Whitney, J.W., Foster, A.L., Uddin, M.N., Majumder, R.K., Ahmed, N., 2007. Arsenic attenuation by oxidized aquifer sediments in Bangladesh. Sci. Total Environ. 379, 133–150. https://doi.org/10.1016/j.scitotenv.2006.11.029

Stopelli, E., Duyen, V.T., Mai, T.T., Trang, P.T.K.K., Viet, P.H., Lightfoot, A., Kipfer, R., Schneider, M., Eiche, E., Kontny, A., Neumann, T., Glodowska, M., Patzner, M., Kappler, A., Kleindienst, S., Rathi, B., Cirpka, O., Bostick, B., Prommer, H., Winkel, L.H.E.E., Berg, M., 2020. Spatial and temporal evolution of groundwater arsenic contamination in the Red River delta, Vietnam: Interplay of mobilisation and retardation processes. Sci. Total Environ. 717, 137143. https://doi.org/10.1016/j.scitotenv.2020.137143

Stover, R., Crisp, G., 2008. ENVIRONMENTALLY SOUND DESALINATION AT THE PERTH SEAWATER DESALINATION PLANT, in: Australia's Environmental and Sutainability Conference and Exhibition. Melbourne.

Subiela, V.J., Peñate, B., Castellano, F., Domínguez, F.J., 2012. Solar PV powered RO systems, in: Bundschuh, J., Hoinkis, J. (Eds.), Renewable Energy Applications for Freshwater Production. CRC Press, Boca Raton, FL, pp. 135–160.

Suss, M.E., 2017. Size-Based Ion Selectivity of Micropore Electric Double Layers in Capacitive Deionization Electrodes. J. Electrochem. Soc. 164, E270–E275. https://doi.org/10.1149/2.1201709jes

Suss, M.E., Porada, S., Sun, X., Biesheuvel, P.M., Yoon, J., Presser, V., 2015a. Water desalination via capacitive deionization: What is it and what can we expect from it? Energy Environ. Sci. 8, 2296–2319. https://doi.org/10.1039/c5ee00519a

Suss, M.E., Porada, S., Sun, X., Biesheuvel, P.M., Yoon, J., Presser, V., 2015b. Water desalination via capacitive deionization: what is it and what can we expect from it? Energy Environ. Sci. 8, 2296–2319. https://doi.org/10.1039/c5ee00519a

Tan, C., He, C., Tang, W., Kovalsky, P., Fletcher, J., Waite, T.D., 2018. Integration of photovoltaic energy supply with membrane capacitive deionization (MCDI) for salt removal from brackish watersfile:///W:/01_Literatur/CDI/2018_Tan-Waite - IntegrPVwithMCDIBrackish.pdf. Water Res. 147, 276–286. https://doi.org/10.1016/j.watres.2018.09.056

Tang, W., He, D., Zhang, C., Kovalsky, P., Waite, T.D., 2017a. Comparison of Faradaic reactions in capacitive deionization (CDI) and membrane capacitive deionization (MCDI) water treatment processes. Water Res. 120, 229–237. https://doi.org/10.1016/j.watres.2017.05.009

Tang, W., He, D., Zhang, C., Waite, T.D., 2017b. Optimization of sulfate removal from brackish water by membrane capacitive deionization (MCDI). Water Res. 121, 302–310. https://doi.org/10.1016/j.watres.2017.05.046

Tang, W., Kovalsky, P., Cao, B., He, D., Waite, T.D., 2016a. Fluoride Removal from Brackish Groundwaters by Constant Current Capacitive Deionization (CDI). Environ. Sci. Technol. 50, 10570–10579. https://doi.org/10.1021/acs.est.6b03307

Tang, W., Kovalsky, P., Cao, B., Waite, T.D., 2016b. Investigation of fluoride removal from low-salinity groundwater by single-pass constant-voltage capacitive deionization. Water Res. 99, 112–121. https://doi.org/10.1016/j.watres.2016.04.047

Tansel, B., Sager, J., Rector, T., Garland, J., Strayer, R.F., Levine, L., Roberts, M., Hummerick, M., Bauer, J., 2006. Significance of hydrated radius and hydration shells on ionic permeability during nanofiltration in dead end and cross flow modes. Sep. Purif. Technol. 51, 40–47. https://doi.org/10.1016/j.seppur.2005.12.020

Thampy, S., Desale, G.R., Shahi, V.K., Makwana, B.S., Ghosh, P.K., 2011. Development of hybrid electrodialysis-reverse osmosis domestic desalination unit for high recovery of product water. Desalination 282, 104–108. https://doi.org/10.1016/j.desal.2011.08.060

Thanh-Nho, N., Strady, E., Nhu-Trang, T.T., David, F., Marchand, C., 2018. Trace metals partitioning between particulate and dissolved phases along a tropical mangrove estuary (Can Gio, Vietnam). Chemosphere 196, 311–322. https://doi.org/10.1016/j.chemosphere.2017.12.189

Thu, V.T.H., Tabata, T., Hiramatsu, K., Ngoc, T.A., Harada, M., 2020. Assessing Impacts of Sea Level Rise and Sea Dike Construction on Salinity Regime in Can Gio Bay, South Vietnam. J. Waterw. Port, Coastal, Ocean Eng. 146, 05020006. https://doi.org/10.1061/(ASCE)WW.1943-5460.0000608

Tian, J., Xu, Y., Chen, Z., Nan, J., Li, G., 2010. Air bubbling for alleviating membrane fouling of immersed hollow-fiber membrane for ultrafiltration of river water. Desalination 260, 225–230. https://doi.org/10.1016/j.desal.2010.04.026

Tong, X., Zhang, B., Chen, Y., 2016. Fouling resistant nanocomposite cation exchange membrane with enhanced power generation for reverse electrodialysis. J. Memb. Sci. 516, 162–171. https://doi.org/10.1016/J.MEMSCI.2016.05.060

Tuan, L.N., Tran, H.X., 2018. Assessing Climate Change Exposure of Rural Fresh Water and Sanitation – A Case Study in Can Gio District. Vietnam J. Sci. Technol. 56, 71. https://doi.org/10.15625/2525-2518/56/1/8826

Tzen, E., 2012. Wind energy powered technologies for freshwater production: Fundamentals and case studies, in: Bundschuh, J., Hoinkis, J. (Eds.), Renewable Energy Applications for Freshwater Production. CRC Press, pp. 167–178.

UN WATER, 2017. UN World Water Development Report: Wastewater, the Untapped Resource. UNESCO WWAP, Paris.

UNDP, 2016. Human Development Report 2016 Human Development for Everyone. United Nations Development Programme, New York.

UNDP, 2006. Human Development Report 2006 - Beyond scarcity: Power, poverty and the global water crisis. New York.

UNESCO, 2019. The United Nations world water development report 2019: leaving no one behind .

Van Der Laan, H., 2009. Modeling subsurface iron Removal. "Application of a Geochemical Model to describe subsurface aeration at pumping station Schuwacht". Delft University of Technology.

van Halem, D., 2011. Subsurface iron and arsenic removal for drinking water treatment in Bangladesh. Water Management Academic Press.

van Halem, D., Heijman, S.G.J., Johnston, R., Huq, I.M., Ghosh, S.K., Verberk, J.Q.J.C., Amy, G.L., Van Dijk, J.C., 2010. Subsurface iron and arsenic removal: Low-cost technology for community-based water supply in Bangladesh. Water Sci. Technol. 62, 2702–2709. https://doi.org/10.2166/wst.2010.463

Varcoe, J.R., Atanassov, P., Dekel, D.R., Herring, A.M., Hickner, M.A., Kohl, P.A., Kucernak, A.R., Mustain, W.E., Nijmeijer, K., Scott, K., Xu, T., Zhuang, L., 2014. Anion-exchange membranes in electrochemical energy systems. Energy Environ. Sci. 7, 3135–3191. https://doi.org/10.1039/C4EE01303D

Vidyanandan, K.V., 2017. An Overview of Factors Affecting the Performance of Solar PV Systems.

Visoottiviseth, P., Ahmed, F., 2008. Technology for remediation and disposal of arsenic, in: Reviews of Environmental Contamination and Toxicology. Springer New York, New York, NY, pp. 77–128. https://doi.org/10.1007/978-0-387-79284-2_4

Voltea, 2016a. Technical Bulletin: CapDI Ion removal comparison. Sassenheim.

Voltea, 2016b. Technical Bulletin: Feedwater Guidelines. Sassenheim.

Voutchkov, N., 2018. Energy use for membrane seawater desalination – current status and trends. Desalination 431, 2–14. https://doi.org/10.1016/j.desal.2017.10.033

Vu, D.T., Yamada, T., Ishidaira, H., 2018. Assessing the impact of sea level rise due to climate change on seawater intrusion in Mekong Delta, Vietnam. Water Sci. Technol. 77, 1632–1639. https://doi.org/10.2166/wst.2018.038

WaKap, 2016. WaKap - Ein Projekt zur Wasseraufbereitung mittels Kapazitiver Deionisierung [WWW Document]. URL www.wakap.de (accessed 8.30.19).

Wang, C., Song, H., Zhang, Q., Wang, B., Li, A., 2015. Parameter optimization based on capacitive deionization for highly efficient desalination of domestic wastewater biotreated effluent and the fouled electrode regeneration. Desalination 365, 407–415. https://doi.org/10.1016/j.desal.2015.03.025

Wang, T., Bai, L., Zhang, C., Zhu, X., Xing, J., Guo, Y., Wang, J., Lin, D., Li, G., Liang, H., 2020. Formation mechanism of iron scale in membrane capacitive deionization (MCDI) system. Desalination 495, 114636. https://doi.org/10.1016/j.desal.2020.114636

Wang, Z., Guo, H., Xiu, W., Wang, J., Shen, M., 2018. High arsenic groundwater in the Guide basin, northwestern China: Distribution and genesis mechanisms. Sci. Total Environ. 640–641, 194–206. https://doi.org/10.1016/j.scitotenv.2018.05.255

Wassmann, R., Hien, N.X., Hoanh, C.T., Tuong, T.P., 2004. Sea level rise affecting the Vietnamese Mekong Delta: Water elevation in the flood season and implications for rice production. Clim. Change 66, 89–107. https://doi.org/10.1023/B:CLIM.0000043144.69736.b7

WEISE WATER, 2020. The AQQA® Innovation [WWW Document]. W. WATER GmbH. URL http://www.weise-water.de/aqqacube (accessed 12.12.20).

Welgemoed, T.J., Schutte, C.F., 2005. Capacitive Deionization Technology TM : An alternative desalination solution 183, 327–340. https://doi.org/10.1016/j.desal.2005.02.054

Wencki, K., Thöne, V., Ante, A., Hogen, T., Hohmann, C., Tettenborn, F., Pohl, D., Preiss, P., Jungfer, C., 2020. Approaches for the evaluation of future-oriented technologies and concepts in the field of water reuse and desalination. J. Water Reuse Desalin. 10, 269–283. https://doi.org/10.2166/wrd.2020.022

Wheeler, D., 2011. Quantifying Vulnerability to Climate Change: Implications for Adaptation Assistance (No. 240). Washington DC.

WHO, 2017. Guidelines for Drinking-water Quality: fourth edition incorporating the first addendum, 4th ed. World Health Organization.

WHO, 2012. WHO | Arsenic [WWW Document]. Fact sheet N°372. URL http://www.who.int/mediacentre/factsheets/fs372/en/ (accessed 12.5.16).

WHO, 2011. Arsenic in Drinking-water. Background document for development of WHO Guidelines for Drinking-water Quality.

Winkel, L.H.E., Trang, P.T.K., Lan, V.M., Stengel, C., Amini, M., Ha, N.T., Viet, P.H., Berg, M., 2011. Arsenic pollution of groundwater in Vietnam exacerbated by deep aquifer exploitation for more than a century. Proc. Natl. Acad. Sci. 108, 1246–1251. https://doi.org/10.1073/pnas.1011915108

World Bank Group, 2019. The Role of Desalination in an Increasingly Water-Scarce World. Washington DC.

Xie, X., Wang, Y., Pi, K., Liu, C., Li, J., Liu, Y., Wang, Z., Duan, M., 2015. In situ treatment of arsenic contaminated groundwater by aquifer iron coating: Experimental study. Sci. Total Environ. 527–528, 38–46. https://doi.org/10.1016/j.scitotenv.2015.05.002

Yeboah, N.N.N., Burns, S.E., 2011. Geological disposal of energy-related waste. KSCE J. Civ. Eng. 15, 697–705. https://doi.org/10.1007/s12205-011-0010-x

Youssef, P.G., Al-Dadah, R.K., Mahmoud, S.M., 2014. Comparative analysis of desalination technologies, in: Energy Procedia. Elsevier Ltd, pp. 2604–2607. https://doi.org/10.1016/j.egypro.2014.12.258

Yu, T.-H., Shiu, H.-Y., Lee, M., Chiueh, P.-T., Hou, C.-H., 2016. Life cycle assessment of environmental impacts and energy demand for capacitive deionization technology. Desalination 399, 53–60. https://doi.org/10.1016/j.desal.2016.08.007

Zhang, C., He, D., Ma, J., Tang, W., Waite, T.D., 2018a. Faradaic reactions in capacitive deionization (CDI) - problems and possibilities: A review. Water Res. 128, 314–330. https://doi.org/10.1016/j.watres.2017.10.024

Zhang, C., Ma, J., He, D., Waite, T.D., 2018b. Capacitive Membrane Stripping for Ammonia Recovery (CapAmm) from Dilute Wastewaters. Environ. Sci. Technol. Lett. 5, 43–49. https://doi.org/10.1021/acs.estlett.7b00534

Zhang, C., Ma, J., Song, J., He, C., Waite, T.D., 2018c. Continuous Ammonia Recovery from Wastewaters Using an Integrated Capacitive Flow Electrode Membrane Stripping System. Environ. Sci. Technol. 52, 14275–14285. https://doi.org/10.1021/acs.est.8b02743

Zhang, C., Ma, J., Waite, T.D., 2020. The impact of absorbents on ammonia recovery in a capacitive membrane stripping system. Chem. Eng. J. 382, 122851. https://doi.org/10.1016/j.cej.2019.122851

Zhang, D., Guo, H., Xiu, W., Ni, P., Zheng, H., Wei, C., 2017. In-situ mobilization and transformation of iron oxides-adsorbed arsenate in natural groundwater. J. Hazard. Mater. 321, 228–237. https://doi.org/10.1016/j.jhazmat.2016.09.021

Zhao, R., Biesheuvel, P.M., van der Wal, A., 2012. Energy consumption and constant current operation in membrane capacitive deionization. Energy Environ. Sci. 5, 9520. https://doi.org/10.1039/c2ee21737f

Zhao, R., Porada, S., Biesheuvel, P.M., van der Wal, A., 2013a. Energy consumption in membrane capacitive deionization for different water recoveries and flow rates, and comparison with reverse osmosis. Desalination 330, 35–41. https://doi.org/10.1016/j.desal.2013.08.017

Zhao, R., Satpradit, O., Rijnaarts, H.H.M., Biesheuvel, P.M., van der Wal, A., 2013b. Optimization of salt adsorption rate in membrane capacitive deionization. Water Res. 47, 1941–1952. https://doi.org/10.1016/j.watres.2013.01.025

Zhou, Y., Gao, C., 2010. Comparison between BWRO membrane and SWRO membrane. Huagong Xuebao/CIESC J. 61, 2590–2595.
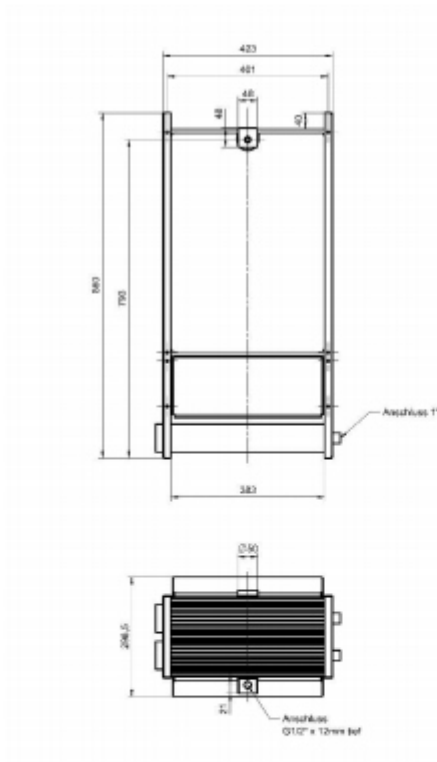
APPENDICES

APPENDIX I TECHNICAL DATA SHEET UF

AQQA®

technical data sheet AQQA®8 Article-No. 80100108

Complete pre-assembled unit for the filtration of water with submerged membrane plates. The unit comprises:

- AQQA® membrane plates
- frame
- AQQA® air diffusor for optimal sized bubbles

parameter	unit	value
dimension of filter housing (incl. flange for aeration)	l x w x h mm	423 x 299 x 860
air connection	G	1"
filtrate connection	G	½"
number of AQQA® membrane plates		18
total membrane surface area	m²	8
typical design flow in MBR [1]	l/h	200
max. flow in MBR [1]	l/h	400
max. air flow	l/min	200
min. air flow	l/min	100
filtration pressure	mbar	-30 ...-500
backflush pressure	mbar	350
pore size nominal	µm	0,04
frame material		1.4301
frame material (optional)		1.4571
membrane material		PES
max. operating temperature	°C	50
max. pH-range		1-12
weight dry	kg	10
weight wet	kg	15

[1] depending on wastewater characterisics

Design pressure: -50 mbar

Source: WEISE WATER (2020)

APPENDIX 2 TECHNICAL DATA SHEET SW30

‹DUPONT›

Product Data Sheet

FILMTEC™ Membranes
FILMTEC™ Seawater RO Elements for Marine Systems

Description

Improved FILMTEC™ seawater reverse osmosis elements offer the highest productivity while maintaining excellent salt rejection.
- FILMTEC™ SW30 membrane elements have the highest flow rates available to meet the water demands of both sea-based and land-based desalinators.
- FILMTEC™ SW30 elements may also be operated at lower pressure to reduce pump size, cost and operating expenses.
- Improved FILMTEC™ seawater membrane combined with automated, precision element fabrication result in the most consistent product performance available.

Typical Properties

Product	Part Number	Applied Pressure psig (bar)	Permeate Flow Rate gpd (m³/d)	Stabilized Salt Rejection (%)
SW30-2514	80733	800 (55)	150 (0.6)	99.4
SW30-2521	80734	800 (55)	300 (1.1)	99.4
SW30-2540	80737	800 (55)	700 (2.6)	99.4
SW30-4021	80740	800 (55)	800 (3.0)	99.4
SW30-4040	80741	800 (55)	1,950 (7.4)	99.4

1. Permeate flow and salt rejection based on the following test conditions: 32,000 ppm NaCl, pressure specified above, 77°F (25°C) and the following recovery rates:
   SW30-2514 – 2%, SW30-2521 & SW30-4021 – 5%, SW30-2540 & SW30-4040 – 8%.
2. Permeate flows for individual elements may vary +/-20%.
3. For the purpose of improvement, specifications may be updated periodically.

Element Dimensions
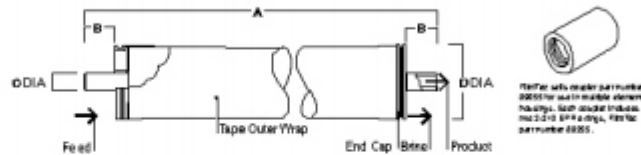
Product	Maximum Feed Flow Rate gpm (m³/h)	Dimensions – Inches (mm) A	B	C	D
SW30-2514	6 (1.4)	14.0 (356)	1.19 (30.2)	0.75 (19)	2.4 (61)
SW30-2521	6 (1.4)	21.0 (533)	1.19 (30.2)	0.75 (19)	2.4 (61)
SW30-2540	6 (1.4)	40.0 (1,016)	1.19 (30.2)	0.75 (19)	2.4 (61)
SW30-4021	16 (3.6)	21.0 (533)	1.05 (26.7)	0.75 (19)	3.9 (99)
SW30-4040	16 (3.6)	40.0 (1,016)	1.05 (26.7)	0.75 (19)	3.9 (99)

1. Refer to FilmTec Design Guidelines for multiple-element systems. 1 inch = 25.4 mm
2. SW30-2514, SW30-2521 and SW30-2540 elements fit nominal 2.5-inch I.D. pressure vessels. SW30-4021 and SW30-4040 elements fit nominal 4-inch I.D. pressure vessel.

APPENDIX 3 TECHNICAL DATA SHEET XLE

‹DUPONT›

Product Data Sheet

FILMTEC™ Membranes
FILMTEC™ Extra Low Energy (XLE) Elements for Commercial Systems

Description

New FILMTEC™ XLE elements offer better system performance and economics by operating at very low applied pressure. XLE membrane, made with a patented technology, provides consistent and reliable system performance. And for added convenience, XLE elements are available in a dry state for rapid start-up (see Figure 2 on reverse). The new XLE series of elements replaces TW30LE elements which were made with an older membrane technology.

Typical Properties

Product	Part Number	Applied Pressure psig (bar)	Permeate Flow Rate gpd (m³/d)	Stabilized Salt Rejection (%)
XLE-2521	154530	100 (6.9)	365 (1.4)	99.0
XLE-2540	154543	100 (6.9)	850 (3.2)	99.0
XLE-4021	154540	100 (6.9)	1,025 (3.9)	99.0
XLE-4040	154546	100 (6.9)	2,600 (9.8)	99.0

1. Permeate flow and salt rejection based on the following test conditions: 500 ppm NaCl feedstream, pressure specified above, 77°F (25°C) and the following recovery rates: XLE-2521, XLE-4021 – 8%; XLE-2540, XLE-4040 – 15%.
2. Permeate flows for individual elements may vary +/-20%.
3. For the purpose of improvement, specifications may be updated periodically.

Element Dimensions
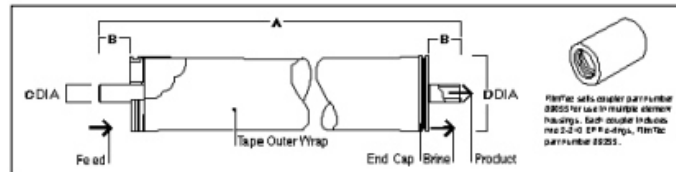
Product	Maximum Feed Flow Rate gpm (m³/h)	Dimensions – Inches (mm) A	B	C	D
XLE-2521	6 (1.4)	21.0 (533)	1.19 (30.2)	0.75 (19)	2.4 (61)
XLE-2540	6 (1.4)	40.0 (1,016)	1.19 (30.2)	0.75 (19)	2.4 (61)
XLE-4021	14 (3.2)	21.0 (533)	1.05 (26.7)	0.75 (19)	3.9 (99)
XLE-4040	14 (3.2)	40.0 (1,016)	1.05 (26.7)	0.75 (19)	3.9 (99)

1. Refer to FilmTec Design Guidelines for multiple-element systems.1 inch = 25.4 mm
2. XLE-2521 and XLE-2540 elements fit nominal 2.5-inch I.D. pressure vessel. XLE-4021 and XLE-4040 elements fit nominal 4-inch I.D. pressure vessel.
3. Refer to FilmTec Design Guidelines for multiple-element systems.1 inch = 25.4 mm
4. Refer to FilmTec Design Guidelines for multiple-element systems.1 inch = 25.4 mm
5. Refer to FilmTec Design Guidelines for multiple-element systems.1 inch = 25.4 mm

APPENDIX 4 ELECTRICAL SCHEME LPRO+MCDI